PUBLICATIONS OF
THE UNIVERSITY OF EASTERN FINLAND

Dissertations in Forestry and Natural Sciences

LUTFUL AHAD

TEMPORAL AND SPECTRAL COHERENCE OF QUASI-STATIONARY PULSED LIGHT: APPLICATION TO FREE-ELECTRON LASERS

PUBLICATIONS OF THE UNIVERSITY OF EASTERN FINLAND
DISSERTATIONS IN FORESTRY AND NATURAL SCIENCES

No 331

Lutful Ahad

TEMPORAL AND SPECTRAL COHERENCE OF QUASI-STATIONARY PULSED LIGHT: APPLICATION TO FREE-ELECTRON LASERS

ACADEMIC DISSERTATION

To be presented by the permission of the Faculty of Science and Forestry for public examination in the Auditorium M103 in Metria Building at the University of Eastern Finland, Joensuu, on December 21, 2018, at 12 o'clock noon.

University of Eastern Finland
Institute of Photonics
Joensuu 2018

Grano Oy
Jyväskylä, 2018
Editors: Pertti Pasanen, Matti Tedre,
Jukka Tuomela, and Matti Vornanen

Distribution:
University of Eastern Finland Library / Sales of publications
julkaisumyynti@uef.fi
http://www.uef.fi/kirjasto

ISBN: 978-952-61-2990-7 (print)
ISSNL: 1798-5668
ISSN: 1798-5668
ISBN: 978-952-61-2991-4 (pdf)
ISSNL: 1798-5668
ISSN: 1798-5676

Author's address:
University of Eastern Finland
Institute of Photonics
P. O. Box 111
80101 JOENSUU
FINLAND
email: lutful.ahad@uef.fi

Supervisors:
Professor Tero Setälä, D.Sc. (Tech)
University of Eastern Finland
Institute of Photonics
P. O. Box 111
80101 Joensuu
FINLAND
email: tero.setala@uef.fi

Dr. Ismo Vartiainen, Ph.D.
Dispelix Oy
02130 Espoo
FINLAND
email: ismo.vartiainen@dispelix.com

Reviewers:
Assistant Professor Andrej Singer
Cornell University
Department of Materials Science and Engineering
327 Bard Hall
Ithaca, NY 14853-1501
USA
email: asinger@cornell.edu

Associate Professor Markku Vainio
University of Helsinki
Department of Chemistry
P. O. Box 55 (A. I. Virtasen aukio 1)
00014 Helsinki
FINLAND
email: markku.vainio@helsinki.fi

Opponent:
Professor Tatiana Alieva
University Complutense of Madrid
Department of Optics
Ciudad Universitaria s/n
28040 Madrid
SPAIN
email: talieva@fis.ucm.es

Lutful Ahad
Temporal and spectral coherence of quasi-stationary pulsed light: application to free-electron lasers
Joensuu: University of Eastern Finland, 2018
Publications of the University of Eastern Finland
Dissertations in Forestry and Natural Sciences

ABSTRACT

This work deals with modeling the spectral and temporal coherence properties of pulsed random light fields. First, we develop an iterative mathematical technique which can be used to form an ensemble of spectral and temporal complex pulses for the construction of the related coherence functions. The proposed model is based on the information of the spectrum of individual pulses and the average temporal length of the pulse ensemble. In particular, we apply the algorithm to simulate pulses of the free-electron laser facility at Stanford. Utilizing the pulses from the algorithm, we examine the coherence properties of the laser facility which turns out to emit quasi-stationary pulse trains.

Second, a new time-domain pseudo-modal expansion is presented for random, quasi-stationary scalar light pulses. The expansion is an elegant approach to the study of pulse coherence as it requires only the average spectrum and the mean temporal intensity of the pulse train. The proposed modal expansion is applied to the case of a self-amplified spontaneous emission based free-electron laser. The new time-domain pseudo-modal representation is extended to quasi-stationary partially polarized electromagnetic beams. A novel harmonic mode representation for statistically stationary partially polarized electromagnetic beams is also presented.

Third, we elaborate on the interpretation of autocorrelation measurements for free-electron lasers and the information that can be extracted from such experiments. We also propose a field cross-correlation method which can provide additional information on a pulsed field.

Universal Decimal Classification: *535, 537.87, 621.375.826*
Keywords: *Photonics; Coherence (Optics); Light; Electromagnetic fields; Polarization; Pulsed radiation; Laser pulses, Ultrashort; Free-electron lasers; Mathematical models; Algorithms; Computer simulation*

ACKNOWLEDGEMENTS

I am very grateful to my supervisors Prof. Tero Setälä and Dr. Ismo Vartiainen for their continuous guidance and support throughout the course of this work. I am especially thankful to Prof. Setälä, without his patience and help this work would not have been possible. I am indebted to Prof. Ari T. Friberg and Prof. Jari Turunen for their support during all these years. I am also thankful to the current Head of the Department, Prof. Jyrki Saarinen, and his predecessors, Prof. Seppo Honkanen and Prof. Timo Jääskeläinen, for providing me an opportunity to work at the University of Eastern Finland (UEF).

I owe special thanks to Dr. Noora Heikkilä, Ms. Katri Mustonen, Ms. Hannele Karppinen, and Ms. Marita Ratilainen for providing marvellous administrative support throughout my stay at the Institute of Photonics. Dr. Juha-Matti Huusko is appreciated for being an excellent IT support person of the department.

Many thanks also goes to Dr. Kimmo Saastamoinen for providing me assistance with Latex, and both Dr. Henri Partanen and Dr. Toni Saastamoinen for their help with MATLAB. I am also thankful to Dr. Pertti Pääkkönen for helping me with the use of MAXWELL for my simulations. I am grateful to M.Sc. Matias Koivurova and Dr. Gianluca Geloni (European XFEL, Hamburg) for their collaboration on GENESIS. The reviewers of this thesis, Prof. Markku Vainio and Prof. Andrej Singer, are much appreciated for their comments and suggestions.

I am extremely thankful to my current and previous office mates, all the colleagues in the Institute of Photonics and at UEF who have provided me a joyful and caring company during my stay at the university. Thank you all!

Lastly, I cannot express enough gratitude to my parents who stood by my side during all these years. All I have in life today is thanks to them. I deeply miss my mom for she was my most sincere friend who stood by my side during truly testing times of my life but could not live long enough to witness this day. Finally, I am thankful to my wife for her support and understanding during the completion of this work.

Joensuu, November 21, 2018

Lutful Ahad

LIST OF PUBLICATIONS

This thesis is based on the following selection of the author's publications:

I L. Ahad, I. Vartiainen, T. Setälä, A. T. Friberg, C. David, M. Makita, and J. Turunen, "On spectral and temporal coherence of x-ray free-electron laser beams," *Opt. Express* **24**, 13081–13090 (2016).

II L. Ahad, I. Vartiainen, T. Setälä, A. T. Friberg, and J. Turunen, "Quasi-monochromatic modes of quasi-stationary, pulsed scalar optical fields," *J. Opt. Soc. Am. A.* **34**, 1469–1475 (2017).

III L. Ahad, J. Turunen, A. T. Friberg, and T. Setälä, "Temporal modes of stationary and pulsed quasistationary electromagnetic beams," *J. Opt. Soc. Am. A.* **35**, 830–839 (2018).

IV M. Koivurova, L. Ahad, G. Geloni, T. Setälä, J. Turunen, and A. T. Friberg, "Interferometry and coherence of nonstationary light," submitted (2018).

Throughout the overview, these papers will be referred to by Roman numerals.

AUTHOR'S CONTRIBUTION

The publications selected in this dissertation are original research papers based on the investigation of the coherence properties of random pulsed light.

The idea for paper **I** arose while the author was performing the literature review. The author wrote the algorithm in paper **I**. In paper **II**, the author participated in the theoretical calculations and numerical simulations. In paper **III**, the author participated in the mathematical derivations. In paper **IV**, the author performed the simulations related to the free-electron laser pulses. The author contributed to the discussions, interpretation of the results, and writing of all papers.

All the publications involved active cooperation with the co-authors.

TABLE OF CONTENTS

1 Introduction

Life on the earth exists due to the presence of light. In colloquial language, the term 'light' is used for the part of the electromagnetic spectrum that is visible to the naked human eye. The spectral range that stimulates the sensation of sight lies in the 400 nm to 800 nm wavelength region, approximately. In scientific terms, light not only refers to the tiny stretch of the electromagnetic spectrum visible to the unaided eye but it also encompasses the wavelengths from the radio and microwave regions down to the ultraviolet (UV) and x-ray regimes [1].

When light from a single-mode laser is shined on a two pinhole aperture, high contrast interference fringes (alternating regions of low and high intensity) appear on the observation screen. However, if light from natural sources, such as the sun or wood fire or an artificial thermal source of radiation, for example, an incandescent bulb, is incident on a two pinhole mask, the fringe pattern is either extremely weak or even invisible. This simple experiment which is commonly called Young's double-pinhole experiment shows that light from man-made and natural sources differ from each other. In the case of a laser, the light fields at different points across the beam are correlated, and therefore, they interfere perfectly creating a set of dark and bright intensity fringes, while for a natural source, the field is often uncorrelated and hence there is no interference. This characteristic of light to create interference fringes was decisive in proving the wave nature of light [2,3] and is called coherence.

Coherence is a fundamental property of light fields. It can be classified broadly into two categories: spatial and temporal coherence. While Young's double-pinhole experiment describes the spatial coherence properties of an optical field, the classic Michelson's interferometer characterizes the temporal coherence of light. Spatial coherence refers to the correlation of an optical field at two different spatial points. Temporal coherence refers to the ability of a wave to interfere at two temporal points. In order words, spatial coherence implies how consistent the wavefront of an optical field is and temporal coherence usually entails how narrowband a field is. All light fields have random fluctuations. These fluctuations take place typically on the femtosecond (10^{-15} s) time scale. It is not possible to observe the instantaneous fluctuations of an optical field with the eye or measure these directly with a detector. Therefore, the properties of optical fields are studied in an averaged sense with the help of correlation functions within the framework of optical coherence theory [4]. The correlation functions describe the extent of statistical unison in the light field at a single spatial point or at two different points in space and time. The correlation among the field components manifests itself in the form of interference phenomenon leading to intensity fringes in a Young's double-pinhole or Michelson's experiment. The visibility of the fringes is a measure of the strength of the correlations, i.e., coherence, of an optical field [4, 5]. In essence, optical coherence theory studies the randomness of light fields in terms of physically observable quantities [6].

Moreover, light from some sources like a continuous-wave laser or sunlight has fluctuations whose characteristics stay essentially the same over the time and hence the fields from such sources are called statistically stationary. For pulsed lasers, the character of fluctuations change in time and the fields emanating from such sources

are called non-stationary optical fields.

Studies on the coherence of light fields can be dated back to the latter half of the nineteenth century when Verdet observed that sunlight vibrates in unison within a small region [7]. Zernike introduced the degree of coherence which provides a quantitative measure for the correlations of an optical field [8]. Wolf laid the foundations of modern coherence theory in the space–time domain for stationary fields [9–11]. Later, the coherence properties of stationary fields were formulated in the space–frequency domain [12–16]. Many important optical fields are non-stationary. Although the formalisms developed for the stationary fields were extended in some studies to the more generalized case of non-stationary fields [17–20], yet the coherence of non-stationary fields has not got as much attention as that of the stationary light fields. In this thesis, we address this unexplored domain. We utilize the coherence theory of non-stationary light to investigate the coherence properties of pulsed fields.

Since the first demonstration of laser in 1960 [21], there has been a continuous development towards fabrication of such light sources which can generate coherent radiation at short wavelengths with femtosecond duration. With conventional lasers, femtosecond pulses can be generated which provide the requisite temporal resolution for the study of ultrafast processes. The spatial resolution is linked with the wavelength and with the traditional lasers which are based on the excitation and de-excitation of the atoms and molecules, generation of shorter wavelengths down to the nanometer scale is not a feasible task. First, the reflectivity of the mirrors falls off drastically for shorter wavelengths making the construction of an efficient optical cavity difficult and, second, a large amount of pumping is required to achieve the population inversion by raising the inner shell electrons to higher energy levels [22]. Therefore, over the years, researchers explored alternate possibilities to generate radiation in the extreme wavelength regions. The years of development and research gave rise to the free-electron lasers (FELs). Unlike the conventional lasers whose output wavelength range is confined by the discrete energy levels, FELs have a beam of free electrons which serves as the pump and the gain medium simultaneously. In an FEL, the beam of free electrons travels at a relativistic speed in an undulator (a periodic arrangement of magnets). By changing the period of the undulator, the wavelength of the emitted radiation can be tuned on a wide scale. Especially the FELs operating in the x-ray region which are called as x-ray FELs (XFELs) are important in the modern scientific research in the fields like material science, biology, and condensed matter physics. The radiation from an XFEL has a wavelength of the order of a few angstroms (which is in the size range of atoms) and thus enables to study the structure of materials on an angstrom level [23]. Apart from providing atomic level spatial resolution, x-rays have weak interaction with materials that enables imaging of thick specimens [24]. The FELs equip the scientists with a tunability on an unprecedented scale from the microwave down to the extreme UV and x-ray regions. The FELs typically deliver approximately 10^{12} photons in about 100 fs pulses. The extremely bright and ultrashort pulses can enable to detect and record the motion of atoms and molecules, a prodigious task which was not possible with the third-generation synchrotron sources [25]. In addition to high brightness and ultrashort pulse durations, FELs have nearly perfect transverse coherence which makes them useful in experiments like coherent diffraction imaging. Due to the ever growing importance of these fourth-generation light sources, we have focused on studying the coherence properties of the FELs. A description of the FELs, their operational principle, and applications is given elsewhere in the thesis.

In the literature, coherent-mode representations have been commonly employed for treating partially coherent optical fields. In the coherent-mode representation, a partially coherent field is expressed as an incoherent sum of fully coherent modes [26]. Such modal expansions were already presented for stationary [15,16] and non-stationary scalar fields [27,28]. There are, however, many important pulsed optical sources, for example, FELs, which emit quasi-stationary random pulses and there had not been a convenient modal expansion for such pulsed fields. In this thesis, we present a novel modal expansion for quasi-stationary, random pulses where the modes can be obtained by using the knowledge of the average pulse intensity and the mean spectrum only. For electromagnetic beams, we present a time-domain harmonic modal expansion which is an extension of an earlier work for the scalar stationary beams [29]. We also propose a pseudo-modal decomposition for pulsed, quasi-stationary, partially polarized electromagnetic beams. The proposed mode representations can find applications in the cases where the structures that interact with partially coherent light are on a wavelength or sub-wavelength scale.

This thesis is organized as follows. In Chapter 2, we describe the concept of complex analytic signal and the basics of the coherence theory of non-stationary scalar fields. Chapter 2 contains an elucidation of the traditional coherent-mode representation method for stationary and non-stationary scalar fields. We introduce here a novel pseudo-modal (the modes are not orthonormal) time-domain representation for quasi-stationary random pulses. We briefly present the notion of the Gaussian Schell model (GSM) and a description of an iterative Fourier transform algorithm (IFTA) that can be used to construct ensembles of spectral and temporal pulses. For studying the spectral and temporal coherence properties of pulsed light sources, such ensembles are then used to construct the correlation functions in the spectral and temporal domains.

Chapter 3 deals with the basics of electromagnetic coherence. We elaborate the concepts of coherence matrices and the degree of polarization. Chapter 3 also contains the electromagnetic extension to the modal representation methods presented in Chap. 1 for stationary, non-stationary, and quasi-stationary optical fields.

Chapter 4 describes the coherence measurements of pulsed light. In Chap. 4, we present a comprehensive discussion on the challenges involved in the characterization of ultrashort optical pulses. It also addresses the intricacies involved in the coherence measurements of pulsed fields that need to be considered in practical investigations.

Chapter 5 includes a description of the FELs, their operational principle and applications. Some results from the IFTA are presented in the chapter. In addition, it briefly describes the simulation results that were obtained with the three-dimensional time-dependent code GENESIS for the FELs. Finally, the conclusions drawn from the work and the future prospects are summarized in Chapter 6.

The major findings of this thesis are:

- An iterative technique which can be used to construct ensembles of complex spectral and temporal fields for a pulsed light source.

- A new time-domain pseudo-modal expansion for quasi-stationary pulsed scalar fields.

- An elegant harmonic time-domain coherent-mode expansion for stationary partially polarized electromagnetic beams.

- A novel pseudo-modal expansion for quasi-stationary partially polarized electromagnetic beams in time domain.
- New insights on the autocorrelation and cross-correlation measurements of pulsed sources.

2 Coherence of non-stationary scalar fields

In statistical optics, random optical fields can be generally divided into two categories: stationary [4, 5, 30] and non-stationary [18–20]. If the average behavior of the fluctuations in an optical field does not change with time, the field is said to be stationary [4, 5]. If the random characteristics of the field change over time, for example, in the case of optical pulses, then the field is non-stationary.

2.1 COMPLEX ANALYTIC SIGNAL

A real-valued scalar function can be associated with a complex function which greatly facilitates the mathematical treatment of optical signals. Let us consider a real-valued scalar function $V_{\mathrm{r}}(\mathbf{r}, t)$, where $\mathbf{r}$ denotes the position vector, t is the time, and the subscript r signifies that $V_{\mathrm{r}}(\mathbf{r}, t)$ is a real function. The function $V_{\mathrm{r}}(\mathbf{r}, t)$ may correspond to any Cartesian electric or magnetic component of the electromagnetic field. If $V_{\mathrm{r}}(\mathbf{r}, t)$ is square integrable (with respect to time), then it can be expressed as a superposition of harmonic functions of different frequencies via a Fourier integral

$$V_{\mathrm{r}}(\mathbf{r}, t) = \int_{-\infty}^{\infty} \tilde{V}_{\mathrm{r}}(\mathbf{r}, \omega) \exp(-\mathrm{i}\omega t) \mathrm{d}\omega, \tag{2.1}$$

where the spectral function $\tilde{V}_{\mathrm{r}}(\mathbf{r}, \omega)$ is obtained by taking the inverse of Eq. (2.1)

$$\tilde{V}_{\mathrm{r}}(\mathbf{r}, \omega) = \frac{1}{2\pi} \int_{-\infty}^{\infty} V_{\mathrm{r}}(\mathbf{r}, t) \exp(\mathrm{i}\omega t) \mathrm{d}t. \tag{2.2}$$

Equation (2.1) holds for pulses but for non-pulsed non-stationary and stationary light, it can be interpreted in terms of generalized functions [4].

As $V_{\mathrm{r}}(\mathbf{r}, t)$ is a real-valued function, Eq. (2.2) implies that $\tilde{V}_{\mathrm{r}}(\mathbf{r}, -\omega) = \tilde{V}_{\mathrm{r}}^{*}(\mathbf{r}, \omega)$ which connotes that the negative frequency components carry no additional information that is not already contained in the positive ones. The asterisk $*$ denotes the complex conjugate. Employing this observation, Eq. (2.1) is rewritten as

$$V_{\mathrm{r}}(\mathbf{r}, t) = 2\mathrm{Re}\left[\int_{0}^{\infty} \tilde{V}_{\mathrm{r}}(\mathbf{r}, \omega) \exp(-\mathrm{i}\omega t) \mathrm{d}\omega\right], \tag{2.3}$$

where Re denotes the real part. Using the function $V_{\mathrm{r}}(\mathbf{r}, t)$, the associated complex analytic signal $V(\mathbf{r}, t)$ is expressed as

$$V(\mathbf{r}, t) = 2\int_{0}^{\infty} \tilde{V}_{\mathrm{r}}(\mathbf{r}, \omega) \exp(-\mathrm{i}\omega t) \mathrm{d}\omega. \tag{2.4}$$

The concept of complex analytic signal is attributed to Gabor [4, 31]. The real function is related to the complex analytic signal by

$$V_{\mathrm{r}}(\mathbf{r}, t) = \mathrm{Re}\left[V(\mathbf{r}, t)\right] = \frac{1}{2}\left[V(\mathbf{r}, t) + V^{*}(\mathbf{r}, t)\right]. \tag{2.5}$$

The complex analytic signal and the associated complex spectral amplitude can be represented by a Fourier transform pair

$$V(\mathbf{r},t) = \int_0^\infty \tilde{V}(\mathbf{r},\omega)\exp(-\mathrm{i}\omega t)\mathrm{d}\omega, \tag{2.6}$$

$$\tilde{V}(\mathbf{r},\omega) = \frac{1}{2\pi}\int_{-\infty}^\infty V(\mathbf{r},t)\exp(\mathrm{i}\omega t)\mathrm{d}t. \tag{2.7}$$

The lower limit in Eq. (2.6) is justified by the definition that $\tilde{V}(\mathbf{r},\omega) = 2\tilde{V}_\mathrm{r}(\mathbf{r},\omega)$ for $\omega > 0$ and $\tilde{V}(\mathbf{r},\omega) = 0$ otherwise. We employ the complex analytic signal representation throughout the thesis.

2.2 COHERENCE FUNCTIONS

Typically light sources found in nature or used in the laboratories are composed of numerous tiny radiators (atoms, molecules) each emitting spontaneously with a finite spectral bandwidth. At a certain instant of time, one can not be sure which radiator is active and which one is in a dormant state. The probabilistic nature of emission manifests itself in the form of rapid fluctuations in the total field. The total field is a sum of all the fields from the individual radiators. The fluctuations occur typically on a femtosecond time scale and hence cannot be detected by the naked eye or even with the fastest detectors. Therefore, the average statistical behavior of light is studied using correlation functions. This area of optics which deals with the statistical analysis of the average behavior of optical fields is termed as optical coherence theory [4,30].

In this section, the correlation functions for non-stationary fields in the space–time and space–frequency domains are introduced utilizing the complex analytic signal representation described in Sec. 2.1.

2.2.1 Non-stationary fields in the space–time domain

Mutual coherence function (MCF) is a fundamental quantity in the study of optical coherence [4, 10, 30]. The MCF describes the two-point space–time correlation of a field. To elucidate this concept, consider $V(\mathbf{r}_1,t_1)$ and $V(\mathbf{r}_2,t_2)$ which are the complex scalar amplitudes of a non-stationary (pulsed) field at two spatial points $\mathbf{r}_1$ and $\mathbf{r}_2$ and at two instants of time t_1 and t_2. The MCF is expressed as [18–20, 28, 32]

$$\Gamma(\mathbf{r}_1,\mathbf{r}_2,t_1,t_2) = \langle V^*(\mathbf{r}_1,t_1)V(\mathbf{r}_2,t_2)\rangle, \tag{2.8}$$

where the angle brackets $\langle\rangle$ denote the average taken over an ensemble $\{V(\mathbf{r},t)\}$ of space–time realizations. The average is defined by

$$\langle g(\mathbf{r},t)\rangle = \lim_{N\to\infty}\frac{1}{N}\sum_{n=1}^{N} g_n(\mathbf{r},t), \tag{2.9}$$

where $g_n(\mathbf{r},t)$ represents an individual realization in the ensemble.

If we consider the field at a single spatial point and the temporal coherence properties are spatially uniform, then for the sake of brevity, we can drop $\mathbf{r}$ dependence in Eq. (2.8) and rewrite it in the form

$$\Gamma(t_1,t_2) = \langle V^*(t_1)V(t_2)\rangle. \tag{2.10}$$

Also it is clear from the above definition that the MCF is Hermitian

$$\Gamma(t_2, t_1) = \Gamma^*(t_1, t_2). \tag{2.11}$$

It is also continuous and square integrable with respect to t_1 and t_2

$$\iint_{-\infty}^{\infty} |\Gamma(t_1, t_2)|^2 \mathrm{d}t_1 \mathrm{d}t_2 < \infty. \tag{2.12}$$

Properties (2.11) and (2.12) imply that the MCF is a Hilbert–Schmidt kernel [4]. In addition, the MCF is non-negative definite in the sense that

$$\sum_{i=1}^{N} \sum_{j=1}^{N} a_i^* a_j \Gamma(t_i, t_j) \geq 0, \tag{2.13}$$

where N is a positive integer and a_1, a_2,..., a_N are arbitrary complex numbers. The general form of the square-integrability and the non-negative definiteness conditions expressed in Eqs. (2.12) and (2.13) can be written as [28]

$$\iint_D \iint_{-\infty}^{\infty} |\Gamma(\mathbf{r}_1, \mathbf{r}_2, t_1, t_2)|^2 \mathrm{d}t_1 \mathrm{d}t_2 \mathrm{d}^3 r_1 \mathrm{d}^3 r_2 < \infty, \tag{2.14}$$

$$\iint_D \iint_{-\infty}^{\infty} f^*(\mathbf{r}_1, t_1) f(\mathbf{r}_2, t_2) \Gamma(\mathbf{r}_1, \mathbf{r}_2, t_1, t_2) \mathrm{d}t_1 \mathrm{d}t_2 \mathrm{d}^3 r_1 \mathrm{d}^3 r_2 \geq 0, \tag{2.15}$$

where D is the spatial domain under consideration and $f(\mathbf{r}, t)$ is an arbitrary function.

When Eq. (2.8) is calculated at a single spatio–temporal point $(\mathbf{r}, t)$, then it gives the temporal intensity $I(\mathbf{r}, t)$

$$I(\mathbf{r}, t) = \Gamma(\mathbf{r}, \mathbf{r}, t, t) = \langle |V(\mathbf{r}, t)|^2 \rangle, \tag{2.16}$$

which shows that non-stationary fields have time-dependent intensity.

The intensity-normalized MCF is called the complex degree of coherence and is given by [12, 33]

$$\gamma(\mathbf{r}_1, \mathbf{r}_2, t_1, t_2) = \frac{\Gamma(\mathbf{r}_1, \mathbf{r}_2, t_1, t_2)}{\sqrt{I(\mathbf{r}_1, t_1) I(\mathbf{r}_2, t_2)}}, \tag{2.17}$$

with the magnitude bounded in the interval

$$0 \leq |\gamma(\mathbf{r}_1, \mathbf{r}_2, t_1, t_2)| \leq 1. \tag{2.18}$$

If $|\gamma(\mathbf{r}_1, \mathbf{r}_2, t_1, t_2)| = 1$, it signifies that the field is fully coherent at the points $(\mathbf{r}_1, t_1)$ and $(\mathbf{r}_2, t_2)$ while $|\gamma(\mathbf{r}_1, \mathbf{r}_2, t_1, t_2)| = 0$ shows that the field is completely incoherent. The intermediate values correspond to partial spatio–temporal coherence of the field.

2.2.2 Non-stationary fields in the space–frequency domain

The complex analytic signal representation introduced in Sec. 2.1 provides an ensemble of realizations in the space–frequency domain. The ensemble $\{\tilde{V}(\mathbf{r}, \omega)\}$ can be used to construct the cross-spectral density (CSD) function [18, 28]

$$W(\mathbf{r}_1, \mathbf{r}_2, \omega_1, \omega_2) = \langle \tilde{V}^*(\mathbf{r}_1, \omega_1) \tilde{V}(\mathbf{r}_2, \omega_2) \rangle, \tag{2.19}$$

which gives the correlation between the frequency components ω_1 and ω_2 at two spatial points. Equation (2.19) computed at a single frequency and at a single point gives the spectral density of the field

$$S(\mathbf{r},\omega) = W(\mathbf{r},\mathbf{r},\omega,\omega) = \langle|\tilde{V}(\mathbf{r},\omega)|^2\rangle. \tag{2.20}$$

Analogously to Eq. (2.17) of time domain, Eq. (2.19) is normalized to get the complex spectral degree of coherence [12]

$$\mu(\mathbf{r}_1,\mathbf{r}_2,\omega_1,\omega_2) = \frac{W(\mathbf{r}_1,\mathbf{r}_2,\omega_1,\omega_2)}{\sqrt{S(\mathbf{r}_1,\omega_1)S(\mathbf{r}_2,\omega_2)}}, \tag{2.21}$$

which satisfies the condition

$$0 \leq |\mu(\mathbf{r}_1,\mathbf{r}_2,\omega_1,\omega_2)| \leq 1, \tag{2.22}$$

where the lower limit corresponds to complete incoherence and the upper limit to full coherence of the field at positions $\mathbf{r}_1$, $\mathbf{r}_2$ and at frequencies ω_1, ω_2. The intermediate values of $|\mu(\mathbf{r}_1,\mathbf{r}_2,\omega_1,\omega_2)|$ indicate partial spatio–spectral coherence of the field.

The MCF and the CSD functions are connected by

$$\Gamma(\mathbf{r}_1,\mathbf{r}_2,t_1,t_2) = \iint_0^\infty W(\mathbf{r}_1,\mathbf{r}_2,\omega_1,\omega_2)\exp\left[i\left(\omega_1 t_1 - \omega_2 t_2\right)\right]\mathrm{d}\omega_1\mathrm{d}\omega_2, \tag{2.23}$$

and

$$W(\mathbf{r}_1,\mathbf{r}_2,\omega_1,\omega_2) = \frac{1}{(2\pi)^2}\iint_{-\infty}^\infty \Gamma(\mathbf{r}_1,\mathbf{r}_2,t_1,t_2)\exp\left[-i\left(\omega_1 t_1 - \omega_2 t_2\right)\right]\mathrm{d}t_1\mathrm{d}t_2. \tag{2.24}$$

Equations (2.23) and (2.24) constitute a form of the generalized Wiener–Khintchine theorem which can be readily derived by utilizing Eqs. (2.6), (2.7), (2.8), and (2.19).

2.2.3 Stationary fields

For stationary fields, the average fluctuations of the field remain the same over time, and the MCF of such a field depends on the time arguments only via their difference $\Delta t = t_2 - t_1$. The MCF of stationary fields can be expressed in the form [4,30]

$$\Gamma(\mathbf{r}_1,\mathbf{r}_2,\Delta t) = \langle V^*(\mathbf{r}_1,t)V(\mathbf{r}_2,t+\Delta t)\rangle_\mathrm{t}, \tag{2.25}$$

where the subscript t stands for time average which is computed as

$$\langle f(t)\rangle_\mathrm{t} = \lim_{T\to\infty}\frac{1}{2T}\int_{-T}^{T} f(t)\mathrm{d}t. \tag{2.26}$$

As remarked in the beginning of Sec. 2.2 that the fluctuations in optical fields typically occur on a femtosecond scale and are too rapid for a detector to measure. In practice, detectors integrate the signal over time, i.e., the quantity $\langle f(t)\rangle_\mathrm{t}$ defined in Eq. (2.26), is measured. Since we may regard an optical field as ergodic, the time-average in Eq. (2.25) is equal to the ensemble average [4].

The averaged intensity of a stationary field at a point $\mathbf{r}$ is defined by

$$I(\mathbf{r}) = \Gamma(\mathbf{r},\mathbf{r},0), \tag{2.27}$$

and it is time independent. Analogously to Eq. (2.17), Eq. (2.25) is normalized by

$$\gamma(\mathbf{r}_1, \mathbf{r}_2, \Delta t) = \frac{\Gamma(\mathbf{r}_1, \mathbf{r}_2, \Delta t)}{\sqrt{\Gamma(\mathbf{r}_1, \mathbf{r}_1, 0)\Gamma(\mathbf{r}_2, \mathbf{r}_2, 0)}}. \tag{2.28}$$

The quantity $\gamma(\mathbf{r}_1, \mathbf{r}_2, \tau)$ is the complex degree of coherence for stationary fields and it is bounded in the interval

$$0 \leq |\gamma(\mathbf{r}_1, \mathbf{r}_2, \Delta t)| \leq 1, \tag{2.29}$$

where the extreme values have similar meanings as described in the following text of Eq. (2.18).

Using Eq. (2.7) in the context of stationary fields leads to

$$\langle \tilde{V}(\mathbf{r}_1, \omega)\tilde{V}(\mathbf{r}_2, \omega')\rangle = W(\mathbf{r}_1, \mathbf{r}_2, \omega)\delta(\omega - \omega'), \tag{2.30}$$

where the CSD function is

$$W(\mathbf{r}_1, \mathbf{r}_2, \omega) = \frac{1}{2\pi}\int_{-\infty}^{\infty} \Gamma(\mathbf{r}_1, \mathbf{r}_2, \Delta t) \exp(i\omega\Delta t)\, \mathrm{d}\Delta t, \tag{2.31}$$

and the Dirac delta function is

$$\delta(\omega - \omega') = \frac{1}{2\pi}\int_{-\infty}^{\infty} \exp\left[-i\left(\omega - \omega'\right)t\right] \mathrm{d}t. \tag{2.32}$$

The inverse of the CSD function reads as

$$\Gamma(\mathbf{r}_1, \mathbf{r}_2, \Delta t) = \int_{0}^{\infty} W(\mathbf{r}_1, \mathbf{r}_2, \omega) \exp(-i\omega\Delta t)\, \mathrm{d}\omega. \tag{2.33}$$

Equations (2.31) and (2.33) above are regarded as the generalized Wiener–Khintchine theorem for stationary fields.

The CSD function computed at a single spatial point $\mathbf{r}$ gives the spectral density of the field

$$S(\mathbf{r}, \omega) = W(\mathbf{r}, \mathbf{r}, \omega), \tag{2.34}$$

analogously to Eq. (2.20). The CSD is normalized by

$$\mu(\mathbf{r}_1, \mathbf{r}_2, \omega) = \frac{W(\mathbf{r}_1, \mathbf{r}_2, \omega)}{\sqrt{S(\mathbf{r}_1, \omega)S(\mathbf{r}_2, \omega)}}, \tag{2.35}$$

to get the spectral degree of spatial coherence [5]. The quantity is bounded in the interval $0 \leq |\mu(\mathbf{r}_1, \mathbf{r}_2, \omega)| \leq 1$, for all values of the arguments $\mathbf{r}_1$, $\mathbf{r}_2$, and ω with physical meanings the same as described below Eq. (2.22) but at a frequency ω.

2.3 COHERENT-MODE REPRESENTATION

In the early 1980's, it was shown that the CSD function of a stationary scalar optical field of any state of coherence can be expressed in terms of the CSD functions of fields, or modes, which are spatially fully coherent in the frequency domain [13, 15, 16]. Full description of the propagation, interaction and scattering of a random optical field is computationally quite arduous when performed in terms

of coherence functions. Since the CSD function of a completely coherent field factors in spatial variables [14], the modal method allows to express the correlation functions in terms of deterministic fields which are numerically easier to analyze compared to the coherence functions. In this section, first we discuss the basic idea of the coherent-mode representation of a stationary field and then present the mode representation of a non-stationary pulsed field in the time and frequency domains [27,28].

2.3.1 Stationary fields

Since the CSD function $W(\mathbf{r}_1, \mathbf{r}_2, \omega)$ is Hermitian, continuous, and square-integrable with respect to the spatial variable in a volume D, it is a Hilbert-Schmidt kernel [4]. Also the CSD function is nonnegative definite [4]. These properties admit the CSD function can be expressed in terms of a (uniformly and absolutely convergent) Mercer series of the form [4,13,15]

$$W(\mathbf{r}_1, \mathbf{r}_2, \omega) = \sum_{m=1}^{\infty} \lambda_m(\omega) \psi_m^*(\mathbf{r}_1, \omega) \psi_m(\mathbf{r}_2, \omega), \tag{2.36}$$

where $\lambda_m(\omega)$ are frequency dependent, real, and non-negative eigenvalues and $\psi_m(\mathbf{r}, \omega)$ are the eigenfunctions of the frequency-domain Fredholm integral equation

$$\int_D W(\mathbf{r}_1, \mathbf{r}_2, \omega) \psi_m(\mathbf{r}_1, \omega) \mathrm{d}^3 r_1 = \lambda_m(\omega) \psi_m(\mathbf{r}_2, \omega). \tag{2.37}$$

The eigenfunctions $\psi_m(\mathbf{r}, \omega)$ are orthonormal

$$\int_D \psi_m^*(\mathbf{r}, \omega) \psi_n(\mathbf{r}, \omega) \mathrm{d}^3 r = \delta_{mn}, \tag{2.38}$$

where δ_{mn} is the Kronecker delta symbol. We introduce

$$W^{(m)}(\mathbf{r}_1, \mathbf{r}_2, \omega) = \psi_m^*(\mathbf{r}_1, \omega) \psi_m(\mathbf{r}_2, \omega), \tag{2.39}$$

for which the magnitude of the spectral degree of spatial coherence, defined by Eq. (2.35), is unity for all $\mathbf{r}_1, \mathbf{r}_2 \in D$ and at all ω. Now, in terms of Eq. (2.39), Eq. (2.36) can be modified as

$$W(\mathbf{r}_1, \mathbf{r}_2, \omega) = \sum_{m=1}^{\infty} \lambda_m(\omega) W^{(m)}(\mathbf{r}_1, \mathbf{r}_2, \omega), \tag{2.40}$$

which demonstrates that the CSD function of the field can be represented as a sum of the CSD functions of fully coherent modes.

2.3.2 Non-stationary pulsed fields

The mode decomposition introduced in the preceding section does not hold for fields which are statistically non-stationary. In this section, we aim to derive the coherent-mode representation for a non-stationary pulsed field in the time and frequency domains [27,28].

Temporal domain

Let us consider a pulsed field defined on the finite interval, $t \in [-T/2, T/2]$, outside of which the field is assumed to vanish. The field can be expressed in terms of the Karhunen–Loéve expansion [4, 29]

$$E(t) = \sum_{m=1}^{\infty} c_m \psi_m(t), \tag{2.41}$$

with the coefficients $\{c_m\}$ being uncorrelated random variables,

$$\langle c_m^* c_n \rangle = \alpha_m \delta_{mn}, \tag{2.42}$$

where α_m are real, nonnegative numbers. The eigenfunctions $\psi_m(t)$ are orthonormal

$$\int_{-T/2}^{T/2} \psi_m^*(t) \psi_n(t) \mathrm{d}t = \delta_{mn}, \tag{2.43}$$

and the uncorrelated coefficients are given by

$$c_m = \int_{-T/2}^{T/2} E(t) \psi_m^*(t) \mathrm{d}t. \tag{2.44}$$

Substitution of Eq. (2.41) into Eq. (2.10) leads to the expansion for the MCF

$$\Gamma(t_1, t_2) = \sum_{m=1}^{\infty} \alpha_m \psi_m^*(t_1) \psi_m(t_2), \tag{2.45}$$

where α_m are the eigenvalues and $\psi_m(t)$ are the eigenfunctions of the Fredholm integral equation

$$\int_{-T/2}^{T/2} \Gamma(t_1, t_2) \psi_m(t_1) \mathrm{d}t_1 = \alpha_m \psi_m(t_2). \tag{2.46}$$

As mentioned in Sec. 2.2.1, the MCF is a non-negative definite Hilbert–Schmidt kernel. This property ensures that the expansion for the MCF given by Eq. (2.45) is a Mercer series [4, 15].

Substitution of $t_1 = t_2 = t$ in Eq. (2.45), integration and utilization of the orthonormality of the eigenfunctions, Eq. (2.43), links the eigenvalues to the temporal intensity defined in Eq. (2.16) (ignoring the spatial dependence)

$$\sum_{m=1}^{\infty} \alpha_m = \int_{-T/2}^{T/2} I(t) \mathrm{d}t. \tag{2.47}$$

The modulus of the MCF is related to the eigenvalues by the relation

$$\sum_{m=1}^{\infty} \alpha_m^2 = \iint_{-T/2}^{T/2} |\Gamma(t_1, t_2)|^2 \, \mathrm{d}t_1 \mathrm{d}t_2, \tag{2.48}$$

which can be readily derived by using Eq. (2.45) in conjunction with Eq. (2.43).

Figure 2.1: Schematic illustration of a quasi-stationary source.

Frequency domain

Substitution of Eq. (2.45) into Eq. (2.24), ignoring the spatial dependence, yields the coherent-mode representation in the frequency domain

$$W(\omega_1, \omega_2) = \sum_{m=1}^{\infty} \alpha'_m \psi^*_m(\omega_1)\psi_m(\omega_2), \tag{2.49}$$

where the coefficients α'_m are the eigenvalues and $\psi_m(\omega)$ are the eigenfunctions of the frequency-domain Fredholm integral equation

$$\int_0^{\infty} W(\omega_1, \omega_2)\psi_m(\omega_1)\mathrm{d}\omega_1 = \alpha'_m \psi_m(\omega_2). \tag{2.50}$$

The spectral eigenfunctions $\psi_m(\omega)$ are given by

$$\psi_m(\omega) = \frac{1}{\sqrt{2\pi}} \int_{-T/2}^{T/2} \psi_m(t) \exp(i\omega t)\, \mathrm{d}t, \tag{2.51}$$

obeying the orthonormality condition

$$\int_0^{\infty} \psi^*_m(\omega)\psi_n(\omega)\mathrm{d}\omega = \delta_{mn}. \tag{2.52}$$

The coefficients of the spectral domain CMD are related to those of the time domain expansion by the relation $\alpha'_m = \alpha_m/2\pi$.

The eigenvalues in the frequency domain are related to the spectral density and the modulus square of the CSD by the relations

$$\sum_{m=1}^{\infty} \alpha'_m = \int_0^{\infty} S(\omega)\mathrm{d}\omega, \tag{2.53}$$

and

$$\sum_{m=1}^{\infty} \alpha'^2_m = \iint_0^{\infty} |W(\omega_1, \omega_2)|^2 \mathrm{d}\omega_1 \mathrm{d}\omega_2. \tag{2.54}$$

Equations (2.53) and (2.54) are the frequency-domain analogs of Eqs. (2.47) and (2.48), respectively.

2.3.3 Quasi-stationary fields

Let us consider a non-stationary pulsed (or non-pulsed) source whose complex degree of temporal coherence depends only on the time difference, $\Delta t = t_2 - t_1$, and

the coherence time is short compared to the width of the average temporal intensity. In addition, the temporal intensity varies slowly over the coherence time. In other words, the temporal intensity is a slow function of time while the complex degree of coherence is a fast function of Δt as schematically shown in Fig. 2.1. The field from such a source is termed as quasi-stationary [32] and can be regarded as the temporal analog of quasi-homogenous fields [4]. Equation (2.17) evaluated at a single spatial point allows to write the MCF as

$$\Gamma(t_1, t_2) = \sqrt{I(t_1) I(t_2)}\gamma(t_1, t_1) \approx I(\bar{t})\gamma(\Delta t) = \Gamma(\bar{t}, \Delta t), \tag{2.55}$$

where $\bar{t} = (t_1 + t_2)/2$ is the average time and $\gamma(\Delta t)$ is the complex degree of temporal coherence whose effective width is a measure for the coherence time. In the second step, we used the assumption that the temporal intensity is a slow function in comparison with the variation of the degree of coherence which implies that the intensity distribution is essentially constant inside the interval where the degree is significant, $I(t_1) \approx I(t_2) \approx I(\bar{t})$.

Next we consider pulsed sources within the interval $[-T/2, T/2]$. As before, the field is taken zero outside of this temporal region. In the frequency domain, let us introduce the average frequency, $\bar{\omega} = (\omega_1 + \omega_2)/2$, and the difference frequency variable, $\Delta\omega = \omega_2 - \omega_1$. Then using the coordinate transformation from the variables ω_1 and ω_2 to the average and difference coordinates, the Wiener–Khintchine theorem of Eq. (2.24) (without $\mathbf{r}$ dependence) transforms into the form

$$W(\bar{\omega}, \Delta\omega) = \frac{1}{(2\pi)^2} \int_{-T}^{T} \int_{\frac{|\Delta t|}{2} - \frac{T}{2}}^{-\frac{|\Delta t|}{2} + \frac{T}{2}} \Gamma(\bar{t}, \Delta t) \exp\left[i\left(\Delta\omega\bar{t} + \bar{\omega}\Delta t\right)\right] \mathrm{d}\bar{t}\mathrm{d}\Delta t. \tag{2.56}$$

Substitution of Eq. (2.55) into Eq. (2.56) leads to

$$W(\bar{\omega}, \Delta\omega) = \frac{1}{2\pi} \int_{-T}^{T} P(\Delta t; \Delta\omega)\gamma(\Delta t) \exp(i\bar{\omega}\Delta t)\mathrm{d}\Delta t, \tag{2.57}$$

where

$$P(\Delta t; \Delta\omega) = \frac{1}{2\pi} \int_{\frac{|\Delta t|}{2} - \frac{T}{2}}^{-\frac{|\Delta t|}{2} + \frac{T}{2}} I(\bar{t}) \exp(i\Delta\omega\bar{t})\mathrm{d}\bar{t}. \tag{2.58}$$

As $\gamma(\Delta t)$ is a narrow function for quasi-stationary fields and $I(\bar{t})$ is negligibly small at the distances on the order of the coherence time from the boundaries of the time window $[-T/2, T/2]$, we can approximate $P(\Delta t; \Delta\omega) \approx P(0; \Delta\omega)$ in the integrand of Eq. (2.56). This leads to

$$W(\bar{\omega}, \Delta\omega) = s(\bar{\omega})\tilde{I}(\Delta\omega), \tag{2.59}$$

where

$$s(\bar{\omega}) = \frac{1}{2\pi} \int_{-T}^{T} \gamma(\Delta t) \exp\left(i\bar{\omega}\Delta t\right) \mathrm{d}\Delta t, \tag{2.60}$$

and

$$\tilde{I}(\Delta\omega) = \frac{1}{2\pi} \int_{-T/2}^{T/2} I(\bar{t}) \exp\left(i\Delta\omega\bar{t}\right) \mathrm{d}\bar{t}. \tag{2.61}$$

We can also write Eq. (2.59) in the form

$$W(\bar{\omega}, \Delta\omega) = S(\bar{\omega})\mu(\Delta\omega), \tag{2.62}$$

where the spectral density is given by

$$S(\bar{\omega}) = W(\bar{\omega}, 0) = s(\bar{\omega})\tilde{I}(0), \tag{2.63}$$

and the complex degree of spectral coherence is

$$\mu(\Delta\omega) = \frac{W(\bar{\omega}, \Delta\omega)}{S(\bar{\omega})} = \frac{\tilde{I}(\Delta\omega)}{\tilde{I}(0)}. \tag{2.64}$$

Utilizing Eqs. (2.47), (2.53), (2.61), and (2.63), it is evident that $s(\bar{\omega})$ is the normalized spectrum expressed as,

$$s(\bar{\omega}) = \frac{S(\bar{\omega})}{\int_0^\infty S(\bar{\omega})\mathrm{d}\bar{\omega}}. \tag{2.65}$$

Equation (2.64) signifies that to compute the degree of spectral coherence, $\mu(\Delta\omega)$, for a quasi-stationary field information only on the temporal intensity, $I(t)$, is needed whereas Eq. (2.60) shows that the normalized spectrum, $s(\bar{\omega})$, is specified by the degree of temporal coherence, $\gamma(\Delta t)$, alone.

2.3.4 Representation for the MCF of quasi-stationary pulsed fields

In this section, we describe a new time-domain method introduced in Publication II which expresses the MCF of a quasi-stationary pulsed field in terms of deterministic quasi-monochromatic functions. To elaborate this method, let us first consider a stationary random field within the time interval, $t \in [-T/2, T/2]$. If the coherence time of the field under consideration is much less than T, then the eigenvalues of Eq. (2.46) are known to be [29]

$$\alpha_m \approx 2\pi S_\mathrm{s}(\omega_m). \tag{2.66}$$

The subscript s in $S_\mathrm{s}(\omega_m)$ refers to stationarity and $\omega_m = m2\pi/T$, with m being a positive integer, which affirms the orthogonality of the corresponding eigenfunctions,

$$\psi_m(t) \approx \frac{1}{\sqrt{T}} \exp\left(-i\omega_m t\right), \tag{2.67}$$

within $[-T/2, T/2]$. In terms of Eqs. (2.66) and (2.67), the coherent-mode expansion for the MCF expressed in Eq. (2.45) becomes

$$\Gamma(t_1, t_2) = \Gamma(\Delta t) = \sum_{m=1}^{\infty} \left[\frac{2\pi S_\mathrm{s}(\omega_m)}{T}\right] \exp\left(-i\omega_m \Delta t\right), \tag{2.68}$$

which is the positive-frequency part of the complex Fourier series of $\Gamma(\Delta t)$ [34]. The series (2.68) also constitutes an approximative time-domain coherent-mode expansion for the stationary fields.

The technique to obtain an approximative time-domain expansion for stationary fields can be applied to the degree of temporal coherence of quasi-stationary pulsed

fields. In terms of the envelope representation [35], the complex degree of temporal coherence of a quasi-stationary field can be decomposed into a rapidly oscillating part and a slowly varying envelope $\gamma_{\mathrm{A}}(\Delta t)$ as

$$\gamma(\Delta t) = \gamma_{\mathrm{A}}(\Delta t) \exp\left(-i\omega_0 \Delta t\right), \tag{2.69}$$

where ω_0 can be any frequency within the spectrum. The slowly changing part obeys the Hermiticity condition, $\gamma_{\mathrm{A}}^*(\Delta t) = \gamma_{\mathrm{A}}(-\Delta t)$. Since the width of $\gamma_{\mathrm{A}}(\Delta t)$ is much smaller than the length T of the interval, we can express it approximately in a form of the coherent-mode representation

$$\gamma_{\mathrm{A}}(\Delta t) = \sum_{m=-\infty}^{\infty} \alpha_m \psi_m^*(t_1) \psi_m(t_2), \tag{2.70}$$

with the eigenfunctions $\psi_m(t)$ given in Eq. (2.67). Substitution of the eigenfunctions into the time-domain Fredholm integral equation, i.e., Eq. (2.46), with $\gamma_{\mathrm{A}}(\Delta t)$ as the kernel, multiplication by $\psi_n^*(t_2)$ and integration with respect to t_2 yields the eigenvalues

$$\alpha_m = \frac{1}{T} \int_{-T/2}^{T/2} \int_{-T/2}^{T/2} \gamma_{\mathrm{A}}(\Delta t) \exp\left(i\omega_m \Delta t\right) \mathrm{d}t_1 \mathrm{d}t_2, \tag{2.71}$$

where we have used the orthonormality of the eigenfunctions expressed in Eq. (2.43). In terms of the average, $\bar{t}$, and difference, Δt, coordinates, Eq. (2.71) can be cast into the form

$$\alpha_m = \int_{-T}^{T} \left(1 - \frac{|\Delta t|}{T}\right) \gamma_{\mathrm{A}}(\Delta t) \exp\left(i\omega_m \Delta t\right) \mathrm{d}\Delta t. \tag{2.72}$$

It follows from the Hermiticity of $\gamma_{\mathrm{A}}(\Delta t)$ that the coefficients α_m of Eq. (2.72) are real, i.e., $\alpha_m^* = \alpha_m$. As it was remarked in Sec. 2.3.3 that the complex degree of coherence is a narrow function of the variable Δt, the factor $\Delta t / T$ can be discarded in this case, and Eq. (2.72) simplifies into the form

$$\alpha_m \approx \int_{-T}^{T} \gamma_{\mathrm{A}}(\Delta t) \exp\left(i\omega_m \Delta t\right) \mathrm{d}\Delta t. \tag{2.73}$$

The eigenvalues are related to the normalized spectrum given in Eq. (2.60) by the relation

$$\alpha_m \approx 2\pi s(\omega_m + \omega_0), \tag{2.74}$$

which is obtained by using Eq. (2.69) in Eq. (2.73).

In terms of Eq. (2.69), the MCF given in Eq. (2.55) can be modified as

$$\Gamma(t_1, t_2) = I(\bar{t}) \gamma_{\mathrm{A}}(\Delta t) \exp\left(-i\omega_0 \Delta t\right). \tag{2.75}$$

If we define a function

$$\phi_m(t) = \sqrt{I(t)} \psi_m(t) \exp(-i\omega_0 t), \tag{2.76}$$

then Eq. (2.75) with an approximation, $\bar{t} \approx t_1 \approx t_2$, leads to a new time-domain representation for the MCF of the quasi-stationary pulsed field

$$\Gamma(t_1, t_2) = \sum_{m=-\infty}^{\infty} \alpha_m \phi_m^*(t_1) \phi_m(t_2). \tag{2.77}$$

Substitution of the orthonormal eigenfunctions $\psi_m(t)$ from Eq. (2.67) into Eq. (2.76) yields

$$\phi_m(t) = \sqrt{\frac{I(t)}{T}} \exp\left[-i(\omega_0 + \omega_m)t\right], \tag{2.78}$$

which are seen to be quasi-monochromatic, frequency shifted functions of identical shape and are non-orthonormal within the interval, $t \in [-T/2, T/2]$. Therefore, Eq. (2.77) is not the traditional coherent-mode decomposition rather it can be regarded as a pseudo-mode representation [36,37] expressing the MCF as a superposition of quasi-monochromatic and deterministic mode functions.

In comparison to the traditional coherent-mode decomposition in Sec. 2.3.2, the new time-domain method is a more efficient technique to represent the MCF of quasi-stationary pulsed sources as the coherence properties of the source can be investigated by making use of the mean spectrum and the average temporal intensity only. To practically demonstrate the validity of our new time-domain decomposition, the method was applied in Publication II to study the coherence properties of an x-ray free-electron laser (XFEL) source [38]. The degree of temporal coherence constructed from the spectral and temporal information was found to be in perfect agreement with the exact results obtained directly from the known MCF.

2.4 GAUSSIAN SCHELL MODEL

A pulsed source for which the temporal degree of coherence depends on the variables t_1 and t_2 only via their difference is termed as a Schell-model source [4,39,40]. In addition to this property, if the intensity distribution is Gaussian and the degree of coherence is also a Gaussian function, then such a source is called pulsed Gaussian Schell-model (GSM) source.

The MCF of a Schell-model source is written as

$$\Gamma(t_1, t_2) = \sqrt{I(t_1)I(t_2)}\gamma(\Delta t). \tag{2.79}$$

For a pulsed GSM source, the temporal intensity $I(t)$ has a Gaussian distribution,

$$I(t) = I_0 \exp\left[-2t^2/T^2\right], \tag{2.80}$$

where I_0 is the peak intensity and T represents the pulse length. The degree of coherence $\gamma(\Delta t)$ in Eq. (2.79) is also a Gaussian function

$$\gamma(\Delta t) = \exp\left[-(\Delta t)^2/(2T_\gamma^2)\right], \tag{2.81}$$

where T_γ characterizes the width of the complex degree of temporal coherence and may be called the coherence time.

2.5 IFTA FOR THE CONSTRUCTION OF THE FEL REALIZATIONS

Temporal counterpart of the iterative Fourier transform algorithm (IFTA) [41] was employed in Publication I to construct an ensemble of FEL pulses in the spectral and temporal domains using the measured spectra of an XFEL at the Linac coherent light

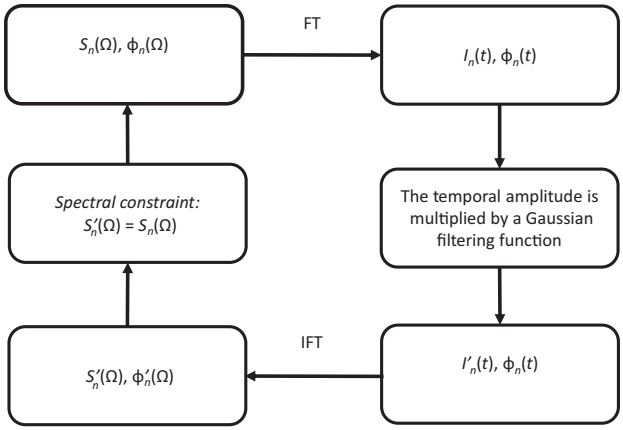

Figure 2.2: Flowchart of the iterative Fourier transform algorithm. The experimentally measured spectrum of the nth field realization is represented by $S_n(\Omega)$, $\phi_n(\Omega)$ is the random spectral phase, $I_n(t)$ is the temporal intensity, and $\phi_n(t)$ is the phase in the time domain. The intensity $I_n(t)$ is multiplied by a Gaussian filtering function to get $I'_n(t)$. Using IFT, the spectrum $S'_n(\Omega)$ is estimated. Many iterations of the algorithm are run until the condition $S'_n(\Omega) = S_n(\Omega)$ is reached.

source (LCLS) [38]. In this section, we elucidate the algorithm that was employed in Publication I.

In the first step of the algorithm (see Fig. 2.2), we associate a random phase $\phi(\Omega)$ to the square root of a measured spectrum, $S_n(\Omega)$, of the nth field realization to get a complex spectral field. The spectral field is Fourier transformed to get the temporal field. The phase of the temporal field, $\phi(t)$, is left untouched and the temporal amplitude is multiplied by a Gaussian filtering function to get a Gaussian distribution for the temporal intensity, $I_n(t)$. In the subsequent step of the algorithm, the temporal field is converted back to the spectral domain via the inverse Fourier transform (IFT). A spectral constraint is applied to the spectral field obtained via IFT by setting the spectrum to the measured spectrum, i.e., $S'_n(\Omega) = S_n(\Omega)$, and the phase is left undisturbed. The process is iterated as long as needed until the estimated spectrum converges to the experimentally measured spectrum. The one-dimensional phase-retrieval algorithm does not possess a unique solution [42], however, the simulated ensemble of spectral and temporal field realizations matches the experimentally measured spectral and temporal characteristics of the FEL in a statistically averaged sense.

The IFTA results in an ensemble of realizations in the spectral and temporal domains. These ensembles were then utilized in Publication I to construct the CSD, MCF, and the complex degrees of spectral and temporal coherence [20] for the XFEL source. A Gaussian filtering function in the time domain was used to get the average temporal intensity of the ensemble of the Gaussian form. However, if the mean temporal intensity of the source is known to be different from the Gaussian form, then an appropriate filtering function for such a source should be used in the IFTA.

A similar approach has been earlier used for generating FEL pulses based on the knowledge of the average spectrum and mean pulse duration [43]. In [43], instead of the measured spectrum of the individual realization, the averaged spectrum is used to get a complex spectral field which is then Fourier transformed to the temporal domain. In essence, the authors in [43] employ a single loop of the IFTA that we described.

In our case, we investigated the coherence properties of the XFEL facility at LCLS and the results demonstrated that this particular FEL emits quasi-stationary pulse trains with low spectral and temporal coherence. However, our proposed model can be applied to any other pulsed light source which may emit pulse trains with any degree of spectral and temporal coherence.

3 Coherence of non-stationary electromagnetic fields

In this chapter, we describe the correlation matrices in the time and frequency domains, the degree of coherence, the degree of polarization, and the coherent-mode decomposition for non-stationary electromagnetic beams. We also present a novel time-domain method for expressing the temporal modes of stationary and pulsed quasistationary beams that was developed in Publication III.

3.1 COHERENCE MATRICES

To describe the temporal correlation matrix, consider a fluctuating, non-stationary electromagnetic beam propagating in the positive z-direction. Employing the formalism described in Sec. 2.1 for the transverse components, $E_x(t)$ and $E_y(t)$, the beam at a fixed spatial point is represented by the vectorial zero-mean complex analytic signal, $\mathbf{E}(t) = [E_x(t)\ E_y(t)]^{\mathrm{T}}$, where T stands for the transpose. The temporal correlation of the electromagnetic beam is described by the mutual coherence matrix (MCM) [4, 44]

$$\mathbf{\Gamma}(t_1, t_2) = \langle \mathbf{E}^*(t_1)\mathbf{E}^{\mathrm{T}}(t_2)\rangle, \tag{3.1}$$

where the angle brackets denote ensemble averaging over a set of realizations. In practice, the members of the ensemble can be the individual pulses of a pulse train emanating from a pulsed light source. The MCM is Hermitian in the sense that $\mathbf{\Gamma}^{\dagger}(t_1, t_2) = \mathbf{\Gamma}(t_2, t_1)$, where the dagger † denotes conjugate transpose. The MCM also satisfies the non-negative definiteness condition [4, 44]. The elements of the MCM are given by $\Gamma_{ij}(t_1, t_2) = \langle E_i^*(t_1)E_j(t_2)\rangle$, $(i, j) \in (x, y)$, and the degree of correlation between the field components at the time instants t_1 and t_2 is

$$\gamma_{ij}(t_1, t_2) = \frac{\Gamma_{ij}(t_1, t_2)}{\sqrt{I_i(t_1)I_j(t_2)}}, \quad (i, j) \in (x, y), \tag{3.2}$$

where $I_i(t) = \Gamma_{ii}(t, t)$ is the intensity of the ith component. The total temporal intensity of the beam is

$$I(t) = \mathrm{tr}[\mathbf{\Gamma}(t, t)], \tag{3.3}$$

where tr denotes the trace. The electromagnetic degree of temporal coherence $\gamma(t_1, t_2)$ is defined in squared form as [45]

$$\gamma^2(t_1, t_2) = \frac{\mathrm{tr}[\mathbf{\Gamma}^{\dagger}(t_1, t_2)\mathbf{\Gamma}(t_1, t_2)]}{I(t_1)I(t_2)}, \tag{3.4}$$

which is bounded in the interval $0 \leq |\gamma(t_1, t_2)| \leq 1$, where zero refers to the complete incoherence while unity signifies full coherence at t_1 and t_2.

Equal-time MCM is called the polarization matrix [4, 5, 9, 11] expressed as

$$\mathbf{J}(t) = \mathbf{\Gamma}(t, t), \tag{3.5}$$

with the elements given by $J_{ij}(t) = \Gamma_{ij}(t,t) = \langle E_i^*(t)E_j(t)\rangle$, $(i,j) \in (x,y)$. The polarization matrix is purely Hermitian, $\mathbf{J}^\dagger(t) = \mathbf{J}(t)$. The diagonal elements of $\mathbf{J}(t)$ give the intensities of the x and y electric field components and the normalized off-diagonal elements provide a measure of the equal-time correlation between the orthogonal components, i.e.,

$$j_{xy}(t) = \frac{J_{xy}(t)}{\sqrt{J_{xx}(t)J_{yy}(t)}}, \tag{3.6}$$

with $0 \leq |j_{xy}(t)| \leq 1$. The upper bound of $|j_{xy}(t)|$ refers to a full correlation of the x and y electric field components while the lower bound indicates a complete lack of correlation.

To develop the correlation matrices in the spectral domain, we Fourier transform the time-domain field [see Sec. 2.1]

$$\mathbf{E}(\omega) = \frac{1}{2\pi}\int_{-\infty}^{\infty} \mathbf{E}(t)\exp(i\omega t)\,\mathrm{d}t. \tag{3.7}$$

The spectral realizations obtained via Eq. (3.7) can be used to define the cross-spectral density matrix (CSDM) as

$$\mathbf{W}(\omega_1,\omega_2) = \langle \mathbf{E}^*(\omega_1)\mathbf{E}^{\mathrm{T}}(\omega_2)\rangle. \tag{3.8}$$

The CSDM is Hermitian, $\mathbf{W}^\dagger(\omega_1,\omega_2) = \mathbf{W}(\omega_2,\omega_1)$, and non-negative definite [44]. The elements of the CSDM are $W_{ij}(\omega_1,\omega_2) = \langle E_i^*(\omega_1)E_j(\omega_2)\rangle$, $(i,j) \in (x,y)$, and the degree of correlation between the spectral field components at ω_1 and ω_2 is

$$\mu_{ij}(\omega_1,\omega_2) = \frac{W_{ij}(\omega_1,\omega_2)}{\sqrt{S_i(\omega_1)S_j(\omega_2)}}, \quad (i,j) \in (x,y), \tag{3.9}$$

where $S_i(\omega) = W_{ii}(\omega)$ is the spectral density of the ith component. The total spectral density of the field is

$$S(\omega) = \mathrm{tr}[\mathbf{W}(\omega,\omega)]. \tag{3.10}$$

The spectral degree of coherence for the electromagnetic beam, $\mu(\omega_1,\omega_2)$, is defined in the form [46]

$$\mu^2(\omega_1,\omega_2) = \frac{\mathrm{tr}[\mathbf{W}^\dagger(\omega_1,\omega_2)\mathbf{W}(\omega_1,\omega_2)]}{S(\omega_1)S(\omega_2)}, \tag{3.11}$$

with $0 \leq |\mu(\omega_1,\omega_2)| \leq 1$. Analogously to the complex degree of temporal coherence, $|\mu(\omega_1,\omega_2)| = 0$ represents complete incoherence while $|\mu(\omega_1,\omega_2)| = 1$ shows full coherence of the field components at ω_1 and ω_2.

The equal-frequency CSDM leads to the spectral polarization matrix, $\mathbf{\Phi}(\omega)$, which contains the spectral polarization properties of the electromagnetic field and is given by the relation

$$\mathbf{\Phi}(\omega) = \mathbf{W}(\omega,\omega). \tag{3.12}$$

The diagonal elements of $\mathbf{\Phi}(\omega)$ are the spectral densities $S_i(\omega) = \Phi_{ii}(\omega)$, $i \in (x, y)$, while the normalized off-diagonal elements give a measure of the equal-frequency correlation between the orthogonal components

$$\phi_{xy}(\omega) = \frac{\Phi_{xy}(\omega)}{\sqrt{\Phi_{xx}(\omega)\Phi_{yy}(\omega)}}, \tag{3.13}$$

with $0 \leq |\phi_{xy}(\omega)| \leq 1$. The upper bound corresponds to full correlation between the x and y field components at a single frequency and the lower bound signifies a complete absence of correlation.

Substituting the spectral realization $\mathbf{E}(\omega)$ from Eq. (3.7) into Eq. (3.8) and using the definition of MCM given in Eq. (3.1), we get a relation between the CSDM and the MCM

$$\mathbf{W}(\omega_1, \omega_2) = \frac{1}{(2\pi)^2} \iint_{-\infty}^{\infty} \mathbf{\Gamma}(t_1, t_2) \exp\left[-i\left(\omega_1 t_1 - \omega_2 t_2\right)\right] \mathrm{d}t_1 \mathrm{d}t_2, \tag{3.14}$$

and

$$\mathbf{\Gamma}(t_1, t_2) = \iint_{0}^{\infty} \mathbf{W}(\omega_1, \omega_2) \exp\left[i\left(\omega_1 t_1 - \omega_2 t_2\right)\right] \mathrm{d}\omega_1 \mathrm{d}\omega_2. \tag{3.15}$$

Equations (3.14) and (3.15) constitute the Wiener–Khintchine theorem for a non-stationary electromagnetic beam at a fixed spatial point. By considering the field at two spatial points $\mathbf{r}_1$ and $\mathbf{r}_2$, we arrive at the generalized Wiener–Khintchine theorem

$$\mathbf{W}(\mathbf{r}_1, \mathbf{r}_2, \omega_1, \omega_2) = \frac{1}{(2\pi)^2} \iint_{-\infty}^{\infty} \mathbf{\Gamma}(\mathbf{r}_1, \mathbf{r}_2, t_1, t_2) \exp\left[-i\left(\omega_1 t_1 - \omega_2 t_2\right)\right] \mathrm{d}t_1 \mathrm{d}t_2, \tag{3.16}$$

and

$$\mathbf{\Gamma}(\mathbf{r}_1, \mathbf{r}_2, t_1, t_2) = \iint_{0}^{\infty} \mathbf{W}(\mathbf{r}_1, \mathbf{r}_2, \omega_1, \omega_2) \exp\left[i\left(\omega_1 t_1 - \omega_2 t_2\right)\right] \mathrm{d}\omega_1 \mathrm{d}\omega_2. \tag{3.17}$$

In Sec. 3.3.2, we employ Eq. (3.17) to derive the time-domain coherent-mode representation for a non-stationary, pulsed electromagnetic beam.

3.2 DEGREE OF POLARIZATION

In a fully polarized beam, the orthogonal components of the electric vector $\mathbf{E}(t)$ are completely correlated, $|j_{xy}(t)| = 1$, and hence the corresponding 2×2 polarization matrix has the form [4, 44]

$$\mathbf{J}^{\mathrm{pol}}(t) = \begin{bmatrix} B(t) & C(t) \\ C^*(t) & D(t) \end{bmatrix}, \tag{3.18}$$

where $B(t) \geq 0$, $D(t) \geq 0$, and $B(t)D(t) - |C(t)|^2 = 0$. In a completely unpolarized beam, the orthogonal components have no correlation, $|j_{xy}(t)| = 0$, and the diagonal elements are equal, $I_x(t) = I_y(t)$. The polarization matrix for a fully unpolarized beam can be written as

$$\mathbf{J}^{\mathrm{unpol}}(t) = A(t) \begin{bmatrix} 1 & 0 \\ 0 & 1 \end{bmatrix}, \tag{3.19}$$

where $A(t) \geq 0$. Utilizing Eqs. (3.18) and (3.19), the polarization matrix of any electromagnetic beam can be expressed as a summation of two polarization matrices each corresponding to a fully polarized and a fully unpolarized beam [5,44]

$$\mathbf{J}(t) = \mathbf{J}^{\text{pol}}(t) + \mathbf{J}^{\text{unpol}}(t). \tag{3.20}$$

The degree of polarization is defined as the ratio of the intensity of the polarized part of the beam to the total intensity [5,44]. It is mathematically expressed as

$$P(t) = \frac{\text{tr}[\mathbf{J}^{\text{pol}}(t)]}{\text{tr}[\mathbf{J}(t)]} = \sqrt{1 - \frac{4\det[\mathbf{J}(t)]}{\text{tr}^2[\mathbf{J}(t)]}}, \tag{3.21}$$

and satisfies $0 \leq P(t) \leq 1$. The lower limit indicates a fully unpolarized beam, the upper limit corresponds to a completely polarized beam, and the intermediate values signify partial polarization.

3.3 COHERENT-MODE DECOMPOSITION OF ELECTROMAGNETIC BEAMS

In Chap. 2, we presented an overview of the coherent-mode decomposition (CMD) for random, scalar, stationary and non-stationary beams. The theory presented therein is not sufficient to describe the coherence properties of partially polarized, partially coherent electromagnetic beams. In this section, we discuss the CMD for stationary and non-stationary electromagnetic beams.

3.3.1 Stationary fields

Gori *et al.* introduced the 2×2 beam coherence-polarization (BCP) matrix for the description of quasi-monochromatic, partially polarized, partially spatially coherent beams [47,48]. The BCP matrix is an equal-time mutual coherence matrix evaluated at two different spatial points. Employing the BCP matrix, the CMD was analyzed for partially spatially coherent, partially polarized beams [49]. Later on, Tervo and co-workers introduced a CMD for stationary, partially coherent electromagnetic fields in the space–frequency domain [50].

Since the CSDM of a random electromagnetic field is a non-negative definite, Hilbert–Schmidt kernel [45], it can be represented in a volume D of interest as a Mercer series in the form

$$\mathbf{W}(\mathbf{r}_1, \mathbf{r}_2, \omega) = \sum_{m=1}^{\infty} \lambda_m(\omega) \boldsymbol{\phi}_m^*(\mathbf{r}_1, \omega) \boldsymbol{\phi}_m^{\text{T}}(\mathbf{r}_2, \omega), \tag{3.22}$$

where $\lambda_m(\omega)$ are the (positive) frequency-dependent eigenvalues and $\boldsymbol{\phi}_m(\mathbf{r}, \omega)$ are the (column-vector) eigenfunctions of the Fredholm integral equation

$$\int_D \boldsymbol{\phi}_m^{\text{T}}(\mathbf{r}_1, \omega) \mathbf{W}(\mathbf{r}_1, \mathbf{r}_2, \omega) \text{d}^3 r_1 = \lambda_m(\omega) \boldsymbol{\phi}_m^{\text{T}}(\mathbf{r}_2, \omega). \tag{3.23}$$

The eigenfunctions $\boldsymbol{\phi}_m(\mathbf{r}, \omega)$ can be taken orthonormal

$$\int_D \boldsymbol{\phi}_m^{\text{T}}(\mathbf{r}, \omega) \boldsymbol{\phi}_n^*(\mathbf{r}, \omega) \text{d}^3 r = \delta_{mn}. \tag{3.24}$$

We can express the CMD of Eq. (3.22) as

$$\mathbf{W}(\mathbf{r}_1, \mathbf{r}_2, \omega) = \sum_{m=1}^{\infty} \lambda_m(\omega) \mathbf{W}^{(m)}(\mathbf{r}_1, \mathbf{r}_2, \omega), \tag{3.25}$$

where $\mathbf{W}^{(m)}(\mathbf{r}_1, \mathbf{r}_2, \omega) = \boldsymbol{\phi}_m^*(\mathbf{r}_1, \omega)\boldsymbol{\phi}_m^{\mathrm{T}}(\mathbf{r}_2, \omega)$. Parallelling Eq. (3.11) for non-stationary fields, the electromagnetic spectral degree of coherence for stationary electromagnetic beams is given in the squared form by [46, 50]

$$\mu^2(\mathbf{r}_1, \mathbf{r}_2, \omega) = \frac{\mathrm{tr}[\mathbf{W}^\dagger(\mathbf{r}_1, \mathbf{r}_2, \omega)\mathbf{W}(\mathbf{r}_1, \mathbf{r}_2, \omega)]}{S(\mathbf{r}_1, \omega)S(\mathbf{r}_2, \omega)}, \tag{3.26}$$

where $S(\mathbf{r}, \omega) = \mathrm{tr}[\mathbf{W}(\mathbf{r}, \mathbf{r}, \omega)]$. Substitution of $\mathbf{W}^{(m)}(\mathbf{r}_1, \mathbf{r}_2, \omega)$ in Eq. (3.26) implies $|\mu(\mathbf{r}_1, \mathbf{r}_2, \omega)| = 1$, indicating that $\mathbf{W}^{(m)}(\mathbf{r}_1, \mathbf{r}_2, \omega)$ corresponds to the CSDM of a (spectrally) spatially fully coherent beam. Therefore, we may regard Eq. (3.22) as a representation of the CSDM in terms of mutually uncorrelated, spatially fully coherent modes.

3.3.2 Non-stationary fields

In random stationary polychromatic electromagnetic fields, the frequency components have no correlation and the formulation is at a certain frequency. For non-stationary fields, the spectral coherence matrix depends on the two-frequency variables ω_1 and ω_2; and due to its properties, it can be expressed in the form of a Mercer's type series [51]

$$\mathbf{W}(\mathbf{r}_1, \mathbf{r}_2, \omega_1, \omega_2) = \sum_{m=1}^{\infty} \lambda_m \boldsymbol{\Phi}_m^*(\mathbf{r}_1, \omega_1)\boldsymbol{\Phi}_m^{\mathrm{T}}(\mathbf{r}_2, \omega_2), \tag{3.27}$$

where λ_m are the eigenvalues and $\boldsymbol{\Phi}(\mathbf{r}, \omega)$ are the eigenfunctions of the vectorial Fredholm integral equation

$$\int_0^\infty \int_D \boldsymbol{\Phi}_m^{\mathrm{T}}(\mathbf{r}_1, \omega_1)\mathbf{W}(\mathbf{r}_1, \mathbf{r}_2, \omega_1, \omega_2)\mathrm{d}^2\mathbf{r}_1\mathrm{d}\omega_1 = \lambda_m \boldsymbol{\Phi}_m^{\mathrm{T}}(\mathbf{r}_2, \omega_2). \tag{3.28}$$

The eigenfunctions can be assumed orthonormal

$$\int_0^\infty \int_D \boldsymbol{\Phi}_m^{\mathrm{T}}(\mathbf{r}, \omega)\boldsymbol{\Phi}_n^*(\mathbf{r}, \omega)\mathrm{d}^3 r\mathrm{d}\omega = \delta_{mn}. \tag{3.29}$$

The time-domain CMD is obtained by substitution of Eq. (3.27) into Eq. (3.17) leading to the MCM of the form

$$\boldsymbol{\Gamma}(\mathbf{r}_1, \mathbf{r}_2, t_1, t_2) = \sum_{m=1}^{\infty} \lambda'_m \boldsymbol{\Psi}_m^*(\mathbf{r}_1, t_1)\boldsymbol{\Psi}_m^{\mathrm{T}}(\mathbf{r}_2, t_2), \tag{3.30}$$

where λ'_m are the eigenvalues and $\boldsymbol{\Psi}_m(\mathbf{r}, t)$ are the eigenfunctions of the vectorial time-domain Fredholm integral equation

$$\int_{-\infty}^\infty \int_D \boldsymbol{\Psi}_m^{\mathrm{T}}(\mathbf{r}_1, t_1)\boldsymbol{\Gamma}(\mathbf{r}_1, \mathbf{r}_2, t_1, t_2)\mathrm{d}^2\mathbf{r}_1\mathrm{d}t_1 = \lambda'_m \boldsymbol{\Psi}_m^{\mathrm{T}}(\mathbf{r}_2, t_2). \tag{3.31}$$

The eigenfunctions are given by

$$\mathbf{\Psi}_m(\mathbf{r},t) = \int_0^\infty \mathbf{\Phi}(\mathbf{r},\omega)\exp(-i\omega t)\,\mathrm{d}\omega. \tag{3.32}$$

and obey the orthonormality condition [51]

$$\int_{-\infty}^{\infty}\int_D \mathbf{\Psi}_m^{\mathrm{T}}(\mathbf{r},t)\mathbf{\Psi}_n^*(\mathbf{r},t)\mathrm{d}^2r\mathrm{d}t = \delta_{mn}. \tag{3.33}$$

The eigenvalues λ'_m are related to those of the spectral CMD by the relation

$$\lambda'_m = 2\pi\lambda_m, \tag{3.34}$$

where the 2π factor comes from the orthonormality requirement of the temporal eigenfunctions. Equations (3.27) and (3.30) show that both the CSDM and MCM of a non-stationary electromagnetic beam can be expressed as incoherent sums of fully coherent modes with suitable weights.

3.4 MODE DECOMPOSITIONS FOR STATIONARY AND PULSED QUASISTATIONARY ELECTROMAGNETIC FIELDS

In Publication III, we introduced a novel time-domain harmonic mode expansion for stationary electromagnetic fields. The new method is an extension of the earlier work concerning the mode decomposition of random scalar fields [29]. The second important result of Publication III is the derivation of a pseudo-mode representation for pulsed quasistationary electromagnetic fields.

3.4.1 Stationary fields

Consider a stationary electromagnetic beam, $\mathbf{E}(t) = [E_x(t)\ E_y(t)]^{\mathrm{T}}$, within a finite time interval $[-T/2, T/2]$. Due to stationarity, the field is not zero outside of the interval. It was shown in Publication III that the MCM of the field can be represented in the form

$$\mathbf{\Gamma}(t_1,t_2) = \sum_{m=1}^{\infty} \alpha_m \mathbf{E}_m^*(t_1)\mathbf{E}_m^{\mathrm{T}}(t_2), \tag{3.35}$$

where α_m are the eigenvalues and $\mathbf{E}_m(t)$ are the orthonormal eigenfunctions of the Fredholm integral equation

$$\int_{-T/2}^{T/2} \mathbf{E}_m^{\mathrm{T}}(t_1)\mathbf{\Gamma}(t_1,t_2)\mathrm{d}t_1 = \alpha_m \mathbf{E}_m^{\mathrm{T}}(t_2). \tag{3.36}$$

Although not explicitly shown, the MCM of Eq. (3.35) depends on Δt only.

If the width of the MCM is small compared with the length T of the time window, then the eigenfunctions are, to a good approximation, harmonic functions given by

$$\mathbf{E}_m(t) = E_m(t)\mathbf{u}_m, \quad E_m(t) = \frac{1}{\sqrt{T}}\exp(-i\omega_m t), \tag{3.37}$$

where $\mathbf{u}_m$ is a unit column vector that specifies the state of the polarization, the subscript $m \in [1, \infty)$, and $\omega_m = m\omega_0$, with $\omega_0 = 2\pi/T$. The corresponding eigenvalues are given by

$$\alpha_m = 2\pi \mathbf{u}_m^{\mathrm{T}} \mathbf{\Phi}(\omega_m) \mathbf{u}_m^*, \tag{3.38}$$

where $\mathbf{\Phi}(\omega_m)$ is the spectral polarization matrix [52] given by the Fourier transform relation

$$\mathbf{\Phi}(\omega) = \frac{1}{2\pi} \int_{-T}^{T} \mathbf{\Gamma}(\Delta t) \exp(i\omega\Delta t) \mathrm{d}\Delta t. \tag{3.39}$$

3.4.2 Pulsed quasistationary fields

In Sec. 2.3.3, we described quasistationary scalar fields. We noted that the complex degree of temporal coherence of such a field depends on the time difference only. Analogously to the scalar case, for vectorial pulsed quasistationary beams, the correlation coefficients defined in Eq. (3.2) depend on the time difference Δt only. In addition, the intensity distributions of the components are much broader than the extensions of the correlations and are essentially uniform over the region where $\gamma_{ij}(\Delta t)$, $(i, j) \in (x, y)$, are significant. Under these conditions, the MCM can be expressed in the form

$$\mathbf{\Gamma}(\bar{t}, \Delta t) = \mathbf{I}^{1/2}(\bar{t}) \boldsymbol{\gamma}(\Delta t) \mathbf{I}^{1/2}(\bar{t}), \tag{3.40}$$

where $\bar{t}$ is the average time coordinate and

$$\mathbf{I}(\bar{t}) = \begin{bmatrix} I_x(\bar{t}) & 0 \\ 0 & I_y(\bar{t}) \end{bmatrix}, \tag{3.41}$$

$$\boldsymbol{\gamma}(\Delta t) = \begin{bmatrix} \gamma_{xx}(\Delta t) & \gamma_{xy}(\Delta t) \\ \gamma_{yx}(\Delta t) & \gamma_{yy}(\Delta t) \end{bmatrix}. \tag{3.42}$$

Invoking the slowly-varying envelope representation, we can express

$$\boldsymbol{\gamma}(\Delta t) = \boldsymbol{\gamma}_{\mathrm{A}}(\Delta t) \exp(-i\omega_0 \Delta t), \tag{3.43}$$

where ω_0 is a frequency within the spectrum. In Publication III, it is demonstrated that the matrix $\boldsymbol{\gamma}_{\mathrm{A}}(\Delta t)$ is a nonnegative definite Hilbert-Schmidt kernel and it can be expressed as a Mercer series

$$\boldsymbol{\gamma}_{\mathrm{A}}(\Delta t) = \sum_{m=1}^{\infty} \alpha_m^{(\mathrm{A})} \mathbf{E}_m^*(t_1) \mathbf{E}_m^{\mathrm{T}}(t_2), \tag{3.44}$$

where the vectors $\mathbf{E}_m(t)$ are given by Eq. (3.37) and the weighting coefficients are

$$\alpha_m^{(\mathrm{A})} = 2\pi \mathbf{u}_m^{\mathrm{T}} \mathbf{s}(\omega_m + \omega_0) \mathbf{u}_m^*, \tag{3.45}$$

with

$$\mathbf{s}(\omega_m) = \frac{1}{2\pi} \int_{-T}^{T} \boldsymbol{\gamma}_{\mathrm{A}}(\Delta t) \exp(i\omega_m \Delta t) \, \mathrm{d}\Delta t. \tag{3.46}$$

Utilizing Eq. (3.43) and Eq. (3.44) in Eq. (3.40), the MCM of a quasistationary pulsed beam assumes the form

$$\mathbf{\Gamma}(t_1, t_2) = \sum_{m=-\infty}^{\infty} \alpha_m^{(\mathrm{A})} \boldsymbol{\mathcal{E}}_m^*(t_1) \boldsymbol{\mathcal{E}}_m^{\mathrm{T}}(t_2), \tag{3.47}$$

where the temporal modes are given by

$$\boldsymbol{\mathcal{E}}_m(t) = \sqrt{\frac{\mathbf{I}(t)}{T}} \mathbf{u}_m \exp\left[-i(\omega_m + \omega_0)t\right]. \tag{3.48}$$

We remark that the modes in the representation of Eq. (3.35) are orthonormal within $[-T/2, T/2]$, therefore, it can be regarded as a coherent-mode representation of stationary electromagnetic beams. For pulsed quasistationary beams, Eq. (3.47) is a pseudo-modal representation as the temporal modes are not orthonormal.

The modal expansion techniques presented in Publication III are useful in the study of stationary and quasistationary electromagnetic beams as the field can be expressed in the time domain in terms of deterministic mode functions. The quantities required for the construction of the expansion, the average intensity and the spectral information, are measurable.

4 Coherence measurements of pulsed light

The coherence properties of pulsed sources, such as FELs, mode-locked lasers, and supercontinuum sources, are described with the aid of two-time and two-frequency correlation functions in the time and frequency domains, respectively. Therefore, measurement of the coherence properties of pulsed optical fields [53, 54] is difficult in comparison to that of the stationary fields where the temporal coherence properties depend on the time difference only and the frequency components are uncorrelated. The conventional interferometric schemes which are usually employed for the analysis of pulsed sources can only measure the time-integrated correlation functions and hence do not provide the two-point measure for the coherence of pulsed fields.

In this chapter, we elucidate the coherence measurements of pulsed light [42, 55]. First, we describe the challenges involved in the characterization of ultrashort pulses. In the proceeding sections, we present an overview of the complexities in the measurement of the two-time and two-frequency correlation functions followed by a discussion on the determination of the time-integrated degree of coherence, autocorrelation, and cross-correlation for the pulse diagnostics.

4.1 CHALLENGES INVOLVED IN THE CHARACTERIZATION OF ULTRASHORT PULSES

What are the shortest engineered events? Possibly the answer would be ultrashort pulses. This section elucidates the complexities involved in characterizing ultrashort pulses.

A pulse can be represented with a complex analytic signal, $V(t)$, discussed in Sec. 2.1. The characterization of a pulse means that $V(t)$ is determined on the time interval in which the pulse exits. Characterization of an ultrashort pulse would require a detector with a response time on the order of the temporal length of the pulse. Even the fastest detectors available have a response time in the picosecond range, therefore, detectors are too slow to directly measure an ultrashort pulse [55]. Determination of the amplitude and phase of the associated electric field of a pulse requires techniques that can overcome the impediment of the detectors for measuring ultrashort events, for example, the femtosecond pulses.

In the investigation of the coherence properties of a partially coherent, pulsed non-stationary field, one needs to characterize a large number of pulses, and then calculate the ensemble average, $\langle V^*(t)V(t')\rangle$, of the pulses to measure their correlations. Ensemble averaging is needed as the output pulses from a partially coherent source are different from one another and each pulse can be considered as a member of an ensemble. In particular, measuring only a single pulse does not provide sufficient information of a random pulsed source.

With the first demonstration of mode-locking in a HeNe laser in the 1960s [56] and the subsequent development of laser sources with femtosecond pulse duration, characterization of ultrashort pulses has been an evolving area of research. Over the course of time, a number of techniques have been developed to address

this domain. Some of the commonly used schemes for characterizing ultrashort pulses are outlined by Walmsley and Dorrer [55] in the review paper. Advanced techniques like frequency-resolved optical gating (FROG) and spectral phase interferometry for direct electric field reconstruction (SPIDER) can be used to obtain all information about the complex waveforms of pulses in the temporal and spectral domain. For example, in the case of partially coherent pulse trains, schemes like FROG or SPIDER, can be used to measure an ensemble of realizations (pulses) and then numerically average them to obtain information about the mean pulse duration and correlation functions (spectral and temporal). Therefore, characterization of ultrashort pulses is much more complex than the time-integrated measurements of stationary and quasi-stationary fields [53, 54]. The remainder of this chapter is devoted to a discussion on the aforementioned intricacy involved in the coherence measurements of partially coherent, pulsed non-stationary fields.

4.2 TWO-TIME AND TWO-FREQUENCY CORRELATION FUNCTIONS

Michelson interferometer is commonly used to measure the temporal coherence of both stationary [4] and pulsed light [53, 54]. In the standard setup for pulses, the Michelson interferometer measures the time-integrated degree of temporal coherence which may not provide a complete picture of the temporal coherence properties. This is due to the fact that the temporal coherence of non-stationary fields depends on the two time variables t_1 and t_2, and the mean intensity of the field is also time dependent [19]. For pulsed quasi-stationary fields such as those emanating from SASE based FELs where the coherence time is much shorter than the temporal length of the pulse, the standard time-integrated measurements are adequate [53, 54], but for pulsed fields which are more temporally coherent, e.g., monochromatized FEL beams considered in [57], and the pulses from a seeded FEL, one needs to perform time-resolved measurements to get the two-time MCF. The intricate subtlety associated with the coherence measurements of non-stationary sources is elaborated in this section.

For pulsed sources having shot-to-shot fluctuations, a modified Michelson interferometer with tilted mirrors was proposed by Papadakis *et al.* [58]. Recently, it was demonstrated that the time-resolved measurements with the modified equal path-length Michelson interferometer can provide sufficient and necessary information to construct the two-time MCF of non-stationary fields [53]. The two-frequency CSD can be obtained from the MCF by using the Wiener-Khintchine theorem of Eq. (2.24).

In the conventional Michelson's interferometry, a light beam is halved into two parts by a 50 : 50 beam splitter. One part of the beam is delayed with respect to the other, either by an axial movement or a small tilt of the mirror. The time-separated copies are made to interfere on a screen and depending on the temporal coherence of the incident beam, an interference pattern is observed. Next we analyze a pulse-train version of this method.

Let us assume that $V_0(t)$ represents a single pulse (in a train) input to the Michelson interferometer schematically shown in Fig. 4.1. A beam splitter divides the pulse into two replicas which travel towards the mirrors M_1 and M_2. A translation of M_1 and M_2 introduces a delay between the pulses propagating in the two arms of the interferometer. The time-separated replicas are then combined on the screen B.

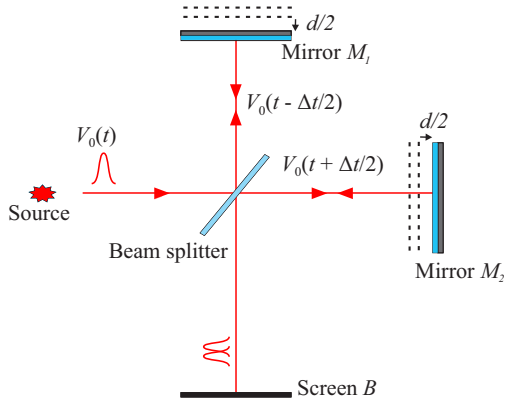

Figure 4.1: Schematic representation of a Michelson's interferometer. An incoming pulse $V_0(t)$ is divided into two equal parts by the beam splitter. The two replicas, that are reflected from the mirrors M_1 and M_2, are combined on a screen B. In the setup illustrated here, M_1 is displaced by a distance $d/2$ from the equilibrium position towards the beam splitter while M_2 is shifted away by the same amount. The displacement of the mirrors introduces a delay between the replicas of a single pulse.

In the setup illustrated in Fig. 4.1, M_1 is moved a distance $d/2$ from the equilibrium position (indicated by the dotted lines) towards the beam splitter and the mirror M_2 is displaced by a distance $d/2$ away from the beam splitter. If c denotes the speed of light in vacuum, then a shift of $d/2$ in the arms of the interferometer corresponds to a time delay of $\Delta t = 2d/c$ between the two halves of the incident pulse. The output field at the detector is

$$V(t, \Delta t) = \frac{1}{2}[V_0(t - \Delta t/2) + V_0(t + \Delta t/2)], \tag{4.1}$$

and the temporal intensity of a single pulse is $I_s(t, \Delta t) = |V(t, \Delta t)|^2$.

In the case of a pulse train, we average the temporal intensity over the ensemble, $I(t, \Delta t) = \langle |V(t, \Delta t)|^2 \rangle$, which can be written as

$$I(t, \Delta t) = \frac{1}{4}\left\{ I_0(t - \Delta t/2) + I_0(t + \Delta t/2) + 2\mathrm{Re}\left[\Gamma_0(t, \Delta t)\right]\right\}, \tag{4.2}$$

where $\mathrm{Re}\left[\Gamma_0(t, \Delta t)\right]$ denotes the real part of the MCF which is defined as $\Gamma_0(t, \Delta t) = \langle V_0^*(t - \Delta t/2) V_0(t + \Delta t/2)\rangle$. Introducing the complex degree of temporal coherence from Eq. (2.17) (without $\mathbf{r}$ dependence), Eq. (4.2) takes the form

$$\begin{aligned} I(t, \Delta t) = \frac{1}{4}\big\{ & I_0(t - \Delta t/2) + I_0(t + \Delta t/2) \\ & + 2\sqrt{I_0(t - \Delta t/2) I_0(t + \Delta t/2)}\,|\gamma_0(t, \Delta t)| \cos[\alpha(t, \Delta t)]\big\}, \end{aligned} \tag{4.3}$$

where $\alpha(t, \Delta t)$ is the argument of $\gamma_0(t, \Delta t)$. Equation (4.3) shows that measurement of the intensities $I(t, \Delta t)$ and $I_0(t)$ gives information about the magnitude and phase of $\gamma_0(t, \Delta t)$. Using the envelope representation for $\gamma_0(t, \Delta t)$, we can write

$$\gamma_0(t, \Delta t) = |\gamma_0(t, \Delta t)| \exp\left\{ \mathrm{i}\left[\alpha'(t, \Delta t) - \omega_0 \Delta t\right]\right\}, \tag{4.4}$$

$$\alpha'(t, \Delta t) = \omega_0 \Delta t + \alpha(t, \Delta t). \tag{4.5}$$

Equation (4.3) in terms of Eq. (4.4) becomes

$$I(t,\Delta t) = \frac{1}{4}\big\{ I_0(t-\Delta t/2) + I_0(t+\Delta t/2) \\ + 2\sqrt{I_0(t-\Delta t/2)I_0(t+\Delta t/2)}|\gamma_0(t,\Delta t)|\cos[\alpha'(t,\Delta t) - \omega_0\Delta t]\big\}. \quad (4.6)$$

In the above interference law, the square-root factor, $|\gamma_0(t,\Delta t)|$, and $\alpha'(t,\Delta t)$ are slowly varying while the term $\omega_0\Delta t$ is a fast varying function. As a consequence, the intensity is cosine modulated and its envelope varies slowly. This results, for all t as a function of Δt, in dark and bright fringes on the observation screen B.

The contrast of the interference pattern observed on the screen B varies as a function of Δt. As Δt increases, the interference pattern becomes dimmer and dimmer, until at a certain Δt, it totally disappears. The extreme value of Δt for which the interference pattern diminishes may be called the coherence time [4,5].

The cosine term in Eq. (4.3) can take on values in the interval $[-1\ 1]$. The adjacent maximum and minimum intensities as a function of Δt on the screen are, respectively, given by

$$I_{\max}(t,\Delta t) = \frac{1}{4}\Big[I_0(t-\Delta t/2) + I_0(t+\Delta t/2) \\ + 2\sqrt{I_0(t-\Delta t/2)I_0(t+\Delta t/2)}|\gamma_0(t,\Delta t)|\Big], \quad (4.7)$$

and

$$I_{\min}(t,\Delta t) = \frac{1}{4}\Big[I_0(t-\Delta t/2) + I_0(t+\Delta t/2) \\ - 2\sqrt{I_0(t-\Delta t/2)I_0(t+\Delta t/2)}|\gamma_0(t,\Delta t)|\Big]. \quad (4.8)$$

The fringe visibility or the contrast of the interference pattern is defined as [4]

$$v(t,\Delta t) = \frac{I_{\max}(t,\Delta t) - I_{\min}(t,\Delta t)}{I_{\max}(t,\Delta t) + I_{\max}(t,\Delta t)}. \quad (4.9)$$

Inserting from Eqs. (4.7) and (4.8) to Eq. (4.9) leads to

$$v(t,\Delta t) = \frac{2\sqrt{I_0(t-\Delta t/2)I_0(t+\Delta t/2)}}{I_0(t-\Delta t/2) + I_0(t+\Delta t/2)}|\gamma_0(t,\Delta t)|, \quad (4.10)$$

which shows that the visibility of the interference fringes gives a quantitative measure of the modulus of the degree of temporal coherence [53, 54]. The quantity $|\gamma_0(t,\Delta t)|$ can be calculated by measuring the average intensities $I(t,\Delta t)$ and $I_0(t)$ (in order to obtain the visibility). The phase of $\gamma_0(t,\Delta t)$ is specified by the fringe positions of the interference patterns.

If the pulses are ultrashort, then there are not fast enough detectors which can provide time-resolved measurements. The available detectors integrate the intensity over a finite time interval so (some of) the information on the time-dependence of the intensity, and subsequently, about the two-time coherence of the pulsed light is lost. Therefore, the measurement of the two-time (and two-frequency) correlation functions for non-stationary fields is more demanding than that of statistically stationary and quasi-stationary fields.

4.3 TIME-INTEGRATED CORRELATION FUNCTIONS

A quantity which is easily measurable with the Michelson interferometer even with slow detectors is the time-integrated MCF which can be defined as

$$\overline{\Gamma}_0(\Delta t) = \int_{-\infty}^{\infty} \Gamma_0(t, \Delta t)\mathrm{d}t, \tag{4.11}$$

and the corresponding time-integrated complex degree of coherence is

$$\overline{\gamma}_0(\Delta t) = \frac{\overline{\Gamma}_0(\Delta t)}{\overline{\Gamma}_0(0)}, \tag{4.12}$$

where $\overline{\Gamma}_0(0) = \int_{-\infty}^{\infty} I_0(t)\mathrm{d}t$ is the total pulse energy. If we integrate the interference distribution in Eq. (4.2) with respect to time t, we obtain

$$\begin{aligned}
\overline{I}(\Delta t) &= \int_{-\infty}^{\infty} I(t, \Delta t)\mathrm{d}t \\
&= \frac{1}{2}\int_{-\infty}^{\infty} I_0(t)\mathrm{d}t + \frac{1}{2}\mathrm{Re}\left[\int_{-\infty}^{\infty} \Gamma_0(t, \Delta t)\mathrm{d}t\right] \\
&= \frac{1}{2}\overline{\Gamma}_0(0) + \frac{1}{2}\mathrm{Re}\left[\overline{\Gamma}_0(\Delta t)\right] \\
&= \frac{1}{2}\overline{\Gamma}_0(0)\left\{1 + |\overline{\gamma}_0(\Delta t)|\cos\left[\alpha(\Delta t)\right]\right\},
\end{aligned} \tag{4.13}$$

where $\alpha(\Delta t)$ is the argument of the integrated degree of coherence, $\overline{\gamma}_0(\Delta t)$. Expressing the interference term in relation (4.13) in an envelope form similar to the one which was utilized in Eq. (4.6), results in interference fringes. We get the absolute value of $\overline{\gamma}_0(\Delta t)$ from the visibility of the interference pattern and its phase from the position of the fringes on the detector.

4.4 AUTOCORRELATION AND CROSS-CORRELATION MEASUREMENTS

In the literature, the FEL temporal coherence experiments are performed in a different way than the approach mentioned in Sec. 4.3. The temporal coherence properties of the FEL pulse trains are commonly studied with the aid of linear autocorrelation measurements [59–61]. The field autocorrelation $A(\Delta t)$ for a pulse $V(t)$ is given by

$$A(\Delta t) = \int_{-\infty}^{\infty} V^*(t - \Delta t/2)V(t + \Delta t/2)\mathrm{d}t. \tag{4.14}$$

In the papers [59–61], the autocorrelation functions of the individual pulses are calculated and then their magnitudes are averaged. In essence, the autocorrelation for an ensemble of pulses is calculated in the FEL experiments as $\langle|A(\Delta t)|\rangle$ which results in losing the phase information, while the more plausible way to estimate the coherence of pulse trains is with the modulus of the ensemble-averaged autocorrelation, $|\langle A(\Delta t)\rangle|$.

Some authors claim that a plot of $\langle|A(\Delta t)|\rangle$ as a function of the time delay Δt provides a measure of the average pulse duration [61,62] while retaining the phase information of the autocorrelation functions in averaging, $\langle A(\Delta t)\rangle$, leads to the loss

of information on the temporal duration of the pulses. In Publication IV, we have addressed this issue and elaborated about the knowledge that can be retrieved from the autocorrelation measurements. We will see next that, $\langle A(\Delta t)\rangle$ gives an estimate about the average spectrum of the pulse train. Substitution of Eq. (2.6) (without $\mathbf{r}$ dependence) into Eq. (4.14) leads to

$$A(\Delta t) = \int_0^\infty |\tilde{V}(\omega)|^2 \exp\left(-i\omega t\right) \mathrm{d}\omega, \tag{4.15}$$

which shows that the field autocorrelation measurement for a single pulse yields the spectrum of the pulse. The result in Eq. (4.15) is the autocorrelation theorem [42] which does not enable to compute the field $V(t)$, because the spectral phase is not included so $V(t)$ can not be determined uniquely. This implies that there are numerous pulses that could yield the same spectrum [42]. If the autocorrelation experiment is done for a partially coherent pulse train and then ensemble-averaged, we get

$$\langle A(\Delta t)\rangle = \int_0^\infty \langle|\tilde{V}(\omega)|^2\rangle \exp\left(-i\omega t\right) \mathrm{d}\omega, \tag{4.16}$$

which yields the average spectrum of the partially coherent pulse train.

A plot of the temporal ultrashort XFEL (SASE based) pulses simulated via GENESIS [63] is shown in Fig. 4.2. The average wavelength is 0.15 nm (8.27 keV). We see that the pulses fluctuate from shot-to-shot and have complicated intensity variations due to the start-up from shot noise.

In Figure 4.3, the red line is a plot of the autocorrelation function, $|\langle A(\Delta t)\rangle|$, and the blue line is calculated by taking the absolute value of the autocorrelation for each pulse and then ensemble averaging, $\langle|A(\Delta t)|\rangle$. The blue curve shows a smooth coherence spike on a pedestal which indicates low coherence of the pulse train as discussed in Publication IV.

Another technique that can be used for the characterization of pulses is the field cross-correlation measurement. The main difference between the autocorrelation and cross-correlation is that in the former method a pulse is split into two replicas which are correlated, while the latter correlates two different pulses $V_i(t)$ and $V_j(t)$ from the source. The cross-correlation function is

$$X(\Delta t) = \int_{-\infty}^\infty V_i^*(t - \Delta t/2) V_j(t + \Delta t/2) \mathrm{d}t, \tag{4.17}$$

which can be re-written in the form

$$X(\Delta t) = \int_0^\infty V_i^*(\omega) V_j(\omega) \exp\left(-i\omega t\right) \mathrm{d}\omega, \tag{4.18}$$

by using the Fourier transform relation given in Eq. (2.6) (without $\mathbf{r}$ dependence). The field cross-correlation retains the spectral phase information which can be used to compute the spectral fields and the corresponding CSD function as demonstrated in Publication IV.

The cross-correlation method is feasible for the diagnostics of pulsed sources with a high repetition rate because this scheme requires two different pulses from the source. For FELs, the cross-correlation technique may not be feasible as the repetition rate is not as high and too long delay line would be needed for the correlation measurements. For example, the European XFEL has a repetition rate of

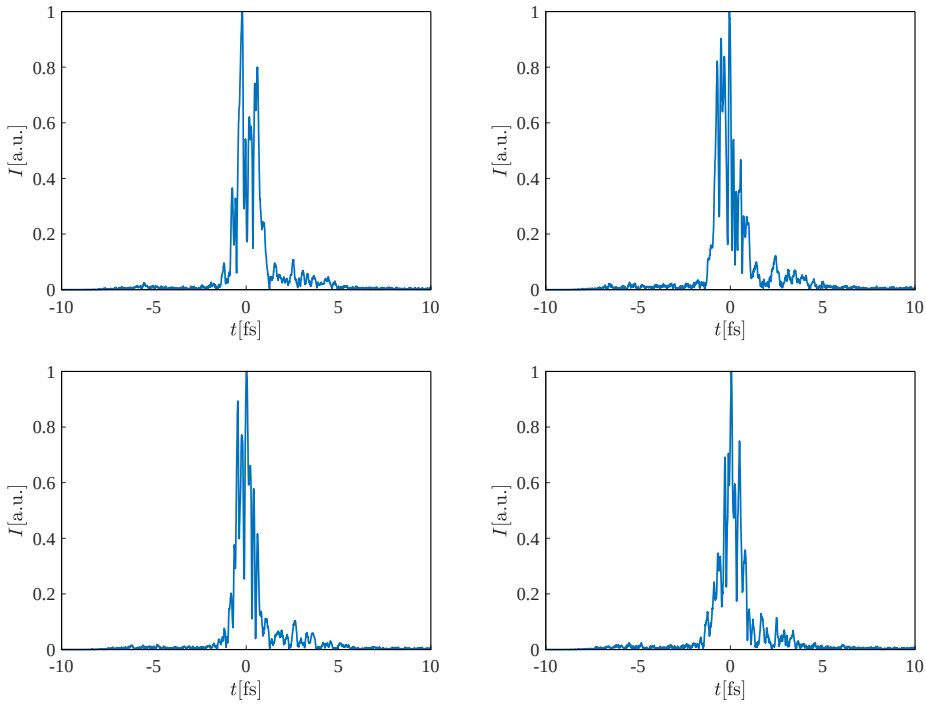

Figure 4.2: Individual temporal realizations simulated via GENESIS.

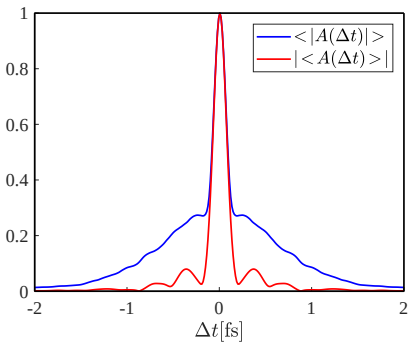

Figure 4.3: Autocorrelation function calculated for a set of XFEL pulses simulated via GENESIS. The red line is the usual autocorrelation function which is calculated by ensemble averaging the single-shot autocorrelation and then taking its absolute value. The blue line corresponds to the autocorrelation of individual realizations calculated by taking the absolute value of the individual autocorrelation functions and then ensemble averaging.

27000 flashes per second which is the highest among all existing XFELs [64], and thus, cross-correlation experiments would require impractically long delay line of about 11.10 km.

5 Coherence of free-electron lasers

This chapter deals with the coherence properties of free-electron lasers (FELs). In the first section, we describe the basics of the FELs. In the subsequent sections, we present an overview of the research on the coherence of FEL radiation and an analysis of the results obtained in Publication I.

5.1 FREE-ELECTRON LASERS

Conventional lasers, first developed in the 1960s, are based on the excitation and de-excitation of atoms and molecules in bound atomic and molecular states, and hence, the output wavelength range is not widely tunable. In the 1970s, the possibility to generate coherent radiation from an electron beam subjected to an undulator was explored. Free-electron lasers are based on the emission of radiation from a relativistic electron beam propagating through a spatially periodic magnetic undulator. John Madey first studied the gain of an electron beam through a periodic magnetic undulator [65] which is considered as the foundation of the FEL. The first operation of an FEL amplifier was demonstrated by Elias *et al.* [66] and an oscillator was also build for the FEL in the infrared region [67].

The gain medium of an FEL is a beam of free electrons. Due to the unique gain medium, unlike the conventional lasers, the FEL radiation is theoretically tunable on a wide wavelength range from the infrared down to the extreme ultraviolet and x-ray regions. With growing interest in sources which can produce coherent radiation in the x-ray regime, a scheme of the self-amplification of the spontaneous emission (SASE) of radiation was proposed by Kondratenko and Saldin [68], and Bonifacio, Pellegrini, and Narducci [69]. The SASE mechanism is a viable technique for generating coherent radiation in the x-ray region because the construction of an optical cavity for shorter wavelengths is not a feasible solution as the reflectivity of mirrors falls off drastically for short wavelengths [70,71]. In a SASE based FEL, the electron beam passes through a long undulator and the spontaneously emitted radiation at the entrance of the laser is amplified in a single pass without the need of a feedback cavity. Free-electron lasers based on this mechanism are termed as SASE FELs and these single-pass lasers can produce intense radiation in the x-ray regime. The FELs with output in the x-ray regime are appropriately named as XFELs.

Due to the high brilliance (the number of photons emitted per second, area and a solid angle within 0.1% of bandwidth [64,71]), almost perfect transverse coherence [71], and extremely short femtosecond pulses, XFELs enable research in the important areas like structural biology, physics, and material science. A typical XFEL can deliver photons per pulse about three orders of magnitude higher than those generated by third-generation synchrotron sources (synchrotron sources based on insertion devices like wigglers and undulators are classified as third-generation synchrotron sources [72]). The unprecedented brilliance and the femtosecond duration of the XFEL pulses can outrun the radiation damage and thus enable imaging of protein molecules and other biological specimen [73–80]. The XFELs are useful for research in the area of condensed matter physics as the techniques like x-ray pho-

ton correlation spectroscopy (XPCS) can now be employed to study the equilibrium dynamics of atoms on an unprecedented spatial and temporal scale [81–86]. The intense XFEL pulses are used to study the electron dynamics and space charge effects when materials are exposed to x-rays [87,88]. All of these techniques described here rely on the coherence properties of the XFEL radiation. Hence, investigation of the coherence of XFELs is of fundamental importance for utilizing these sources in the coherence based experiments.

5.1.1 Operational principle of the free-electron laser

A free-electron laser consists of three main components (see Fig. 5.1): An electron gun that provides a stream of electrons, an accelerator which accelerates the electron beam to relativistic speeds, and a periodic arrangement of magnets called an undulator. When the electron beam which propagates at a relativistic speed after exiting the accelerator enters the undulator, the beam experiences a periodically varying magnetic field, and follows a curved path. An accelerating charge emits electromagnetic radiation and therefore, the deflected electron beam emits a stream of photons. The electron beam is then deflected to a dump via bending magnets at the exit of the undulator [71,89]. If the undulator is helical, the electron beam traverses a helical path, and in the case of a planar undulator, the electron beam follows a sinusoidal trajectory in a plane perpendicular to the direction of the magnetic field [90,91].

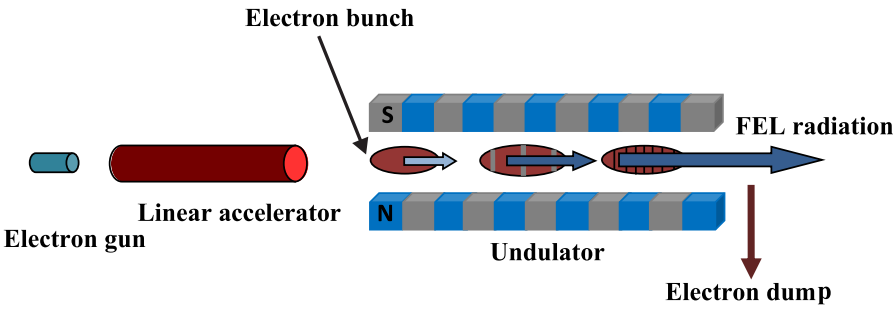

Figure 5.1: Schematic representation of a SASE based FEL. The electron gun generates a beam of electrons which acquire a relativistic speed in the linear accelerator. The relativistic electron beam encounters a periodically varying magnetic field inside the undulator and emits electromagnetic radiation. The spent electron beam then gets deflected to a dump while the FEL radiation propagates to the experimental station.

An FEL has two operation regimes: high-gain linear and saturation. As the electron beam and the radiation co-propagate through the undulator, the radiation power increases exponentially along the length of the undulator. This region is called the linear regime of the FEL operation. Once, the power saturates, the exponential growth ceases further along the undulator, and the FEL is then said to be operating in the saturation (or nonlinear) regime [92,93].

5.1.2 The FEL collective instability

The electrons in a bunch are spatially randomly distributed at the entrance of the undulator. The randomly distributed electrons emit photons which do not have any

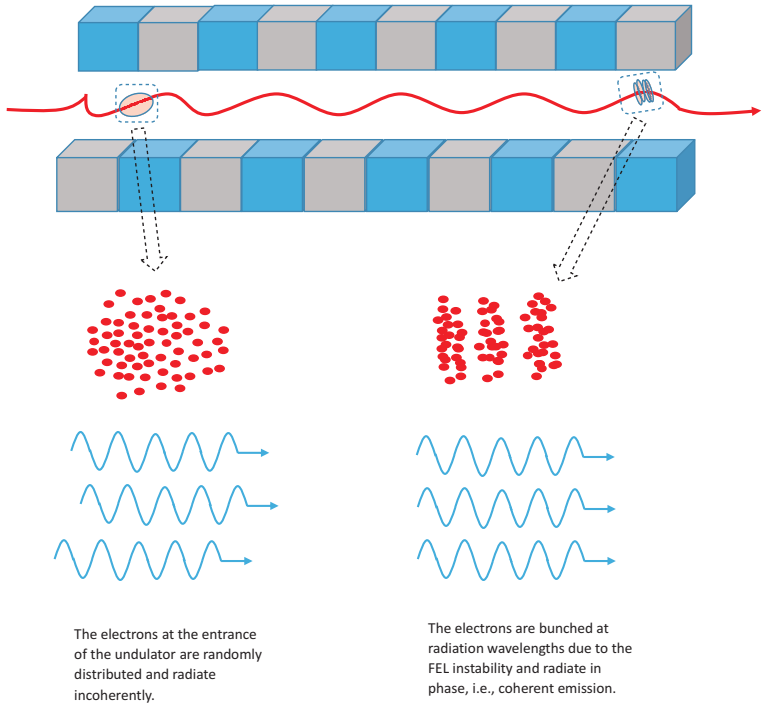

Figure 5.2: Schematic illustration of the FEL instability. The electrons have a random distribution as they enter the undulator. Inside the undulator, the electrons and the radiation field interact which causes the electrons to group into longitudinal slices which are separated on the order of the radiation wavelength. The electrons inside a single slice "microbunch" radiate in phase due to which the output intensity is greatly increased, that is, the intensity of the radiation field is proportional to the number of electrons in the microbunch.

phase relation with one another. However, as the radiation field propagates in the undulator, it interacts with the electron bunch. The electrons that are in phase with the electromagnetic field, gain energy and are accelerated, while those electrons which are out of phase with the field, lose energy, and are, therefore, decelerated [70]. The energy modulation of the electron bunches causes the electrons to group into micro-bunches on the order of the radiation wavelength. This longitudinal density modulation of the electron beam is called FEL's collective instability [25]. A simpler schematic illustration of the microbunching of electrons in the undulator is given in Fig. 5.2.

Electrons which are grouped within a micro-bunch radiate in phase [70] due to which the intensity of the radiation increases quadratically with the number of emitters, i.e., electrons in the microbunch. Typically each microbunch has 10^9 electrons which radiate coherently [71]. Due to the phenomenon of instability, the radiation from the FELs surpass the intensity of third-generation synchrotron sources by sev-

eral orders of magnitude.

Figure 5.2 also schematically demonstrates that the radiation from an FEL has a high degree of transverse coherence because the electrons that are grouped within each microbunch oscillate and radiate in unison [94]. In addition to the microbunching phenomenon, the FEL amplifier serves as a linear filter for transverse radiation modes. Only the modes with the higher gain are amplified. This mode selection is another key reason for the high transverse coherence of the FELs.

5.1.3 X-ray free-electron laser facilities

With the ever increasing demand for generating coherent radiation with high brightness at angstrom wavelengths, FELs attracted a lot of interest from the scientific community. Pellegrini put a proposal for the construction of an XFEL using the linear accelerator at the SLAC National Accelerator Laboratory [95]. Based on Pellegrini's proposal, the first XFEL operating in the hard x-ray region, the Linac Coherent Light Source (LCLS) at Stanford, lased in 2009 [96]. Another hard x-ray FEL in Japan called SACLA (SPring-8 Angstrom Compact free electron LAser) became operational in 2011 and achieved lasing at 10.3 keV (0.12 Å) [97]. FERMI at Trieste, Italy, is a soft x-ray FEL facility that can deliver ultrashort pulses (10–100 fs) with high transverse and longitudinal coherence [98,99]. FLASH (Free-electron LASer in Hamburg) is the world's first soft x-ray facility [89]. The European XFEL at Hamburg became operational in May, 2017. The newly built European XFEL can produce extremely short femtosecond pulses (< 100 fs) in the $0.26 - 24.8$ keV range ($4.7 - 0.05$ nm wavelength region) with a repetition rate of 27000 pulses per second [64]. FLASH and the European XFEL facilities are managed by the Deutsches Elektronen-Synchrotron (DESY). South Korea recently commissioned its first hard x-ray FEL source at Pohang Accelerator Laboratory, PAL-XFEL which lased at 8.60 keV (0.144 nm) [100]. Currently, a new XFEL facility is near the commissioning phase at Paul Scherrer Institute (PSI) in Switzerland [101]. These seven XFEL facilities will equip the scientific community with the brightest probe to investigate the nanoworld of atoms and molecules on the elusive ultrashort and ultrafast angstrom–femtosecond scale.

5.2 COHERENCE OF FELS

Coherence is one of the fundamental properties of FEL sources that has made these devices useful in techniques like serial femtosecond crystallography (SFX) [74], x-ray holographic imaging [102], and XPCS [84, 85]. Most of the FEL experiments depend on the coherence properties of the radiation [23]. Effect of the FEL coherence on the outcome of such experiments has not been extensively studied. Therefore, investigation of the coherence of FELs is a topic of prime interest for the scientific community. In this section, we present an overview of the coherence properties of FELs that has been carried out in the literature.

The radiation in a SASE based FEL starts from the shot noise in the electron beam. Therefore, a number of transverse modes are excited as the electron beam enters the undulator. The fundamental mode overlaps the electron beam the most and is amplified the most, while the higher order modes grow relatively weaker until the onset of saturation [70, 90]. In other words, a SASE based FEL amplifier behaves as a spatial and temporal filter for the shot noise fluctuations in the electron beam resulting in high transverse coherence. Due to startup from the shot noise such FELs have shot to shot variations in wavelength and pulse energy [71] which

is very different from the conventional lasers. The longitudinal coherence of SASE FELs is poor [93]. As the FEL radiation travels along the undulator, the longitudinal and transverse coherence builds and reaches a maximum level until the end of the linear regime of operation [70, 92]. The longitudinal coherence of the FEL [60] is measured usually with a split and delay unit [103].

The classic Young's double-slit or double-pinhole experiment [3] is commonly employed for characterizing the transverse coherence properties of FELs operating in the far-UV region to the extreme UV and soft x-ray wavelengths [60, 94, 104, 105]. Ischebeck *et al.* developed an in-vacuum setup to study the transverse coherence of the FEL operating at 100 nm wavelength at DESY. The measurements showed that the vacuum ultraviolet (VUV) radiation from the FEL at DESY is highly spatially coherent [94]. Singer *et al.* analyzed the transverse coherence properties of FLASH operating at 13.7 nm using a set of horizontal and vertical slits with different separations at a distance of 20 m from the source [104]. The analysis showed that FLASH has a high degree of transverse coherence with a coherence length of about 300 μm and the transverse coherence properties of the FLASH beam are isotropic along the horizontal and vertical axis. Measurement of the coherence properties of FLASH at a wavelength of 8 nm was performed at a distance of 70 m from the source [60]. The beam spot size at the pinhole apertures' position was 10×10 μm^2 (full width of the half maximum of a Gaussian function). The coherence length was determined to be about 6.2 ± 0.9 μm in the horizontal and 8.7 ± 1.0 μm in the vertical direction. Using a split and delay unit based on wavefront division [103], the temporal coherence time was estimated to be 1.75 ± 0.01 fs, which for a radiation of 8 nm wavelength is equivalent to about 65.5 wavecycles. Further measurements of the temporal coherence of FLASH for wavelengths $\lambda = 32$ nm to $\lambda = 8$ nm exhibited a decrease in the coherence time from 6 ± 0.5 fs for $\lambda = 32$ nm to 2.9 ± 0.5 fs for $\lambda = 8$ nm. Transverse coherence length was estimated to be 2.3 mm (rms) for $\lambda = 24$ nm, while the beam size was recorded to be 2.5 mm [59]. Vartanyants *et al.* used an aperture array (see Fig. 5.3) with different pinhole separations to investigate the coherence properties of the XFEL at LCLS at $\lambda = 1.6$ nm and a pulse duration of approximately 300 fs [105]. The apertures were placed at a distance of about 139.4 m downstream from the source. The spot size (FWHM) of the focused beam at the apertures was about 5.7 ± 0.4 μm in the horizontal and 17.3 ± 2.4 μm in the vertical direction. The transverse coherence length along the vertical direction was found to be 17 μm. Because a single aperture cannot withstand the energetic x-ray photons, the measurement was done in a 'diffraction before destruction mode'. After each shot, the aperture was moved to a new position and the interference pattern was recorded. The degree of transverse coherence was estimated to be 56% and the temporal coherence time was found to be 0.55 fs. The Young's double-pinhole experimental setup, based on the diffract and destroy principle, for the measurement of the coherence properties of intense pulses, such as x-rays, is diagrammatically shown in Fig. 5.3. A thick beamstop protects the camera from direct exposure to the FEL beam.

With the current state-of-the art, Young's interferometry is practically not viable for XFELs operating in the hard x-ray region due to the difficulty in fabricating apertures which can endure the radiation damage due to the impinging energetic x-ray photons. Analyzing the coherence properties of hard x-ray pulses using Young's double-pinhole experiment is challenging as it requires preparing a set of apertures and re-aligning the interferometer after each shot as the aperture is destroyed by a single exposure. To overcome these difficulties, different approaches have been proposed to study the coherence of the hard x-ray FELs [106–108]. For the

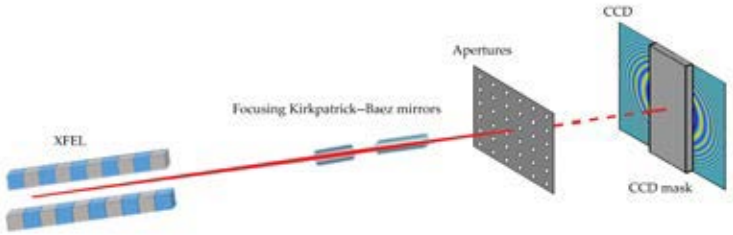

Figure 5.3: Pictorial demonstration of the Young's double-pinhole experiment for measuring the coherence properties of an XFEL in the diffract and destroy mode. The rectangular beamstop shields the camera from direct exposure to the x-ray pulses.

x-ray regime of XFELs, transverse and longitudinal coherence measurements have been performed by using the coherent diffraction speckle patterns from colloidal nanoparticles using small-angle scattering geometry (SAXS) and gold nanopowder using wide-angle scattering geometry (WAXS).

Apart from the coherent diffraction methods which estimates the coherence properties of hard x-ray FEL beams based on diffraction pattern from nanoparticles, the intensity correlations, that is, Hanbury Brown–Twiss interferometry (HBT), might be another tenable technique for analysis of the coherence of XFELs in the hard x-ray region. For the FEL in Hamburg (commonly called FLASH) operating in the extreme ultraviolet region, HBT has been performed which corroborated that the FEL beam has a high degree of transverse coherence (about 80%) [109]. Recently, HBT interferometry has been performed for the hard x-ray FEL facility LCLS operating at a wavelength of 1.5 Å [110]. Unlike the interferometry in [109] which was performed without the use of a sample in the path of the FEL beam, the latest setup employs a colloidal crystal sample placed in the path of the monochromatized XFEL beam. The diffracted intensities from the sample are recorded on a pixel detector. The diffraction based HBT interferometry demonstrated that LCLS has almost full transverse coherence of about 80% and its monochromatized beam has a temporal coherence time of 7.5 fs.

In addition to the autocorrelation based on wavefront division which geometrically splits a pulse to produce its' two jitter-free replicas [103], Michelson interferometry based on amplitude division is another technique which can be used for the measurement of the spatial and temporal coherence properties of FELs in the XUV regime [111]. Utilizing the interferometer developed in [111], spatio–temporal properties of monochromatized beam of FLASH were measured at a wavelength of 13.5 nm [57]. The temporal coherence was estimated to be 59 ± 8 fs which corresponds to about 1300 wavecycles. The transverse coherence lengths were measured to be approximately 12% of the beam size in the horizontal and 15% of the beam size in the vertical direction. The coherence measurements of various FEL facilities are summarized in Table 5.1.

As the FEL amplifier filters out the modes with high loss and only a few transverse modes survive the SASE process, it is logical to apply the CMD for analyzing the coherence properties of FELs [114]. In the temporal domain, the FEL radiation has a number of longitudinal coherent modes which do not have phase relation with each other. The FELs based on SASE mechanism have poor temporal coherence. Dif-

Table 5.1: Coherence measurements of different FEL facilities. Here, λ is the operating wavelength of the FEL, l_c is the transverse coherence length, the % values show the degree of transverse coherence, T_c is the coherence time, T represents the pulse duration, and SDU stands for a split and delay unit. . The horizontal and vertical directions of the beam cross-section are represented by H and V, respectively. The single asterisk $*$ refers to the fundamental while double asterisks $**$ to the 3rd harmonic of the wavelength.

Facility	λ [nm]	l_c, %	T_c [fs]	T [fs]	Information
FLASH [112]	23.9	63%	6		SDU
FLASH [104]	13.7	300 μm (H), 250 μm (V)			double-slit, beam radius 890 μm
FLASH [59]	32 $*$ 24 8 $*$ 8 $**$	2.3 mm 42%	6 ± 0.5 6 ± 0.5 2.9 ± 0.5 2.4 ± 0.5	 30	autocorrelator, beam size 2.5 mm (rms)
FLASH [60]	8	6.25 ± 0.9 μm (H), 8.7 ± 1 μm (V)	1.75 ± 0.01	100	double-pinhole, SDU, beam size 10×10 μm^2
LCLS [105]	1.6	56%	0.6	300	double-pinhole
LCLS [106]	0.137	fully coherent	2 ± 1	29 ± 14	nanoparticles, monochromator
LCLS [107]	0.138	93 %	2.2	29	nanoparticles, monochromator
SACLA [108]	0.206	1.7 ± 0.2 μm (H) 1.3 ± 0.1 μm (V)			nanoparticles, beam size 1.8 μm (H) 1.3 μm (V)
SACLA [113]	0.155	79%	0.1	5.2	nanoparticles
FLASH [109]		80 %		50	HBT
LCLS [110]	0.155	80%	7.5	10	HBT monochromator
FLASH [57]	13.5	12% (H) 15% (V) (of beam diameter)	59 ± 9	100-150	Michelson interferometer, monochromator

ferent schemes have been suggested for improving the partial temporal coherence of the SASE based FELs. For instance, one approach is to seed the SASE based FEL with a temporally coherent seed source, the SASE radiation will have imprints of the seed's coherence and the temporal fluctuations due to the noise in the electron beam can be suppressed. This seeding scheme would improve the temporal coherence of the SASE based FELs. A number of schemes for improving the temporal coherence of XFELs are listed by McNeil and Thompson in the Review [115] and Feldhaus *et al.* in [70]. In the literature, the FELs are modeled with the GSM, for instance in the Refs. [59,104,116].

5.3 AN ITERATIVE MODEL TO SIMULATE FEL PULSES

In Publication I, we analyzed the spectral and temporal coherence properties of the XFEL source at LCLS Stanford. First, using IFTA (discussed in Sec. 2.5), we constructed an ensemble of complex pulses in both domains using the measured spectra of individual pulses recorded for the XFEL. We utilized the ensemble of the simulated XFEL pulses to construct the two-frequency CSD and two-time MCF functions. The normalized correlation functions illustrated that the spectral coherence width of the XFEL source under consideration is very narrow compared to the average spectral width of the pulses and the coherence time is short compared to the average pulse duration. This demonstrated that the XFEL at LCLS emits quasistationary pulse trains with low spectral and temporal coherence. Our result regarding the quasistationarity of the XFEL conforms with the physics of the SASE based XFELs. A SASE based XFEL, like the one at the LCLS Stanford, amplifies the shot noise fluctuations in the electron beam density and as a consequence of this nature of the SASE process, the output pulses have shot-to-shot variations. These fluctuations manifest in the form of low spectral and temporal coherence of the pulses.

In Publication I, our analysis also proved that the XFEL source obeys the Gaussian Schell model (GSM). Our findings concerning the applicability of the GSM to the XFEL sources corroborated the earlier results [116] on modeling these sources with the classic GSM.

The iterative model developed in Publication I is an elegant way to simulate an ensemble of spectral and temporal pulses not only for the XFEL facilities but it is also equally suitable to mimic the output of any other pulsed light source. The proposed model is based on the knowledge of the spectra of individual pulses and the mean pulse duration which can be easily measured.

5.4 FEL SIMULATIONS WITH GENESIS

In Publication IV , we simulated the output of the European XFEL SASE-1 undulator with the three-dimensional (3D) time-dependent simulation code Genesis [63]. We generated a set of 100 time-domain pulses (like those shown in Fig. 4.2) for the SASE-1 undulator and Fourier transformed the set of the simulated pulses to get an ensemble of pulses in the spectral domain. Utilizing the ensemble of the time and frequency domain pulses, we calculated the complex degrees of temporal and spectral coherence, respectively, which are narrow lines as shown in Fig. 5.4.

As illustrated in Fig. 5.4, the width of the complex degree of temporal coherence (0.13 fs) is short compared to the mean pulse duration (0.70 fs). In the spectral domain, the width of the complex degree of spectral coherence (0.40 PHz) is short

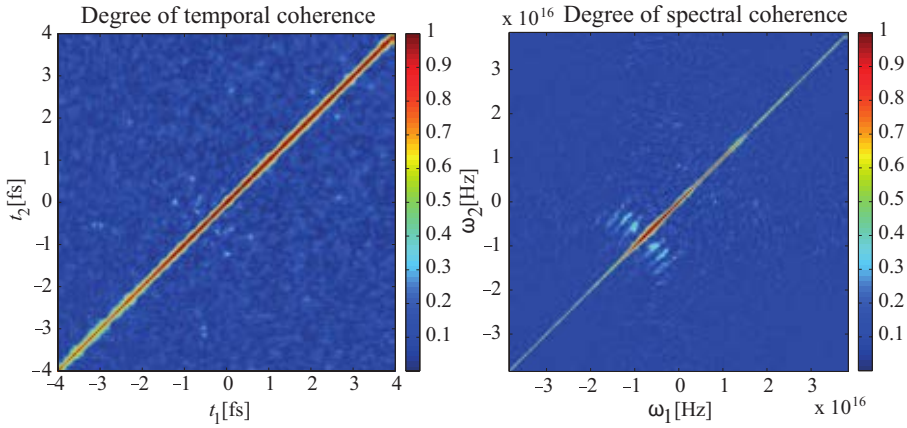

Figure 5.4: The complex degrees of temporal and spectral coherence computed for the European XFEL SASE-1. An ensemble of 100 temporal and spectral realizations was utilized to calculate the correlation functions.

in comparison to the average spectral width of the pulses (4.47 PHz). Therefore, based on the results in Publication IV, we conclude that the European XFEL SASE-1 undulator emits quasistationary pulse trains. As already mentioned the SASE based FELs have large shot-to-shot fluctuations due to start-up from the shot noise in the electron beam. As a consequence, these FELs have low spectral and temporal coherence and can be classified as quasistationary. Hence, the results of the simulation are in excellent agreement with the underlying physics of the SASE based FELs.

The FELs considered in this work, that is, LCLS at Stanford (Sec. 5.3) and the European XFEL at Hamburg (Sec. 5.4), are based on the SASE principle. Analysis of their coherence properties using IFTA and Genesis provides qualitatively similar results.

6 Conclusions

This thesis deals with the second-order coherence theory of pulsed light. The output fields of many important light sources, like pulsed lasers, have time-dependent random fluctuations and such sources are routinely employed in a large array of scientific applications. Although considerable work has been done in the coherence theory of stationary optical fields, yet the coherence of non-stationary light has not attracted much interest despite its ever increasing importance. To address this important area of the coherence theory, in this work, we developed novel modal expansions which can be utilized to explore the coherence properties of pulsed optical fields.

In this chapter, we present a summary of the main results of this thesis, and, the future prospects of the techniques developed herein for the analysis of the coherence properties of pulsed optical fields.

6.1 SUMMARY OF THE MAIN RESULTS

In Publication I, we investigated the spectral and temporal coherence properties of a free-electron laser facility. We need an ensemble of realizations in the spectral and temporal domain to construct the correlation functions in both domains. To obtain a set of spectral and temporal realizations (electric fields), we introduced an iterative Fourier transform algorithm (IFTA), imposing constraints both in time (Gaussian form for the mean temporal evolution of the pulse train) and frequency (measured spectra of pulses) domain. The iterative model we presented is based on the knowledge of the spectra of individual pulses and the average pulse duration. The ensuing simulated complex pulsed fields from our model form an ensemble that matches the measured results in the time and frequency domain and thus represent the actual realizations from the FEL in a statistically averaged sense. In Publication I, we then used our model to study the second-order coherence properties of the Linac Coherent Light Source (LCLS) at Stanford. Our analysis demonstrated that the SASE based FEL at Stanford emits quasi-stationary pulse trains with limited spectral and temporal coherence. Importantly, our work not only provided an improved iterative scheme for modeling pulsed light sources but it also corroborated the earlier works in the field by demonstrating that FELs typically obey the Gaussian Schell-model. Our proposed model is not limited only to the analysis of quasi-stationary pulsed sources but it can be applied equally well to study the coherence properties of other pulsed sources which may emit pulse trains with a lower or higher degree of correlation.

In Publication II, we proposed a new time-domain method for studying the coherence properties of a quasi-stationary train of random pulses. In the literature, several modal representations have been introduced for stationary and non-stationary, pulsed, scalar as well as electromagnetic fields. Publication II dealt with the formulation of a new modal expansion for quasi-stationary, pulsed optical fields in a finite time interval. We demonstrated that the MCF of a quasi-stationary field can be represented to a good approximation as a sum of fully deterministic,

quasi-monochromatic temporal functions of identical form and centered at different frequencies. In comparison with the traditional mode representations which necessitate the solution of a Fredholm integral equation, the new pseudo-modal representation is easier to implement as it requires only the information on the average spectrum and mean temporal intensity of a quasi-stationary pulsed field. The new time-domain method developed in Publication II was applied to a SASE based FEL which emits quasi-stationary pulse trains. We achieved an excellent agreement between the exact and the new approximative complex degree of coherence for the FEL source. The application of the pseudo-mode time-domain technique to a quasi-stationary FEL confirmed its validity for modeling the coherence properties of partially coherent sources.

Although a mode representation for scalar stationary beams in terms of scalar harmonic functions has already been suggested about four decades ago, an electromagnetic extension was missing. Publication III addresses two important unexplored problems. First, we introduced a harmonic coherent-mode expansion for stationary partially polarized electromagnetic beams for which the coherence time is much shorter than the length of the time interval in which the field is considered. Second, we provided an extension of the pseudo-modal time-domain method of Publication II from the scalar to the vector case. The vectorial extension of the time-domain expansion can be used to study the electromagnetic coherence properties of quasi-stationary sources, like SASE based FELs and supercontinuum light.

Publication IV concerns with the field interference techniques for pulsed light. In the literature, the linear autocorrelation experiment is mostly used to measure the coherence properties of FELs. Some literatures mention that first by measuring the single-shot autocorrelations, then disregarding the phase information (i.e. taking the absolute value), and finally ensemble averaging the single-shot autocorrelations results in a pedestal shaped curve which gives information about the average pulse length. In Publication IV, we demonstrated that, in general, the field autocorrelation measurements provide information only on the average pulse spectrum. However, for the special case of Schell-model sources, the field interferometric methods also yield time-domain information. We also propose a field cross-correlation scheme which can provide both the amplitude and spectral phase of the individual pulses. The cross-correlation method is suitable in the coherence studies of pulsed sources with high repetition rate. A long delay line will be required for the cross-correlation measurements if the repetition rate is low and for such a case, autocorrelation is the appropriate interferometric technique.

In a nutshell, the main new contributions of this work are:

- Introduction of an IFTA model to construct ensembles of complex electric fields in the spectral and temporal domains for pulsed light sources.
- A new time-domain pseudo-modal representation for quasi-stationary pulsed scalar fields which was applied to a SASE based FEL.
- A novel time-domain coherent-mode representation for stationary partially polarized electromagnetic beams in terms of harmonic fields.
- A new time-domain pseudo-modal expansion for quasi-stationary partially polarized electromagnetic beams.
- Analysis of field interferometric techniques for pulsed light.

6.2 FUTURE PROSPECTS

There is a continuous development to improve the longitudinal coherence of the FELs. Seeded FELs are being planned and some are already in operation. The seeded FELs can have nearly perfect longitudinal and transverse coherence. Other FELs like the one at Fermi facility, Trieste, which are based on high-gain harmonic generation method also have improved longitudinal coherence. The methods developed in the thesis can be applied to the currently commissioned and any other future FEL to get a better understanding of their coherence properties. This would strengthen the contributions of these fourth-generation light sources to science by enabling new discoveries in a wide range of fields such as structural biology, physics, and material science. Success of the experiments like coherent-diffraction imaging and XPCS performed with the FELs depends on a better comprehension of the coherence properties of these sources. The present work adds a valuable set of knowledge to this domain of science which is useful not only in the present but also in the foreseeable future.

The mode decomposition of quasi-stationary, scalar and electromagnetic random pulsed fields developed in this thesis are applicable not only to the radiation from the FELs but can also be applied to many other types of pulsed fields. For example, it would be of interest to explore the use of the proposed modal techniques in modeling the coherence properties of pulsed excimer lasers and the pulses generated by electro–optical modulation of an LED or the radiation from a superluminescent diode. For stationary LEDs, which are spatially quasi-homogeneous, a corresponding model could be formulated in the spatial–frequency domain. Then the spatial and the temporal models could be combined for investigating the coherence properties of temporally modulated LEDs.

At present, XFELs have low repetition rates. When XFEL sources with higher repetition rates become available, the field cross-correlation scheme can be utilized to get insights on their pulse characteristics and coherence properties.

BIBLIOGRAPHY

[1] International commission for optics, `http://e-ico.org/node/286` (visited on 2018-08-15).

[2] T. Young, "The Bakerian Lecture: On the theory of light and colors," *Phil. Trans. R. Soc. Lond.* **92**, 12–48 (1802).

[3] T. Young, "The Bakerian lecture: Experiments and calculations relative to physical optics," *Phil. Trans. R. Soc. Lond.* **94**, 1–16 (1804).

[4] L. Mandel and E. Wolf, *Optical Coherence and Quantum Optics* (Cambridge University Press, Cambridge, 1995).

[5] E. Wolf, *Introduction to the Theory of Coherence and Polarization of Light* (Cambridge University Press, Cambridge, 2007).

[6] G. Gbur and T. D. Visser, "The structure of partially coherent fields," in *Progress in Optics*, Vol. 55, E. Wolf, ed. (Elsevier, 2010), pp. 285–341.

[7] E. M. Verdet, "Étude sur la constitution de la lumière non polarisée et de la lumière partiellement polarisée," *Ann. Sci. ÉNS* **2**, 291–316 (1865).

[8] F. Zernike, "The concept of degree of coherence and its application to optical problems," *Physica* **5**, 785–795 (1938).

[9] E. Wolf, "Optics in terms of observable quantities," *Nuovo Cimento* **12**, 884–888 (1954).

[10] E. Wolf, "A macroscopic theory of interference and diffraction of light from finite sources II. Fields with a spectral range of arbitrary width," *Proc. Roy. Soc. A* **230**, 246–265 (1955).

[11] E. Wolf, "Coherence properties of partially polarized electromagnetic radiation," *Nuovo Cimento* **13**, 1165–1181 (1959).

[12] L. Mandel and E. Wolf, "Spectral coherence and the concept of spectral purity," *J. Opt. Soc. Am.* **66**, 529–535 (1976).

[13] E. Wolf, "New spectral representation of random sources and of the partially coherent fields that they generate," *Opt. Commun.* **38**, 3–6 (1981).

[14] L. Mandel and E. Wolf, "Complete coherence in the space–frequency domain," *Opt. Commun.* **36**, 247–249 (1981).

[15] E. Wolf, "New theory of partial coherence in the space-frequency domain. Part I: spectra and cross spectra of steady-state sources," *J. Opt. Soc. Am.* **72**, 343–351 (1982).

[16] E. Wolf, "New theory of partial coherence in the space-frequency domain. Part II: steady-state fields and higher-order correlations," *J. Opt. Soc. Am. A.* **3**, 76–85 (1986).

[17] B. Cairns and E. Wolf, "The instantaneous cross-spectral density of nonstationary wavefields," *Opt. Commun.* **62**, 215–218 (1987).

[18] M. Bertollotti, A. Ferrari, and L. Sereda, "Coherence properties of nonstationary light sources," *J. Opt. Soc. Am. B.* **12**, 341–347 (1995).

[19] M. Bertolotti, L. Sereda, and A. Ferrari, "Application of the spectral representation of stochastic processes to the study of nonstationary light radiation: a tutorial," *Pure Appl. Opt.* **6**, 153–171 (1997).

[20] L. Sereda, M. Bertollotti, and A. Ferrari, "Coherence properties of nonstationary light wave fields," *J. Opt. Soc. Am. A.* **15**, 695–705 (1998).

[21] T. H. Maiman, "Stimulated optical radiation in ruby," *Nature* **187**, 493 (1960).

[22] C. Pellegrini, "The histroy of X-ray free-electron lasers," *Eur. Phys. J. H* **37**, 659–708 (2012).

[23] C. Pellegrini, "X-ray free-electron lasers: from dreams to reality," *Phys. Scr.* **T169**, 014004 (2017).

[24] A. Sakdinawat and D. Attwood, "Nanoscale X-ray imaging," *Nat. Photonics* **4**, 840–848 (2010).

[25] C. Pellegrini and J. Stöhr, "X-ray free-electron lasers–principles, properties and applications," *Nucl. Instrum. Methods Phys. Res. A* **500**, 33–40 (2003).

[26] A. S. Ostrovsky, *Coherent-Mode Representations in Optics* (SPIE, 2006).

[27] H. Lajunen, J. Tervo, and P. Vahimaa, "Overall coherence and coherent-mode expansion of spectrally partially coherent plane-wave pulses," *J. Opt. Soc. Am. A.* **21**, 2117–2123 (2004).

[28] H. Lajunen, P. Vahimaa, and J. Tervo, "Theory of spatially and spectrally partially coherent pulses," *J. Opt. Soc. Am. A.* **22**, 1536–1545 (2005).

[29] B. Saleh, *Photoelectron Statistics* (Springer, 1978).

[30] J. Goodman, *Statistical Optics* (Joh Wiley , New York, 1985).

[31] D. Gabor, "Theory of communication," *J. Inst. Elect. Eng.* **93**, 429–441 (1946).

[32] H. Lajunen, A. T. Friberg, and P. Östlund, "Quasi-stationary plane-wave optical pulses and the van Cittert–Zernike theorem in time," *J. Opt. Soc. Am. A.* **23**, 2530–2537 (2006).

[33] L. Mandel and E. Wolf, "Coherence properties of optical fields," *Rev. Mod. Phys.* **37**, 231–287 (1965).

[34] G. J. Gbur, *Mathematical Methods for Optical Physics and Engineering* (Cambridge University Press, Cambridge, 2011).

[35] B. E. A. Saleh and M. C. Teich, *Fundamentals of Photonics* (Wiley, New York, 1991).

[36] R. Martínez-Herrero, P. M. Mejías, and F. Gori, "Genuine cross-spectral densities and pseudo-modal expansions," *Opt. Lett.* **34**, 1399–1401 (2009).

[37] S. Yang, S. A. Ponomarenko, and Z. Chen, "Coherent pseudo-mode decomposition of a new partially coherent source class," *Opt. Lett.* **40**, 3081–3084 (2009).

[38] M. Makita, P. Karvinen, D. Zhu, P. N. Juranic, J. Grünert, S. Cartier, J. H. Jungmann-Smith, H. T. Lemke, A. Mozzanica, S. Nelson, L. Patthey, M. Sikorski, S. Song, Y. Feng, and C. David, "High-resolution single-shot spectral monitoring of hard x-ray free-electron laser radiation," *Optica* **2**, 912–916 (2015).

[39] A. C. Schell, "A technique for the determination of the radiation pattern of a partially coherent aperture," *IEEE Trans. Antennas Propag.* **AP-15**, 187–188 (1967).

[40] P. Pääkkönen, J. Turunen, P. Vahimaa, A. T. Friberg, and F. Wyrowski, "Partially coherent Gaussian pulses," *Opt. Commun.* **204**, 53–58 (2002).

[41] O. Bryngdahl and F. Wyrowski, "Digital holography–computer-generated holograms," in *Progress in Optics*, Vol. 28, E. Wolf, ed. (North-Holland, 1990), pp. 1–86.

[42] R. Trebino, *Frequency-Resolved Optical Gating: The Measurement of Ultrashort Laser Pulses* (Kluwer Academic Publishers, Boston, MA, 2000).

[43] T. Pfeifer, Y. Jiang, S. Düsterer, R. Moshammer, and J. Ullrich, "Partial-coherence method to model experimental free-electron laser pulse statistics," *Opt. Lett.* **35**, 3441–3443 (2010).

[44] T. Voipio, T. Setälä, and A. T. Friberg, "Partial polarization theory of pulsed optical beams," *J. Opt. Soc. Am. A* **30**, 71–81 (2013).

[45] J. Tervo, T. Setälä, and A. T. Friberg, "Degree of coherence for electromagnetic fields," *Opt. Express* **11**, 1137–1143 (2003).

[46] T. Setälä, J. Tervo, and A. T. Friberg, "Complete electromagnetic coherence in the space–frequency domain," *Opt. Lett.* **29**, 328–330 (2004).

[47] Gori, "Matrix treatment for patially polarized, partially coherent beams," *Opt. Lett.* **23**, 241–243 (1998).

[48] F. Gori, M. Santarsiero, S. Vicalvi, R. Borghi, and G. Guattar, "Beam coherence-polarization matrix," *Pure Appl. Opt.* **7**, 941–951 (1998).

[49] F. Gori, M. Santarsiero, R. Simon, G. Piquero, R. Borghi, and G. Guattari, "Coherent-mode decomposition of partially polarized, partially coherent sources," *J. Opt. Soc. Am. A* **20**, 78–84 (2003).

[50] J. Tervo, T. Setälä, and A. T. Friberg, "Theory of partially coherent electromagnetic fields in the space–frequency domain," *J. Opt. Soc. Am. A* **21**, 2205–2215 (2004).

[51] T. Voipio, T. Setälä, and A. T. Friberg, "Coherent-mode representation of partially polarized pulsed electromagnetic beams," *J. Opt. Soc. Am. A* **30**, 2433–2443 (2013).

[52] A. T. Friberg and T. Setälä, "Electromagnetic theory of optical coherence [Invited]," *J. Opt. Soc. Am. A* **33**, 2431–2442 (2016).

[53] R. Dutta, J. Turunen, and A. T. Friberg, "Michelson's interferometer and the temporal coherence of pulse trains," *Opt. Lett.* **40**, 166–169 (2015).

[54] R. Dutta, A. T. Friberg, G. Genty, and J. Turunen, "Two-time coherence of pulse trains and the integrated degree of temporal coherence," *J. Opt. Soc. Am. A* **32**, 1631–1637 (2015).

[55] I. A. Walmsley and C. Dorrer, "Characterization of ultrashort electromagnetic pulses," *Adv. Opt. Photon.* **1**, 308–437 (2009).

[56] L. E. Hargrove, R. L. Fork, and M. A. Pollack, "Locking of HeNe laser modes induced by synchronous intracavity modulation," *Appl. Phys. Lett.* **5**, 4 (1964).

[57] V. Hilbert, C. Rödel, G. Brenner, T. Döppner, S. Düsterer, S. Dziarzhytski, L. Fletcher, E. Förster, S. H. Glenzer, M. Harmand, N. J. Hartley, L. Kazak, D. Komar, T. Laarmann, H. J. Lee, T. Ma, M. Nakatsutsumi, A. Przystawik, H. Redlin, S. Skruszewicz, P. Sperling, J. Tiggesbäumker, S. Toleikis, and U. Zastrau, "Spatio–temporal coherence of free-electron laser radiation in the extreme ultraviolet determined by a Michelson interferometer," *Apl. Phys. Lett.* **105**, 101102 (2014).

[58] V. M. Papadakis, A. Stassinopoulos, D. Anglos, S. H. Anastasiadis, E. P. Giannelis, and D. G. Papazoglou, "Single-shot temporal coherence measurements of random lasing media," *J. Opt. Soc. Am. B* **24**, 31–36 (2007).

[59] S. Roling, B. Siemer, M. Wöstmann, H. Zacharias, R. Mitzner, A. Singer, K. Tiedtke, and I. A. Vartanyants, "Temporal and spatial coherence properties of free-electron laser pulses in the extreme ultaviolet regime," *Phys. Rev. ST Accel. Beams* **14**, 080701 (2011).

[60] A. Singer, F. Sorgenfrei, A. P. Mancuso, N. Gerasimova, O. M. Yefanov, J. Gulden, T. Gorniak, T. Senkbeil, A. Sakdinawat, Y. Liu, D. Attwood, S. Dziarzhytski, D. D. Mai, R. Treusch, E. Weckert, T. Salditt, A. Rosenhahn, W. Wurth, and I. A. Vartanyants, "Spatial and temporal coherence properties of single free-electron laser pulses," *Opt. Express* **20**, 17480–17495 (2012).

[61] T. Osaka, T. Hirano, Y. Morioka, Y. Sano, Y. Inubushi, T. Togashi, I. Inoue, K. Tono, A. Robert, K. Yamauchi, J. B. Hastings, and M. Yabashi, "Characterization of temporal coherence of hard X-ray free-electron laser pulses with single-shot interferograms," *IUCrJ* **4**, 728–733 (2017).

[62] A. L. Marec, O. Larroche, and A. Klisnick, "Evidence of partial temporal coherence effects in the linear autocorrelation of extreme ultraviolet laser pulses," *Opt. Lett.* **41**, 3387–3390 (2016).

[63] S. Reiche, "GENESIS 1.3: a fully time-dependent FEL simulation code," *Nucl. Instrum. Methods Phys. Res. A* **429**, 243–248 (1999).

[64] European XFEL: Facts and Figures, `https://www.xfel.eu/facility/overview/facts_amp_figures/index_eng.html` (visited on 2018-04-06).

[65] J. M. J. Madey, "Stimulated emission of bremsstrahlung in a periodic magnetic field," *J. Appl. Phys.* **42**, 1906–1913 (1971).

[66] L. R. Elias, W. M. Fairbank, J. M. J. Madey, H. A. Schwettman, and T. I. Smith, "Observation of stimulated emission of radiation by relativistic electrons in a spatially periodic transverse magnetic field," *Phys. Rev. Lett.* **36**, 717–720 (1976).

[67] D. A. G. Deacon, L. R. Elias, J. M. J. Madey, G. J. Ramian, H. A. Schwettman, and T. I. Smith, "First operation of a free-electron laser," *Phys. Rev. Lett.* **38**, 892–894 (1977).

[68] A. M. Kondratenko and E. L. Saldin, "Generation of coherent radiation by a relativistic electron beam in an ondulator," *Part. Accelerators* **10**, 207–216 (1980).

[69] R. Bonifacio, C. Pellegrini, and L. M. Narducci, "Collective instabilities and high-gain regime in a free-electron laser," *Optics Commun.* **50**, 373–378 (1984).

[70] J. Feldhaus, J. Arthur, and J. B. Hastings, "X-ray free-electron lasers," *J. Phys. B* **38**, S799–S819 (2005).

[71] P. Schmuser, M. Dohlus, and J. Rossbach, "Ultraviolet and soft X-ray free electron lasers," in *Springer tracts in modern physics*, G. Holder, ed. (Springer-Verlag, Berlin Heidelberg, 2008), pp. 1–205.

[72] Third-generation synchrotron, `https://www.diamond.ac.uk/Home/About/FAQs/About-Synchrotrons.html` (visited on 2018-08-10).

[73] R. Neutze, R. Wouts, D. van der Spoel, E. Weckert, and J. Hajdu, "Potential for biomolecular imaging with femtosecond X-ray pulses," *Nature* **406**, 752–757 (2000).

[74] H. N. Chapman, P. Fromme, A. Barty, T. A. White, R. A. Kirian, A. Aquila, M. S. Hunter, J. Schulz, D. P. DePonte, U. Weierstall, R. B. Doak, Filipe R. N. C. Maia, A. V. Martin, I. Schlichting, L. Lomb, N. Coppola, R. L. Shoeman, S. W. Epp, R. Hartmann, D. Rolles, A. Rudenko, L. Foucar, N. Kimmel, G. Weidenspointner, P. Holl, M. Liang, M. Barthelmess, C. Caleman, S. Boutet, M. J. Bogan, J. Krzywinski, C. Bostedt, S. Bajt, L. Gumprecht, B. Rudek, B. Erk, C. Schmidt, A. Hömke, C. Reich, D. Pietschner, L. Strüder, G. Hauser, H. Gorke, J. Ullrich, S. Herrmann, G. Schaller, F. Schopper, H. Soltau, K.-U. Kühnel, M. Messerschmidt, J. D. Bozek, S. P. Hau-Riege, M. Frank, C. Y. Hampton, R. G. Sierra, D. Starodub, G. J. Williams, J. Hajdu, N. Timneanu, M. M. Seibert, J. Andreasson, A. Rocker, O. Jönsson, M. Svenda, S. Stern, K. Nass, R. Andritschke, C.-D. Schröter, F. Krasniqi, M. Bott, K. E. Schmidt, X. Wang, I. Grotjohann, J. M. Holton, T. R. M. Barends, R. Neutze, S. Marchesini, R. Fromme, S. Schorb, D. Rupp, M. Adolph, T. Gorkhover, I. Andersson, H. Hirsemann, G. Potdevin, H. Graafsma, B. Nilsson, and J. C. H. Spence, "Femtosecond X-ray protein nanocrystallography," *Nature* **470**, 73–77 (2011).

[75] M. M. Seibert, T. Ekeberg, Filipe R. N. C. Maia, M. Svenda, J. Andreasson, O. Jönsson, D. Odić, B. Iwan, A. Rocker, D. Westphal, M. Hantke, D. P. Deponte, A. Barty, J. Schulz, L. Gumprecht, N. Coppola, A. Aquila, M. Liang, T. A. White, A. V. Martin, C. Caleman, S. Stern, C. Abergel, V. Seltzer,

J. Claverie, C. Bostedt, J. D. Bozek, S. Boutet, A. A. Miahnahri, M. Messerschmidt, J. Krzywinski, G. Williams, K. O. Hodgson, M. J. Bogan, C. Y. Hampton, R. G. Sierra, D. Starodub, I. Andersson, S. Bajt, M. Barthelmess, J. C. H. Spence, P. Fromme, U. Weierstall, R. A. Kirian, M. S. Hunter, R. B. Doak, S. Marchesini, S. P. Hau-Riege, M. Frank, R. L. Shoeman, L. Lomb, S. W. Epp, R. Hartmann, D. Rolles, A. M. Rudenko, C. Schmidt, L. Foucar, N. Kimmel, P. Holl, B. Rudek, B. Erk, A. Hömke, C. H. Reich, D. Pietschner, G. Weidenspointner, L. Strüder, G. Hauser, H. Gorke, J. Ullrich, I. Schlichting, S. Herrmann, G. Schaller, F. Schopper, H. Soltau, K.-U. Kühnel, R. Andritschke, C.-D. Schröter, F. Krasniqi, M. Bott, S. Schorb, D. Rupp, M. Adolph, T. Gorkhover, H. Hirsemann, G. Potdevin, H. Graafsma, B. A. Nilsson, H. N. Chapman, and J. Hajdu, "Single minivirus particles intercepted and imaged with an X-ray laser," *Nature* **470**, 78–81 (2011).

[76] M. F. Hantke, D. Hasse, Filipe R N C Maia, T. Ekeberg, K. John, M. Svenda, N. D. Loh, A. V. Martin, N. Timneanu, D. S. D. Larsson, G. van der Schot, G. H. Carlsson, M. Ingelman, J. Andreasson, D. Westphal, M. Liang, F. Stellato, D. P. Deponte, R. Hartmann, N. Kimmel, R. A. Kirian, M. M. Seibert, K. Mühlig, S. Schorb, K. Ferguson, C. Bostedt, S. Carron, J. D. Bozek, D. Rolles, A. Rudenko, S. Epp, H. N. Chapman, A. Barty, J. Hajdu, and I. Andersson, "High-throughput imaging of heterogeneous cell organelles with an X-ray laser," *Nat. Photonics* **8**, 943–949 (2014).

[77] T. Ekeberg, M. Svenda, C. Abergel, Filipe R. N. C. Maia, V. Seltzer, J.-M. Claverie, M. Hantke, O. Jönsson, C. Nettelblad, G. van der Schot, M. Liang, D. P. DePonte, A. Barty, M. M. Seibert, B. Iwan, I. Andersson, N. D. Loh, A. V. Martin, H. Chapman, C. Bostedt, J. D. Bozek, K. R. Ferguson, J. Krzywinski, S. W. Epp, D. Rolles, A. Rudenko, R. Hartmann, N. Kimmel, and J. Hajdu, "Three-dimensional reconstruction of the giant mimivirus particle with an X-ray free-electron laser," *Phys. Rev. Lett.* **114**, 098102 (2015).

[78] M. Levantino, B. A. Yorke, D. C. Monteiro, M. Cammarata, and A. R. Pearson, "Using synchrotrons and XFELs for time-resolved X-ray crystallography and solution scattering experiments on biomolecules," *Curr. Opin. Struct. Biol.* **35**, 41–48 (2015).

[79] J. C. H. Spence, "XFELs for structure and dynamics in biology," *IUCrJ* **4**, 322–339 (2017).

[80] H. K. N. Reddy, C. H. Yoon, A. Aquila, S. Awel, K. Ayyer, A. Barty, P. Berntsen, J. Bielecki, S. Bobkov, M. Bucher, G. A. Carini, S. Carron, H. N. Chapman, B. Daurer, H. DeMirci, T. Ekeberg, P. Fromme, J. Hajdu, M. F. Hanke, P. Hart, B. G. Hogue, A. Hosseinizadeh, Y. Kim, R. A. Kirian, R. P. Kurta, D. S. D. Larsson, N. D. Loh, Filipe R. N. C. Maia, A. P. Mancuso, K. Mühlig, A. Munke, D. Nam, C. Nettelblad, A. Ourmazd, M. Rose, P. Schwander, M. M. Seibert, J. A. Sellberg, C. Song, J. C. H. Spence, M. Svenda, G. van der Schot, I. A. Vartanyants, G. J. Williams, and P. L. Xavier, "Coherent soft X-ray diffraction imaging of coliphage PR772 at the Linac coherent light source," *Sci. Data* **4**, 170079 (2017).

[81] G. Grübel, "X-ray photon correlation spectroscopy at the European X-ray free-electron laser (XFEL) facility," *C. R. Physique* **9**, 668–680 (2008).

[82] M. Leitner, B. Sepiol, L.-M. Stadler, B. Pfau, and G. Vogl, "Atomic diffusion studied with coherent X-rays," *Nat. Mater.* **8**, 717–720 (2009).

[83] J. N. Clark, L. Beitra, G. Xiong, A. Higginbotham, D. M. Fritz, H. T. Lemke, D. Zhu, M. Chollet, G. J. Williams, M. Messerschmidt, B. Abbey, R. J. Harder, A. M. Korsunsky, J. S. Wark, and I. K. Robinson, "Ultrafast three-dimensional imaging of lattice dynamics in individual gold nanocrystals," *Science* **341**, 56–59 (2013).

[84] F. Lehmkühler, P. Kwaśniewski, W. Roseker, B. Fischer, M. A. Schroer, K. Tono, T. Katayama, M. Sprung, M. Sikorski, S. Song, J. Glownia, M. Chollet, S. Nelson, A. Robert, C. Gutt, M. Yabashi, T. Ishikawa, and G. Grübel, "Sequential single shot X-ray photon correlation spectroscopy at the SACLA free electron laser," *Sci. Rep.* **5**, 17193 (2015).

[85] E. M. Dufresne, S. Narayanan, A. R. Sandy, D. M. Kline, Q. Zhang, E. C. Landahl, and S. Ross, "Pushing X-ray photon correlation spectroscopy beyond the continuous frame rate limit," *Opt. Express* **24**, 355–364 (2016).

[86] M. H. Seaberg, B. Holladay, J. C. T. Lee, M. Sikorski, A. H. Reid, S. A. Montoya, G. L. Dakovski, J. D. Koralek, G. Coslovich, S. Moeller, W. F. Schlotter, R. Streubel, S. D. Kevan, P. Fischer, E. E. Fullerton, J. L. Turner, F.-J. Decker, S. K. Sinha, S. Roy, and J. J. Turner, "Nanosecond X-ray photon correlation spectroscopy on magnetic skyrmions," *Phys. Rev. Lett.* **119**, 067403 (2017).

[87] L. Young, E. P. Kanter, B. Krässig, Y. Li, A. M. March, S. T. Pratt, R. Santra, S. H. Southworth, N. Rohringer, L. F. DiMauro, G. Doumy, C. A. Roedig, N. Berrah, L. Fang, M. Hoener, P. H. Bucksbaum, J. P. Cryan, S. Ghimire, J. M. Glownia, D. A. Reis, J. D. Bozek, C. Bostedt, and M. Messerschmidt, "Femtosecond electronic response of atoms to ultra-intense X-rays," *Nature* **466**, 56–61 (2010).

[88] S. P. Hau-Riege, R. M. Bionta, D. D. Ryutov, R. A. London, E. Ables, K. I. Kishiyama, S. Shen, M. A. McKernan, D. H. McMahon, M. Messerschmidt, J. Krzywinski, P. Stefan, J. Turner, and B. Ziaja, "Near-ultraviolet luminescence of N_2 irradiated by short X-ray pulses," *Phys. Rev. Lett.* **105**, 043003 (2010).

[89] FLASH, `http://photon-science.desy.de/facilities/flash/the_free_electron_laser/index_eng.html` (visited on 2018-07-11).

[90] E. L. Saldin, E. A. Schneidmiller, and M. V. Yurkov, *The Physics of Free Electron Lasers* (Springer, 2000).

[91] C. Pellegrini, A. Marinelli, and S. Reiche, "The physics of X-ray free-electron lasers," *Rev. Mod. Phys.* **88**, 015006 (2016).

[92] E. Saldin, E. Schneidmiller, and M. Yurkov, "Statistical and coherence properties of radiation from X-ray free-electron lasers," *New J. Phys.* **12**, 035010 (2010).

[93] G. Geloni, E. Saldin, L. Samoylova, E. Schneidmiller, H. Sinn, T. Tschentscher, and M. Yurkov, "Coherence properties of the European XFEL," *New J. Phys.* **12**, 035021 (2010).

[94] R. Ischebeck, J. Feldhaus, C. Gerth, E. Saldin, and P. Schmüser, "Study of the transverse coherence at the TTF free electron laser," *Nucl. Instrum. Methods Phys. Res. A* **507**, 175–180 (2003).

[95] C. Pellegrini, "A 4 to 0.1 nm FEL based on SLAC Linac," *Proceedings of the workshop on 4th generation light sources, SSRL 92/02*, M. Cornacchia and H. Winick, Editors, Proc. SSL, 364–375 (1992).

[96] P. Emma, R. Akre, J. Arthur, R. Bionta, C. Bostedt, J. Bozek, A. Brachmann, P. Bucksbaum, R. Coffee, F.-J. Decker, Y. Ding, D. Dowell, S. Edstrom, A. Fisher, J. Frisch, S. Gilevich, J. Hastings, G. Hays, P. Hering, Z. Huang, R. Iverson, H. Loos, M. Messerschmidt, A. Miahnahri, S. Moeller, H.-D. Nuhn, G. Pile, D. Ratner, J. Rzepiela, D. Schultz, T. Smith, P. Stefan, H. Tompkins, J. Turner, J. Welch, W. White, J. Wu, G. Yocky, and J. Galayda, "First-lasing and operation of an ångstrom-wavelength free-electron laser," *Nat. Photon.* **4**, 641–647 (2010).

[97] T. Ishikawa, H. Aoyagi, T. Asaka, Y. Asano, N. Azumi, T. Bizen, H. Ego, K. Fukami, T. Fukui, Y. Furukawa, S. Goto, H. Hanaki, T. Hara, T. Hasegawa, T. Hatsui, A. Higashiya, T. Hirono, N. Hosoda, M. Ishii, T. Inagaki, Y. Inubushi, T. Itoga, Y. Joti, M. Kago, T. Kameshima, H. Kimura, Y. Kirihara, A. Kiyomichi, T. Kobayashi, C. Kondo, T. Kudo, H. Maesaka, X. M. Maréchal, T. Masuda, S. Matsubara, T. Matsumoto, T. Matsushita, S. Matsui, M. Nagasono, N. Nariyama, H. Ohashi, T. Ohata, T. Ohshima, S. Ono, Y. Otake, C. Saji, T. Sakurai, T. Sato, K. Sawada, T. Seike, K. Shirasawa, T. Sugimoto, S. Suzuki, S. Takahashi, H. Takebe, K. Takeshita, K. Tamasaku, H. Tanaka, R. Tanaka, T. Tanaka, T. Togashi, K. Togawa, A. Tokuhisa, H. Tomizawa, K. Tono, S. Wu, M. Yabashi, M. Yamaga, A. Yamashita, K. Yanagida, C. Zhang, T. Shintake, H. Kitamura, and N. Kumagai, "A compact X-ray free-electron laser emitting in the sub-ångström region," *Nat. Photon.* **6**, 540–544 (2012).

[98] E. Allaria, D. Castronovo, P. Cinquegrana, P. Craievich, M. Dal Forno, M. B. Danailov, G. D'Auria, A. Demidovich, G. De Ninno, S. Di Mitri, B. Diviacco, W. M. Fawley, M. Ferianis, E. Ferrari, L. Froehlich, G. Gaio, D. Gauthier, L. Giannessi, R. Ivanov, B. Mahieu, N. Mahne, I. Nikolov, F. Parmigiani, G. Penco, L. Raimondi, C. Scafuri, C. Serpico, P. Sigalotti, S. Spampinati, C. Spezzani, M. Svandrlik, C. Svetina, M. Trovo, M. Veronese, D. Zangrando, and M. Zangrando, "Two-stage seeded soft-X-ray free-electron laser," *Nat. Photon.* **7**, 913–918 (2013).

[99] Free Electron Laser Radiation for Multidisciplinary Investigations (FERMI), `https://www.elettra.trieste.it/lightsources/fermi.html` (visited on 2018-04-09).

[100] Pohang Accelerator Laboratory: PAL-XFEL, `http://pal.postech.ac.kr/paleng/` (visited on 2018-04-09).

[101] SwissFEL, `https://www.psi.ch/swissfel/` (visited on 2018-04-09).

[102] L. M. Stadler, C. Gutt, T. Autenrieth, O. Leupold, S. Rehbein, Y. Chushkin, and G. Grübel, "Hard X ray holographic diffraction imaging," *Phys. Rev. Lett.* **100**, 245503 (2008).

[103] F. Sorgenfrei, W. F. Schlotter, T. Beeck, M. Nagasono, S. Gieschen, H. Meyer, A. Föhlisch, M. Beye, and W. Wurth, "The extreme ultraviolet split and femtosecond delay unit at the plane grating monochromator beamline PG2 at FLASH," *Rev. Sci. Instr.* **81**, 043107 (2010).

[104] A. Singer, I. A. Vartanyants, M. Kuhlmann, S. Duesterer, R. Treusch, and J. Feldhaus, "Transverse–coherence properties of the free electron laser FLASH at DESY," *Phys. Rev. Lett.* **101**, 254801 (2008).

[105] I. A. Vartanyants, A. Singer, A. P. Mancuso, O. M. Yefanov, A. Sakdinawat, Y. Liu, E. Bang, G. J. Williams, G. Cadenazzi, B. Abbey, H. Sinn, D. Attwood, K. A. Nugent, E. Weckert, T. Wang, D. Zhu, B. Wu, C. Graves, A. Scherz, J. J. Turner, W. F. Schlotter, M. Messerschmidt, J. Lüning, Y. Acremann, P. Heimann, D. C. Mancini, V. Joshi, J. Krzywinski, R. Soufli, M. Fernandez-Perea, S. Hau-Riege, A. G. Peele, Y. Feng, O. Krupin, S. Moeller, and W. Wurth, "Coherence properties of individual femtosecond pulses of an X-ray free-electron laser," *Phys. Rev. Lett.* **107**, 144801 (2011).

[106] C. Gutt, P. Wochner, B. Fischer, H. Conrad, M. Castro-Colin, S. Lee, F. Lehmkühler, I. Steinke, M. Sprung, W. Roseker, D. Zhu, H. Lemke, S. Bogle, P. H. Fuoss, G. B. Stephenson, M. Cammarata, D. M. Fritz, A. Robert, and G. Grübel, "Single shot spatial and temporal coherence properties of the SLAC Linac coherent light source in the hard X-ray regime," *Phys. Rev. Lett.* **108**, 024801 (2012).

[107] S. Lee, W. Roseker, C. Gutt, B. Fischer, H. Conrad, F. Lehmkühler, I. Steinke, D. Zhu, H. Lemke, M. Cammarata, D. M. Fritz, P. Wochner, M. Castro-Colin, S. O. Hruszkewycz, P. H. Fuoss, G. B. Stephenson, G. Grübel, and A. Robert, "Single shot speckle and coherence analysis of the hard X-ray free-electron laser LCLS," *Opt. Express* **21**, 24647–24664 (2013).

[108] I. Inoue, K. Tono, Y. Joti, T. Kameshima, K. Ogawa, Y. Shinohara, Y. Amemiya, and M. Yabashi, "Characterizing transverse coherence of an ultra-intense focused X-ray free-electron laser by an extended Young's experiment," *IUCrJ* **2**, 620–626 (2015).

[109] A. Singer, , U. Lorenz, F. Sorgenfrei, N. Gerasimova, J. Gulden, O. M. Yefanov, R. P. Kurta, A. Shabalin, R. Dronyak, R. Treusch, V. Kocharyan, E. Weckert, W. Wurth, and I. A. Vartanyants, "Hanbury Brown–Twiss interferometry at a free-electron laser," *Phys. Rev. Lett.* **111**, 034802 (2013).

[110] O. Yu. Gorobtsov, N. Mukharamova, S. Lazarev, M. Chollet, D. Zhu, Y. Feng, R. P. Kurta, J.-M. Meijer, G. Williams, M. Sikorski, S. Song, D. Dzhigaev, S. Serkez, A. Singer, A. V. Petukhov, and I. A. Vartanyants, "Diffraction based Hanbury Brown and Twiss interferometry at a hard X-ray free-electron laser," *Sci. Rep.* **8**, 2219 (2018).

[111] V. Hilbert, A. Blinne, S. Fuchs, T. Feigl, T. Kämpfer, C. Rödel, I. Uschmann, M. Wünsche, G. G. Paulus, E. Förster, and U. Zastrau, "An extreme ultraviolet Michelson interferometer for experiments at free-electron lasers," *Rev. Sci. Instrum.* **84**, 095111 (2013).

[112] R. Mitzner, B. Siemer, M. Neeb, T. Noll, F. Siewert, S. Roling, M. Rutkowski1, A. Sorokin, M. Richter, P. Juranic, K. Tiedtke, J. Feldhaus, W. Eberhardt, and H. Zacharias, "Spatio–temporal coherence of free electron laser pulses in the soft x-ray regime," *Opt. Express* **16**, 19909–19919 (2008).

[113] F. Lehmkühler, C. Gutt, B. Fischer, Martin A. Schroer, M. Sikorski, S. Song, W. Roseker, J. Glownia, M. Chollet, S. Nelson, K. Tono, T. Katayama, M. Yabashi, T. Ishikawa, A. Robert, and G. Grübel, "Single shot coherence properties of the free-electron laser SACLA in the hard X-ray regime," *Sci. Rep.* **4**, 5234 (2014).

[114] I. A. Vartanyants and A. Singer, "Coherence properties of hard X-ray synchrotron sources and X-ray free-electron lasers," *New J. Phys.* **12**, 035004 (2010).

[115] B. W. J. McNeil and N. R. Thompson, "X-ray free-electron lasers," *Nature Photon.* **4**, 814–821 (2010).

[116] I. A. Vartanyants, A. P. Mancuso, A. Singer, O. M. Yefanov, and J. Gulden, "Coherence measurements and coherent diffractive imaging at FLASH," *J. Phys. B: AT. Mol. Opt. Phys.* **43**, 194016 (2010).

Paper **I**

L. Ahad, I. Vartiainen, T. Setälä, A. T. Friberg,
C. David, M. Makita, and J. Turunen
"On spectral and temporal coherence
of x-ray free-electron laser beams"
Optics Express **24**,
pp. 13081–13090, 2016.

On spectral and temporal coherence of x-ray free-electron laser beams

Lutful Ahad,[1,*] **Ismo Vartiainen,**[1] **Tero Setälä,**[1] **Ari T. Friberg,**[1] **Christian David,**[2] **Mikako Makita,**[2] **and Jari Turunen**[1]

[1]*Institute of Photonics, University of Eastern Finland, P. O. Box 111, FI-80101 Joensuu, Finland*

[2]*Paul Scherrer Institut, CH-5232 Villigen PSI, Switzerland*

[*]*lutful.ahad@uef.fi*

Abstract: A model for the coherence properties of free-electron lasers (FELs) in time and frequency domains is introduced within the framework of classical second-order coherence theory of nonstationary light. An iterative phase-retrieval algorithm is applied to construct an ensemble of field realizations in both domains, based on single-pulse spectra measured at the Linac Coherent Light Source (LCLS) in self-amplified spontaneous emission mode. Such an ensemble describes the specific FEL pulse train in a statistically averaged sense. Two-time and two-frequency correlation functions are constructed, demonstrating that the hard X-ray free-electron laser at LCLS in this case behaves as a quasistationary source with low spectral and temporal coherence. We also show that the Gaussian Schell model provides a good description of this FEL.

OCIS codes: (030.1640) Coherence; (140.2600) Free-electron lasers (FELs); (340.7480) X-rays, soft x-rays, extreme ultraviolet (EUV).

References and links

1. C. Pellegrini and S. Reiche, "The development of X-ray free-electron lasers," IEEE. J. Sel. Top. Quantum Electron. **10,** 1393–1404 (2004).
2. B. W. J. McNeil and N. R. Thompson, "X-ray free-electron lasers," Nature Photon. **4,** 814–821 (2010).
3. I. A. Vartanyats, A. Singer, A. P. Mancuso, O. M. Yefanov, A. Sakdinawat, Y. Liu, E. Bang, G. J. Williams, G. Cadenazzi, B. Abbey, H. Sinn, D. Attwood, K. A. Nugent, E. Weckert, T. Wang, D. Zhu, B. Wu, C. Graves, A. Scherz, J. J. Turner, W. F. Schlotter, M. Messerschmidt, J. Lüning, Y. Acremann, P. Heimann, D. C. Mancini, V. Joshi, J. Krzywinski, R. Soufli, M. Fernandez-Perea, S. Hau-Riege, A. G. Peele, Y. Feng, O. Krupin, S. Moeller and W. Wurth, "Coherence properties of individual femtosecond pulses of an x-ray free-electron laser," Phys. Rev. Lett. **107,** 144801 (2011).
4. J. P. Marangos, "Introduction to the new science with x-ray free-electron lasers," Contemp. Phys. **52**, 551–569 (2011).
5. J. Spence, "X-ray imaging: ultrafast diffract-and-destroy movies," Nature Photon. **2,** 390–391 (2008).
6. H. N. Chapman, P. Fromme, A. Barty, T. A. White, R. A. Kirian, A. Aquila, M. S. Hunter, J. Schulz, D. P. DePonte, U. Weierstall, R. B. Doak, F. R. N. C. Maia, A. V. Martin, I. Schlichting, L. Lomb, N. Coppola, R. L. Shoeman, S. W. Epp, R. Hartmann, D. Rolles, A. Rudenko, L. Foucar, N. Kimmel, G. Weidenspointner, P. Holl, M. Liang, M. Barthelmess, C. Caleman, S. Boutet, M. J. Bogan, J. Krzywinski, C. Bostedt, S. Bajt, L. Gumprecht, B. Rudek, B. Erk, C. Schmidt, A. Hömke, C. Reich, D. Pietschner, L. Strüder, G. Hauser, H. Gorke, J. Ullrich, S. Herrmann, G. Schaller, F. Schopper, H. Soltau, K-U. Kühnel, M. Messerschmidt, J. D. Bozek, S. P. Hau-Riege, M. Frank, C. Y. Hampton, R. G. Sierra, D. Starodub, G. J. Williams, J. Hajdu, N. Timneanu, M. M. Seibert, J. Andreasson, A. Rocker, O. Jönsson, M. Svenda, S. Stern, K. Nass, R. Andritschke, C-D. Schröter, F. Krasniqi, M. Bott, K. E. Schmidt, X. Wang, I. Grotjohann, J. M. Holton,T. R. M. Barends, R. Neutze, S. Marchesini, R.

#261731 Received 23 Mar 2016; revised 13 May 2016; accepted 14 May 2016; published 6 Jun 2016

Fromme, S. Schorb, D. Rupp, M. Adolph, T. Gorkhover, I. Andersson, H. Hirsemann, G. Potdevin, H. Graafsma, B. Nilsson, and J. C. H. Spence, "Femtosecond x-ray protein nanocrystallography," Nature **470,** 73–77 (2011).
7. H. N. Chapman and K. A. Nugent, "Coherent lensless x-ray imaging," Nature Photon. **4,** 833–839 (2010).
8. M. Tegze and G. Faigel, "X-ray holography with atomic resolution," Nature **380,** 49–51 (1996).
9. G. Grübel and F. Zontone, "Correlation spectroscopy with coherent x-rays," J. Alloys Comp. **362,** 3–11 (2004).
10. R. Mitzner, B. Siemer, M. Neeb, T. Noll, F. Siewert, S. Rolling, M. Rutkowski, A. A. Sorokin, M. Richter, P. Juranic, K. Tiedtke, J. Feldhaus, W. Eberhardt, and H. Zacharias,"Spatio-temporal coherence of free electron laser pulses in the soft x-ray regime," Opt. Express **16,** 19909–19919 (2008).
11. A. Singer, F. Sorgenfrei, A. P. Mancuso, N. Gerasimova, O. M. Yefanov, J. Gulden, T. Gorniak, T. Senkbeil, A. Sakdinawat, Y. Liu, D. Attwood, S. Dziarzhytski, D. D. Mai, R. Treusch, E. Weckert, T. Salditt, A. Rosenhahn, W. Wurth, and I. A. Vartanyants, "Spatial and temporal coherence properties of single free-electron laser pulses," Opt. Express **20,** 17480–17495 (2012).
12. C. Gutt, P. Wochner, B. Fischer, H. Conrad, M. Castro-Colin, S. L. F. Lehmkühler, I. Steinke, M. Sprung, W. Roseker, D. Zhu, H. Lemke, S. Bogle, P. H. Fuoss, G. B. Stephenson, M. Cammarata, D. M. Fritz, A. Robert, and G. Grübel, "Single shot spatial and temporal coherence properties of the SLAC Linac Coherent Light Source in the hard x-ray regime," Phys. Rev. Lett. **108,** 024801 (2012).
13. Y. H. Jiang, T. Pfeifer, A. Rudenko, O. Herrwerth, L. Foucar, M. Kurka, K. U. Kühnel, M. Lezius, M. F. Kling, X. Liu, K. Ueda, S. Düsterer, R. Treusch, C. D. Schröter, R. Moshammer, and J. Ullrich, "Temporal coherence effects in multiple ionization of N2 via XUV pump-probe autocorrelation," Phys. Rev. A **82,** 041403(R) (2010).
14. T. Pfeifer, Y. Jiang, S. Düsterer, R. Moshammer, and J. Ullrich, "Partial-coherence method to model experimental free-electron laser pulse statistics," Opt. Lett. **35,** 3441–3443 (2010).
15. O. Bryngdahl and F. Wyrowski, "Digital holography–computer-generated holograms," in *Progress in Optics*, E. Wolf, ed. (North-Holland, 1990), vol. 28, pp. 1–86.
16. R. Trebino, ed., *Frequency-Resolved Optical Gating: The Measurement of Ultrashort Laser Pulses* (Kluwer, 2002), Chap. 4.
17. L. Sereda, M. Bertolotti, and A. Ferrari, "Coherence properties of nonstationary light wave fields," J. Opt. Soc. Am. A **15,** 695–705 (1998).
18. L. Mandel and E. Wolf, *Optical Coherence and Quantum Optics* (Cambridge University, 1995).
19. R. Dutta, J. Turunen, and A. T. Friberg, "Michelson's interferometer and the temporal coherence of pulse trains," Opt. Lett. **40,** 166–169 (2015).
20. R. Dutta, A. T. Friberg, G. Genty, and J. Turunen, "Two-time coherence of pulse trains and the integrated degree of temporal coherence," J. Opt. Soc. Am. A **32,** 1631–1637 (2015).
21. A. C. Schell, "A technique for the determination of the radiation pattern of a partially coherent aperture," IEEE Trans. Antennas Propag. **AP-15,** 187–188 (1967).
22. G. Genty, M. Surakka, J. Turunen, and A. T. Friberg, "Second-order coherence of supercontinuum light," Opt. Lett. **35,** 3057–3059 (2010).
23. G. Genty, M. Surakka, J. Turunen, and A. T. Friberg, "Complete characterization of supercontinuum coherence," J. Opt. Soc. Am. B **28,** 2301–2309 (2011).
24. S. Düsterer, "Determination of temporal FEL pulse properties: challenging concepts and experiments," Proc. SPIE **8078**, 80780H (2011).
25. J. A. Terschlüsen, M. Agåker, M. Svanqvist, S. Plogmaker, J. Nordgren, J. E. Rubensson, H. Siegbahn, and J. Söderström,"Measuring the temporal coherence of a high harmonic generation setup employing a Fourier transform spectrometer for the VUV/XUV," Nucl. Instrum. Meth. Phys. A **768,** 84–88 (2014).
26. M. Makita, P. Karvinen, D. Zhu, P. N. Juranic, J. Grünert, S. Cartier, J. H. Jungmann-Smith, H. T. Lemke, A. Mozzanica, S. Nelson, L. Patthey, M. Sikorski, S. Song, Y. Feng, and C. David, "High-resolution single-shot spectral monitoring of hard x-ray free-electron laser radiation," Optica **2,** 912–916 (2015).
27. A. M. Kondratenko and E. L. Saldin, "Generation of coherent radiation by a relativistic electron beam in an undulator," Part. Acceler. **10,** 207–216 (1980).
28. P. Pääkkönen, J. Turunen, P. Vahimaa, A. T. Friberg, and F. Wyrowski, "Partially coherent Gaussian pulses," Opt. Commun. **204**, 53–58 (2002).
29. J. Turunen, in *Laser Beam Propagation: Generation and Propagation of Customized Light*, A. Forbes, ed. (CRC Press, 2014), Chap. 10.

1. Introduction

Owing to their high brightness, ultrashort pulse duration, and high degree of transverse spatial coherence, X-ray free-electron lasers (XFELs) [1–3] enable novel research in material science, structural biology, and condensed matter physics [4]. Most of the experimental techniques utilize the coherent fraction of the radiation, including methods such as serial femtosecond crystallography (SFX) [5, 6], coherent X-ray diffraction imaging (CXDI) [7], X-ray holography [8],

#261731 Received 23 Mar 2016; revised 13 May 2016; accepted 14 May 2016; published 6 Jun 2016

and X-ray photon correlation spectroscopy (XPCS) [9]. Hence a thorough understanding of the coherence properties of XFELs [10–13] is of paramount importance.

In this paper we present a numerical method for generating ensembles of pulses representing beams such as those produced by XFELs. These mathematically constructed fields describe the statistical properties of the pulse train in an ensemble-averaged sense. Rather than assuming average spectral and temporal data as in [14], we employ actual measured spectra of individual pulses together with partial knowledge of their average time-domain intensity to construct the spectral phases and the temporal pulse realizations. The XFEL pulses, being rather incoherent in time but originating within similar stochastic conditions, are each represented by an ensemble of realizations. The train of pulses is subsequently statistically governed by a collection of such ensembles, one for each measured spectrum. For the field reconstruction, we apply a temporal-domain counterpart of the spatial iterative Fourier-transform algorithm (IFTA) [15]. The one-dimensional phase retrieval problem does not possess a unique solution [16], and in our case we only have at our disposal the average pulse length in the time domain. The solution would be non-unique even if, in addition to the spectrum, we had access to the individual temporal intensity of each measurement. In our statistical analysis we use this ambiguity to advantage to build ensembles of field realizations for the measured pulses. In the phase retrieval process the correct spectrum is obtained by using it as an explicit condition in the frequency domain. Due to lack of detailed information, the mean temporal intensity is constructed to be Gaussian with the known average pulse length. This is accomplished by employing in the time domain a Gaussian weighting function whose width is appropriately adjusted as the iteration proceeds. Each of the ensuing fields may be regarded as a physically admissible XFEL pulse realization with exact correspondence in the time and frequency domains. Moreover, the ensembles representing the pulses statistically match the experimentally measured spectral and temporal results, and the ensemble associated with the whole pulse train can thereby be expected to faithfully reproduce the statistics of the XFEL source. From the overall ensemble of spectral and temporal field realizations we then construct two-frequency and two-time correlation functions [17], which describe pulse trains of partial spectral and temporal coherence fully within the framework of the classical second-order coherence theory of nonstationary light.

In previous investigations [10–13], time-domain coherence of XFEL pulse trains has been considered using a temporal correlation function that depends only on time delay. Such an approach is adequate for stationary fields [18], whereas two-time correlation functions and time-resolved measurements are needed to completely characterize the temporal coherence properties of pulse trains [19, 20]. We illustrate our model using spectra of individual XFEL pulses measured at the Linac Coherent Light Source (LCLS), which turns out to behave as a quasistationary source despite the femtosecond-scale pulse duration. In addition, the coherence properties of the XFEL source are found to match extremely closely the predictions of the Gaussian Schell model [18, 21].

2. Correlation functions

We denote the frequency-domain and time-domain (scalar, complex) electric fields of the nth individual pulse in a pulse train by $E_n(\omega-\omega_0)$ and $E_n(t)$, respectively. The mean frequency [18] of the pulse train is given by $\omega_0 = \int_0^\infty \omega S^2(\omega)\mathrm{d}\omega / \int_0^\infty S^2(\omega)\mathrm{d}\omega$, where $S(\omega)$ is the average spectrum defined below. Introducing further $\Omega = \omega - \omega_0$, we may write the spectral field representation of an individual pulse in the form

$$E_n(\Omega) = \sqrt{S_n(\Omega)}\exp\left[i\phi_n(\Omega)\right], \tag{1}$$

#261731 Received 23 Mar 2016; revised 13 May 2016; accepted 14 May 2016; published 6 Jun 2016

where $S_n(\Omega) = |E_n(\Omega)|^2$ represents the spectral density of the pulse and $\phi_n(\Omega)$ is its spectral phase. In the envelope representation, the temporal field is

$$E_n(t) = A_n(t)\exp(-i\omega_0 t), \tag{2}$$

where

$$A_n(t) = \sqrt{I_n(t)}\exp[i\phi_n(t)] = \int_{-\infty}^{\infty} E_n(\Omega)\exp(-i\Omega t)\,\mathrm{d}\Omega, \tag{3}$$

and $I_n(t) = |E_n(t)|^2 = |A_n(t)|^2$ is the temporal intensity profile of an individual pulse, $\phi_n(t)$ being the envelope phase.

By regarding the individual pulses (which generally are of different spectral and temporal form) as members of a statistical ensemble, we may introduce correlation functions in both spectral and temporal domains. In the second-order coherence theory of nonstationary light, the appropriate spectral correlation function is the two-frequency cross-spectral density function (CSD), defined as an ensemble average

$$W(\Omega_1,\Omega_2) = \langle E^*(\Omega_1)E(\Omega_2)\rangle = \frac{1}{N}\sum_{n=1}^{N} E_n^*(\Omega_1)E_n(\Omega_2), \tag{4}$$

where N is the number of pulses in the ensemble. We may also view the CSD as a function of the average and difference coordinates $\Omega = \frac{1}{2}(\Omega_1+\Omega_2)$ and $\Delta\Omega = \Omega_2 - \Omega_1$. The mean spectrum of the pulse train is given by $S(\Omega) = W(\Omega,0)$ and its complex degree of spectral coherence is defined as

$$\mu(\Omega,\Delta\Omega) = \frac{W(\Omega,\Delta\Omega)}{\sqrt{S(\Omega-\Delta\Omega/2)S(\Omega+\Delta\Omega/2)}}. \tag{5}$$

Considered as a function of $\Delta\Omega$, the characteristic breadth of $|\mu(\Omega,\Delta\Omega)|$ provides the spectral coherence width of the pulse train at frequency Ω.

Time-domain correlations of nonstationary fields are characterized by the two-time mutual coherence function (MCF), defined as

$$\Gamma(t_1,t_2) = \langle E^*(t_1)E(t_2)\rangle = \exp[-i\omega_0(t_2-t_1)]\frac{1}{N}\sum_{n=1}^{N} A_n^*(t_1)A_n(t_2). \tag{6}$$

We may express the MCF in terms of the average and difference coordinates $t = \frac{1}{2}(t_1+t_2)$ and $\Delta t = t_2 - t_1$. Then the mean temporal intensity is given by $I(t) = \Gamma(t,0)$ and the complex degree of temporal coherence is defined as

$$\gamma(t,\Delta t) = \frac{\Gamma(t,\Delta t)}{\sqrt{I(t-\Delta t/2)I(t+\Delta t/2)}}. \tag{7}$$

Again, if we consider $|\gamma(t,\Delta t)|$ as a function of Δt, its width is a measure of the coherence time at time instant t. We emphasize that the spectral coherence width may depend strongly on Ω and the coherence time on t; extreme variations occur, for instance, in supercontinuum pulse trains [22, 23].

Time-resolved measurements of the temporal (and spectral) intensity and phase of individual ultrashort pulses are possible in the visible region, which in principle allow a direct construction of the two-time and two-frequency correlation functions. Measurement of the temporal properties of XFEL pulses has been intensively studied [24]. However, to our knowledge there are no

#261731 Received 23 Mar 2016; revised 13 May 2016; accepted 14 May 2016; published 6 Jun 2016

methods that can provide the required temporal resolution or information about the temporal phase. Coherence measurements yielding time-integrated results in Michelson-type interferometric setups have been performed [25], but they do not enable the construction of the full two-time MCF. This raises the question what information can be extracted from such measurements.

It follows at once from Eqs. (2)–(4) and (6) that the CSD and MCF are related by the generalized Wiener–Khintcine theorem as

$$\Gamma(t_1,t_2) = \exp\left[-i\omega_0(t_2-t_1)\right] \iint_{-\infty}^{\infty} W(\Omega_1,\Omega_2) \exp\left[i\left(\Omega_1 t_1 - \Omega_2 t_2\right)\right] \mathrm{d}\Omega_1 \mathrm{d}\Omega_2, \tag{8}$$

which, if the average and difference coordinates are used, becomes

$$\Gamma(t,\Delta t) = \exp\left(-i\omega_0 \Delta t\right) \iint_{-\infty}^{\infty} W(\Omega,\Delta\Omega) \exp\left[-i\left(\Omega\Delta t + \Delta\Omega t\right)\right] \mathrm{d}\Omega \mathrm{d}\Delta\Omega. \tag{9}$$

Inverting this expression, we find that the mean spectrum of the pulse train is given by

$$S(\Omega) = \frac{1}{(2\pi)^2} \iint_{-\infty}^{\infty} \Gamma(t,\Delta t) \exp\left[i(\omega_0+\Omega)\Delta t\right] \mathrm{d}t \mathrm{d}\Delta t. \tag{10}$$

Since temporally integrated Michelson-type measurements provide us with the quantity

$$\bar{\Gamma}(\Delta t) = \frac{1}{2\pi} \int_{-\infty}^{\infty} \Gamma(t,\Delta t) \mathrm{d}t, \tag{11}$$

the average spectrum may be written in the form

$$S(\bar{\omega}-\omega_0) = \frac{1}{2\pi} \int_{-\infty}^{\infty} \bar{\Gamma}(\Delta t) \exp\left(i\bar{\omega}\Delta t\right) \mathrm{d}\Delta t, \tag{12}$$

where $\bar{\omega} = (\omega_1+\omega_2)/2$. This result is formally equivalent with the classic Wiener–Khintchine theorem for stationary light [18]. However, instead of the MCF for stationary fields, we consider here the time integral of the two-time MCF. Equation (12) shows that the mean spectrum of a pulse train is obtained from time-integrated Michelson interferometer measurements. In reverse, the time-integrated MCF can be obtained from the mean spectrum according to

$$\bar{\Gamma}(\Delta t) = \int_{0}^{\infty} S(\bar{\omega}-\omega_0) \exp\left(-i\bar{\omega}\Delta t\right) \mathrm{d}\bar{\omega}. \tag{13}$$

The characteristic width of the normalized form of the temporally integrated MCF,

$$\bar{\gamma}(\Delta t) = \bar{\Gamma}(\Delta t)/\bar{\Gamma}(0), \tag{14}$$

may then be considered as a measure of the effective coherence time of the pulse train.

3. Iterative Fourier-transform algorithm (IFTA)

Our model for constructing ensembles of pulses, illustrated in Fig. 1, is based on the knowledge of a large number of spectra of individual pulses that have been measured for XFEL source at LCLS using full pulse energy of ~ 2 mJ, repetition rate of 120 Hz, mean photon energy of ~ 8.37 keV, and pulse length of 34 fs (corresponding to a FWHM of 40 fs). More details of the experiment can be found in [26]. In the time domain we assume that the mean temporal evolution of the pulse train is of the Gaussian form

$$I(t) = I_0 \exp\left(-2t^2/T^2\right), \tag{15}$$

#261731 Received 23 Mar 2016; revised 13 May 2016; accepted 14 May 2016; published 6 Jun 2016

where the mean pulse duration is $T = 34$ fs. Nevertheless, shorter Gaussian pulses and also any non-Gaussian mean pulse shapes, which could arise in different FEL operation regimes, could be considered equally well by using an appropriate average pulse shape. Under such conditions the pulse train might exhibit different statistics, but the method presented here would still be fully applicable.

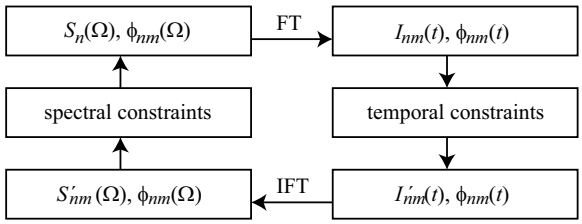

Fig. 1. Flow chart of the temporal iterative Fourier-transform algorithm (IFTA).

In the initialization stage of the algorithm we associate with the (measured) pulse spectrum $S_n(\Omega)$ of the nth field realization a random phase distribution $\phi_{n1}(\Omega)$ to generate the initial spectral field $E_{n1}(\Omega) = \sqrt{S_{n1}(\Omega)}\exp[i\phi_{n1}(\Omega)]$, as in [14]. We then use Eq. (3) to transform into the time domain, which gives $A_{n1}(t) = \sqrt{I_{n1}(t)}\exp[i\phi_{n1}(t)]$. The temporal constraints in Fig. 1 mean that the time-domain intensity distribution of the pulse is multiplied by a Gaussian function of the same form as in Eq. (15), but with the width given by $m \times 37$ fs, where m is the order of the iteration round in question. Starting from $T = 37$ fs and increasing the width at each iteration step (so that eventually the Gaussian is almost flat) was found to lead to the average intensity whose e^{-2}-width is 34 fs. The temporal phase of the field is left untouched implying that the time-domain field at this stage is $A'_{n1}(t) = \sqrt{I'_{n1}(t)}\exp[i\phi_{n1}(t)]$. We next make use of the inverse of Eq. (3), i.e.,

$$E'_{n1}(\Omega) = \frac{1}{2\pi}\int_{-\infty}^{\infty} A'_{n1}(t)\exp(i\Omega t)\,\mathrm{d}t, \tag{16}$$

to convert back into the frequency domain. Here we set the spectrum to its measured form but leave the phase as it is, thus obtaining $E_{n2}(\Omega) = \sqrt{S_{n2}(\Omega)}\exp[i\phi_{n2}(\Omega)]$. The iterative process is continued as long as needed for the results to converge, i.e., until we achieve the situation $S'_{nm}(\Omega) = |E'_{nm}(\Omega)|^2 \approx S_n(\Omega)$.

4. Results and discussion

The algorithm results in an ensemble of pulse realizations with individual spectra that match the measured ones but have certain spectral phase distributions as well as temporal intensity profiles and phases that differ from one another. The CSD and MCF are then constructed using Eqs. (4) and (6). A single execution of the IFTA algorithm was found to lead to a temporal pulse of varying complicated shape, which depends on the chosen random initial spectral phase. This demonstrates a low degree of phase correlations for the individual XFEL pulses, defined as

$$\begin{aligned}\Phi(\Omega_1,\Omega_2) &= \langle \exp[-i\phi(\Omega_1)]\exp[i\phi(\Omega_2)]\rangle \\ &= \frac{1}{L}\sum_{l=1}^{L}\exp[-i\phi_l(\Omega_1)]\exp[i\phi_l(\Omega_2)]\end{aligned} \tag{17}$$

#261731 Received 23 Mar 2016; revised 13 May 2016; accepted 14 May 2016; published 6 Jun 2016

and

$$\Theta(t_1,t_2) = \exp(-i\omega_0\Delta t)\,\langle \exp[-i\phi(t_1)]\exp[i\phi(t_2)]\rangle$$
$$= \exp(-i\omega_0\Delta t)\,\frac{1}{L}\sum_{l=1}^{L}\exp[-i\phi_l(t_1)]\exp[i\phi_l(t_2)] \qquad (18)$$

in the spectral and temporal domains, respectively. The summation here is taken over L realizations obtained for an individual measured spectrum. To construct the CSD and MCF using Eqs. (4) and (6), we therefore average over a grand ensemble consisting of L realizations for each of the M single spectral pulse measurements in the pulse train. These final ensembles, both in time and frequency domains, thus contain a total of $N = M \times L$ realizations.

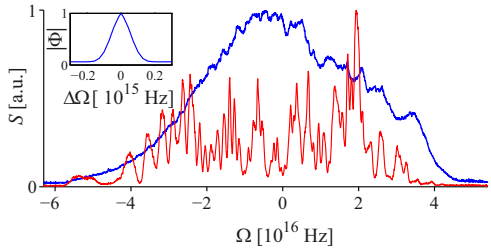

Fig. 2. Experimentally measured spectrum (solid red line) of a single pulse and the mean spectrum (solid blue line) of 1100 measured pulses. The mean spectrum equals the average spectrum calculated through IFTA. The inset shows the magnitude of the normalized average spectral phase-correlation function Φ constructed with 200 spectral field realizations related to the single-pulse spectrum.

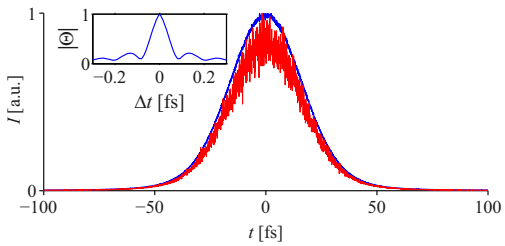

Fig. 3. Temporal intensity distribution (red line) constructed by averaging over 20 field realizations computed by IFTA with different phases associated with the single measured pulse shown in Fig. 2. The mean temporal intensity (blue line) is found by reconstructing with IFTA 20 realizations of varying phase profiles for each of the 1100 measured spectra, to obtain 22000 time-domain realizations, and averaging. The inset shows the magnitude of the normalized temporal phase-correlation function Θ calculated by averaging over 200 realizations with the same measured spectrum.

Numerical results, averaged over $M = 1100$ measured pulses with $L = 20$ realizations for each, are shown in Figs. 2 and 3. The spectral phase correlation function Φ of a single pulse,

#261731 Received 23 Mar 2016; revised 13 May 2016; accepted 14 May 2016; published 6 Jun 2016

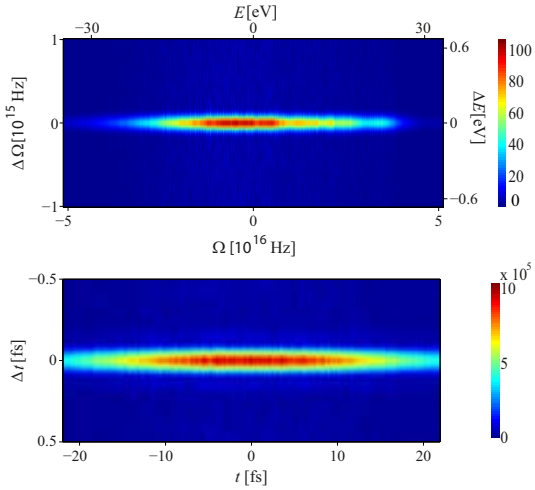

Fig. 4. Absolute values of the CSD (top, shown also in terms of the related photon energies E and ΔE) and the MCF (bottom) corresponding to 22000 reconstructed pulse realizations.

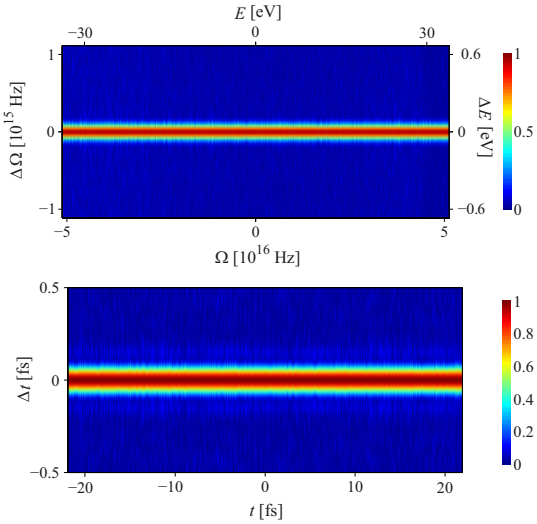

Fig. 5. Complex degrees of spectral (top) and temporal (bottom) coherence of the XFEL pulses. The top figure is shown also in terms of the associated photon energies E and ΔE.

displayed in the inset of Fig. 2, is constructed using Eq. (17) with $L = 200$ realizations (for better accuracy) and averaged over the frequencies. We see that its effective width in $\Delta\Omega$ is only a tiny fraction of the mean spectral spread of the pulses. The corresponding temporal intensity

#261731 Received 23 Mar 2016; revised 13 May 2016; accepted 14 May 2016; published 6 Jun 2016

distributions, together with the time-averaged phase correlation function given by Eq. (18), are illustrated in Fig. 3. Clearly, the effective width of Θ in Δt is a small fraction of the mean temporal pulse duration. Like most FELs operating today, this source is based on self-amplification of spontaneous emission (SASE) [27]. Spontaneous gain gives rise to variations from bunch to bunch leading to large shot-to-shot spectral diversity, as seen from Fig. 2, and indicating a low degree of spectral coherence. This fact is reflected in the CSD and MCF plots displayed in Fig. 4, which appear as narrow horizontal lines (note the different scales on the horizontal and vertical axes).

The normalized CSD and MCF, defined by Eqs. (5) and (7), respectively, are shown in Fig. 5. They confirm the low spectral and temporal coherence and the almost stationary nature of the XFEL pulse train. The width of $|\mu(\Omega,\Delta\Omega)|$ in the $\Delta\Omega$ direction (spectral coherence width) is nearly independent of Ω, i.e., $|\mu(\Omega,\Delta\Omega)| \approx |\mu(\Delta\Omega)|$, and similarly, the width of $|\gamma(t,\Delta t)|$ in the Δt direction (coherence time) is nearly independent of t, i.e., $|\gamma(t,\Delta t)| \approx |\gamma(\Delta t)|$. In this case, $|\gamma(\Delta t)|$ is essentially the integrated quantity $\overline{\gamma}(\Delta t)$ in Eq. (14). Figure 6 shows $|\mu(\Delta\Omega)|$ and $|\gamma(\Delta t)|$, averaged over Ω and t, respectively, together with Gaussian fits. Since the spectral coherence width is small compared to the average spectral spread and the coherence time is short compared to the mean pulse duration, this FEL behaves as a quasistationary source in the language of second-order coherence theory of nonstationary light.

We can approximate the XFEL pulse train using the Gaussian Schell model [18, 21, 28, 29]. The mean intensity then is given by the Gaussian function $I(t)$ of Eq. (15) (with duration T), the spectrum has a Gaussian form

$$S(\Omega) = S_0 \exp\left(-2\Omega^2/\Sigma^2\right), \tag{19}$$

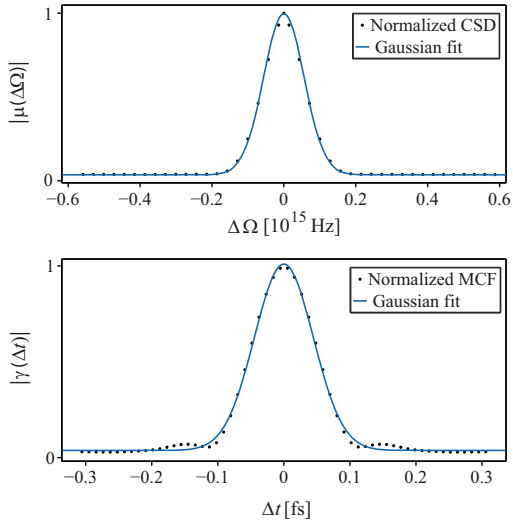

Fig. 6. Widths of the averaged normalized CSD (top) and the MCF (bottom) as functions of the difference coordinates. The dots represent the data points given by IFTA and the solid lines are Gaussian fits.

#261731 Received 23 Mar 2016; revised 13 May 2016; accepted 14 May 2016; published 6 Jun 2016

and we take Gaussian distributions for the complex degrees of spectral and temporal coherence,

$$\mu(\Omega,\Delta\Omega) = \exp\left(-\Delta\Omega^2/2\Sigma_\mu^2\right), \tag{20}$$

$$\gamma(t,\Delta t) = \exp\left(-\Delta t^2/2T_\gamma^2\right)\exp\left(-i\omega_0\Delta t\right), \tag{21}$$

respectively. The parameters T, Σ, Σ_μ, and T_γ are not independent. In the quasistationary case, when $\Sigma \gg \Sigma_\mu$, $T \gg T_\gamma$, and the time–bandwidth product $T\Sigma \gg 1$, the relations $\Sigma_\mu = 2/T$ and $T_\gamma = 2/\Sigma$ hold [29]. A Gaussian fit of the average spectrum shown in Fig. 2 gives $\Sigma = 4.35 \times 10^{16}$ Hz. Hence, with $T = 34$ fs, we have $T\Sigma = 1500$, $\Sigma_\mu = 5.9 \times 10^{13}$ Hz, and $T_\gamma = 0.046$ fs. Figure 6 displays the mean cross-sections $|\mu(\Delta\Omega)|$ and $|\gamma(\Delta t)|$ of the absolute values of the normalized CSD and MCF. The Gaussian fits give $\Sigma_\mu \approx 5.7 \times 10^{13}$ Hz and $T_\gamma \approx 0.046$ fs, in excellent agreement with the Gaussian Schell model. The widths of Gaussian functions in Fig. 6 correspond to a drop from the peak values of unity to $e^{-0.5}$ when the non-zero tails were taken into account.

5. Conclusions

We have introduced an iterative mathematical technique for the construction of ensembles of pulses in both spectral and temporal domains. The model is based on spectral measurements of individual pulses and on knowledge of the mean pulse duration. Such ensembles were used to construct two-time and two-frequency correlation functions that fully describe the second-order coherence properties of the pulse train. In an explicit example we considered a particular FEL, which turned out to emit quasistationary pulse trains (with low spectral and temporal coherence). In addition, the source was found to obey the Gaussian Schell model. We emphasize, however, that the method put forward here is applicable to any other FEL, some of which are likely to be far more coherent, and in fact to any other pulsed laser source.

Acknowledgments

This work was partially funded by the Academy of Finland (projects 268480 and 268705) and Dean's special support for coherence research at the University of Eastern Finland, Joensuu (project 930350). We acknowledge Sven Reiche from Paul Scherrer Institut for his comments on the manuscript. We also thank Diling Zhu and Yiping Feng from the Linac Coherent Light Source, SLAC National Accelerator Laboratory for their contributions in the spectral measurements. Toni Saastamoinen is acknowledged for assistance with the IFTA algorithm.

#261731 Received 23 Mar 2016; revised 13 May 2016; accepted 14 May 2016; published 6 Jun 2016

LUTFUL AHAD

This thesis investigates the temporal and spectral coherence of quasi-stationary pulsed light. An iterative mathematical technique is introduced which can simulate the output of a pulsed light source. A new time-domain pseudo-modal expansion based on the knowledge of the average spectrum and mean temporal intensity of a random, quasi-stationary pulse train is introduced. The pseudo-modal expansion is extended to the electromagnetic case. A novel harmonic mode representation for stationary polarized electromagnetic beams is also presented. The thesis also contains a discussion on the autocorrelation measurements of free-electron laser pulses and elaborates on the information that can be obtained from such measurements.

UNIVERSITY OF
EASTERN FINLAND

uef.fi

PUBLICATIONS OF
THE UNIVERSITY OF EASTERN FINLAND
Dissertations in Forestry and Natural Sciences

ISBN 978-952-61-2990-7
ISSN 1798-5668